University of Genoa

Doctoral Program in Neuroscience

Doctoral School in Clinical and Experimental Neuroscience

XXX Cycle

The paroxysmal disorder gene *PRRT2* downregulates Na_V channels and neuronal excitability in human neurons

Author: Dr. Giorgia Giansante

Supervisor: Dr. Pierluigi Valente

TABLE OF CONTENTS

ABSTRACT

Proline-Rich Transmembrane Protein 2 (*PRRT2*) has been identified as the single causative gene for a group of paroxysmal syndromes, including benign familial infantile seizures, paroxysmal kinesigenic dyskinesia and migraine. Most of the mutations of this gene lead to a premature stop codon, generating an unstable form of mRNA or a truncated protein that is degraded, pointing out the loss of the PRRT2 function as pathogenic mechanism of action. In this thesis, we have used different approaches to investigate the pathophysiological function of PRRT2. An important role for PRRT2 in the neurotransmitter release machinery, brain development and synapse formation has been uncovered by a previous work performed in our laboratory by acute silencing of PRRT2 expression. Here, we analyzed the phenotype of primary hippocampal neurons obtained from mouse *PRRT2* knockout (KO) embryos. Analysis of synaptic function in primary neurons obtained from *PRRT2*-KO showed a largely similar, albeit attenuated, synaptic phenotype with respect to acute *PRRT2* silencing characterized by weakened spontaneous/evoked synaptic transmission and increased facilitation at excitatory synapses. These effects were accompanied by a strengthened inhibitory transmission that, however, displayed faster synaptic depression. At the network level, these synaptic phenotypes, resulted in a state of increased spontaneous and evoked neurotransmitter release with increased excitability of excitatory neurons. To better dissect the physiological role of PRRT2, we characterized the phenotypes of neurons differentiated from Induced Pluripotent Stem Cells (iPSCs) from patients homozygous for the *PRRT2 c.649dupC* mutation. Hence, we observed an increased Na^+ current and firing activity in iPSCs rescued with the re-expression of the human wild-type form of PRRT2. By use of heterologous expression system, we demonstrate that PRRT2 interacts with $Na_V1.2$/$Na_V1.6$, but not with $Na_V1.1$ channels, modulating their membrane exposure and decreasing their conductances.

In brief, our findings highlighted that *PRRT2* mutations might be a negative modulator of $Na_V1.2$/$Na_V1.6$ channels and point out the critical role of this protein in the regulation of the neuronal network functionality.

1. INTRODUCTION

1.1. The Paroxysmal Disorders

Paroxysmal Disorders (PDs) represent a heterogeneous group of rare neurological disorders sharing similar features, such as abnormal movements, dystonia, chorea, athetosis and ballism, or a combination of all these disorders (Bhatia, 2011). These pathological conditions are often associated with epilepsy (**Fig. 1**). PDs usually begin during childhood and tend to improve with age (McGrath and Dure, 2003). They are generally characterized by episodic nature and by short duration of the attacks (Unterberger and Trinka, 2008).

Shuzo Kure clinically reported PD for the first time in 1892 in a 23-year-old Japanese man who showed frequent movement-induced paroxysmal attacks from the age of ten (Kure, 1892). In 1995, Demirkiran and Jankovic proposed a classification of PDs based on precipitating events and differentiated four main types of PDs: Paroxysmal Kinesigenic Dyskinesia (PKD), Paroxysmal Non-Kinesigenic Dyskinesia (PNKD), Paroxysmal Exercise-Induced Dyskinesia (PED) and Paroxysmal Hypnogenic Dyskinesia (PHD) (Demirkiran and Jankovic, 1995). A subsequent classification of PDs was based on the duration of the attacks and on the presumed etiology. By this, the PDs was classified as primary (familial or sporadic) and secondary (Unterberger and Trinka, 2008).

In the first time, primary PD-related disorders were hypothesized to be ion channels-related dysfunctions, indicated with the generical name of “channelopathies” (Bhatia, 2000). This hypothesis was corroborated from the discovery of mutations occurred in genes encoding for ion channels (Fink *et al*., 1996; Fouad *et al*., 1996; Bhatia, 2000). Moreover, it was observed a sensitivity of some subtypes of PDs to anticonvulsant drugs at low dose to modulate the conductance of several ion channels (Bhatia, 2000, Erro *et al*., 2014).

Recently, several studies reported three major PD-related genes: Myofibrillogenesis regulator 1 (*MR-1*) (Raskind *et al*., 1998; Lee *et al*., 2004), Glucose Transporter 1 (*SLC2A1*) (Wang *et al*., 2000; Vermeer *et al*.,

2007) and the Proline-Rich Transmembrane Protein 2 (*PRRT2*) (Chen *et al*., 2011).

Human *MR-1* is located on human chromosome *2q35* and has three isomeric forms: *MR-1L*, *MR-1M* and *MR-1S*, formed by alternative splicing (Lee *et al*., 2004). Mutations in the N-terminal region of *MR-1L* and *MR-1S* are the main causes of PNKD: for this reason, the gene is also known as *PNKD* (Lee *et al*., 2004, Wang *et al*., 2017a). In a previous study, it was found that *MR-1* gene is homologous to the hydroxyacylglutathione hydrolase gene (Lee *et al*., 2004). Because this gene functions in a pathway to detoxify methylglyoxal, a by-product of oxidative stress present in coffee and alcoholic beverages (Wang *et al*., 2011), it was suggested a mechanism whereby alcohol, coffee and stress may act as precipitants of attacks in PKND (Lee *et al*., 2004).

Solute carrier family 2 facilitated glucose transporter member 1 (*SLC2A1*), also known as *GLUT1*, encodes for the D-glucose transporter across the blood brain barrier, GLUT1 protein (Wang *et al*., 2000). Numerous studies have demonstrated that different mutations in *SLC2A1* might be important to lead PED without epilepsy or co-occurrence of PED with epilepsy (Suls *et al*., 2008). Moreover, Wang *et al*. (2016) screened *MR-1* and *SLC2A1* genes in 28 patients who were diagnosed with sporadic PKD but not carrying *PRRT2* mutations.

Until now, *PRRT2* is the major gene accounted for PKD (frequency of 40-90%) (Chen *et al*., 2011), for Benign Familial Infantile Epilepsy (BFIE) (80%) and for Infantile Convulsion and Choreoathetosis (ICCA) (>90%) (Heron *et al*., 2012; Marini *et al*., 2012).

Recent findings associate PRRT2 functions also at presynaptic level (Liu *et al*., 2016; Valente *et al*., 2016a), and this data added that *PRRT2*-related disorders can be considered synaptopathies too (Erro *et al*., 2014).

The broad spectrum of clinical manifestations suggests that there is a marked pleiotropy and variable penetrance of *PRRT2* mutations (Erro *et al*., 2014).

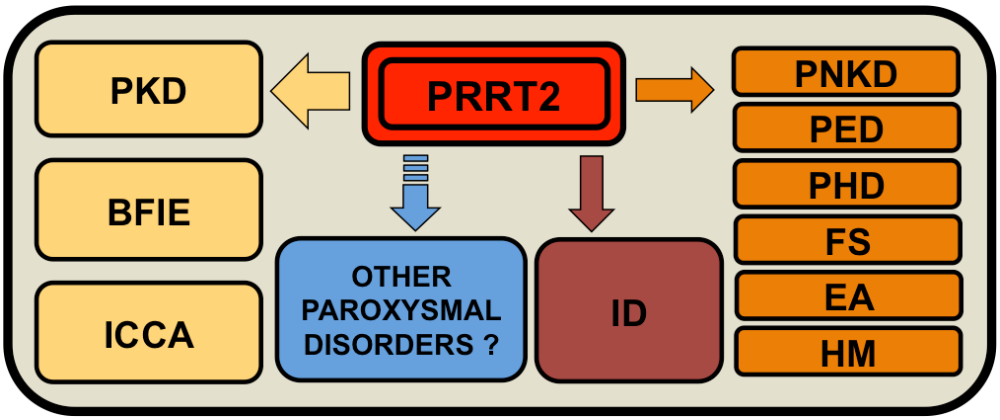

Figure 1. Clinical Spectrum of *PRRT2* Mutations Disorders. The large yellow arrow indicates the most common phenotypes caused by *PRRT2* mutations: paroxysmal kinesigenic dyskinesia (**PKD**), benign familial infantile epilepsy (**BFIE**), infantile convulsions with choreoathetosis syndrome (**ICCA**). The thin orange and brown arrows point to the less frequent clinical spectrum of disorders produced by *PRRT2* mutations: paroxysmal non-kinesigenic dyskinesia (**PNKD**), paroxysmal exercise-induced dyskinesia (**PED**), paroxysmal hypnogenic dyskinesia (**PHD**), febrile seizures (**FS**), episodic ataxia (**EA**) and hemiplegic migraine (**HM**) and intellectual disability (**ID**). The dashed blue arrow indicates the other hypothetical, but at now unverified, clinical manifestations induced by *PRRT2* mutations (From Méneret *et al*., 2013, *modified*).

1.2. The *PRRT2* gene

Over the past five years, numerous studies have identified nonsense, frameshift and missense mutations in the *PRRT2* gene in a large number of patients with various paroxysmal neurological disorders with early-onset manifestations (Chen *et al*., 2011; Lee *et al*., 2012).

The *PRRT2* gene (Entrez Gene: 112476) maps on the short arm of chromosome 16 (*16p11.2*) (Chen et al., 2011) and consists of four exons encoding for a 340 amino-acids (AAs) protein. This structure is highly conserved among mammals (~80%), with some similarities still appreciable in lower vertebrates (~30%) (e.g., *zebrafish*) (Lee *et al*., 2012). The sequence similarity increases in the C-terminal region of the molecule (up to 90%) in mammals and 60% in zebrafish (Lee *et al*., 2012).

It has been reported that families affected by PKD, BFIE and ICCA showed linkage to the large pericentromeric region of chromosome 16 (*16p11.2*), suggesting that these disorders are allelic with variable expressions

(Szepetowski *et al*., 1997; Caraballo *et al*., 2002). Thus, sequences of more than 157 genes in this specific gene region have been sequenced (Kikuchi *et al*., 2007), but a specific gene involved in these pathologies was not identified for more than a decade. A large number of *PRRT2* mutations were identified by the use of the next generation sequencing technique, combined with classical linkage analysis (Chen *et al*., 2011; Wang *et al*., 2011).

A vast majority of *PRRT2* mutations reported (about 95%) are nonsense or frameshift (Liu *et al*., 2013). Among these mutations, a common frameshift mutation occurs in an unstable region of nine cytosines (*c.641-c.649*), causing the introduction of a stop codon seven AAs downstream of insertion (*c.649-650insC>p.Arg217Profs*7*) (Lee *et al*., 2012). This mutation segregates in about 80% of the *PRRT2* mutant families resulting in diverse paroxysmal disorders (Ebrahimi-Fakhari *et al*., 2015). The *c.649dupC* frameshift mutation leads to an unstable mRNA or a truncated form of the protein that is degraded, resulting in a *loss-of-function* pathogenetic mechanism (Lee *et al*., 2012; Li *et al*., 2015; Liu *et al*., 2016).

A variety of other nonsense or frameshift mutations are mostly located in the long N-terminal domain of the protein, scattered in the proline-rich domain, and only a few involve the transmembrane domains or the cytoplasmic loop (Heron *et al*., 2012). In addition to these truncated mutants, a few missense mutations were also identified (Gardiner *et al*., 2012). All mutations described so far are depicted in **Fig. 2**.

In contrast, other common non-paroxysmal movement disorders, typical in many neurodegenerative disorders, such as in Parkinson's disease, are not associated with *PRRT2* mutations (Kumar *et al*., 2012).

The shared paroxysmal nature of symptoms and genetic findings in *PRRT2*-associated diseases suggested a common pathophysiology that involve *PRRT2* gene encoding for a protein that it might be important in synaptic vesicle (SV) release machinery and in neuronal excitability (Ebrahimi-Fakhari *et al*., 2015).

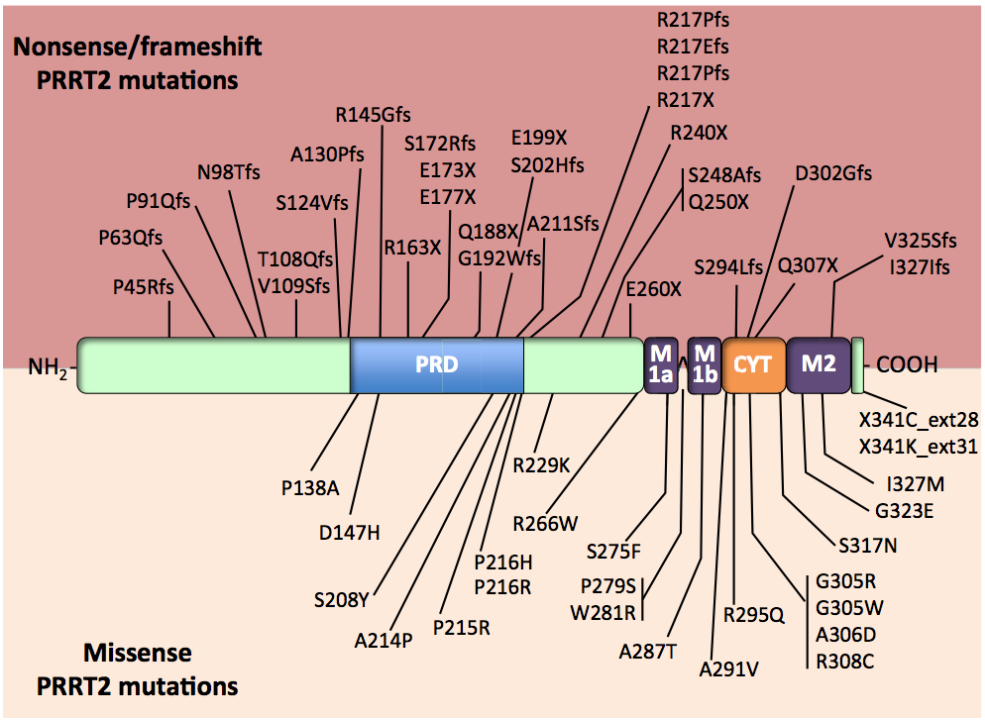

Figure 2. Mapping of *PRRT2* mutations superimposed to the domain structure of Proline-Rich Transmembrane Protein 2 (PRRT2). Mutations in *PRRT2* have been recently identified as the cause for a heterogeneous group of paroxysmal neurological diseases. The identified nonsense/frameshift and missense mutations are reported on the PRRT2 domain structure in the upper and lower panels, respectively (from Valtorta *et al*., 2016).

1.2.1. PRRT2 and the Paroxysmal Kinesigenic Dyskinesia

PKD (Online Mendelian Inheritance of Man, OMIM: 128200), together with BFIE and ICCA, represents the core of *PRRT2*-associated disorders (Chen *et al*., 2011; Wang *et al*., 2011; Heron *et al*., 2012; Lee *et al*., 2012; Ono *et al*., 2012). *PRRT2* mutations in BFIE and PKD are inherited in an autosomal-dominant manner and affect both females and males in populations with various ethnic backgrounds (Ebrahimi-Fakhari *et al*., 2015). The general clinical features of BFIE-PKD/ICCA will be herein discussed.

PKD is the most frequent of the paroxysmal dyskinesia syndromes but has an estimated prevalence of only 1:150,000 in the population (Spacey and Adams, 2013). PKD was first described in 1892 in a young Japanese patient presenting with short attacks of purposeless involuntary movements triggered by rapid voluntary motion, with no loss of consciousness (Kure, 1892).

Then, Kertesz and colleagues described the phenotypes in 1967 in ten patients from six families. The patients showed "*short paroxysms of unilateral or generalized tonic, choreiform, and athetoid movements that were usually precipitated by movement*", suggesting that the disorder was often familial and therefore a genetic cause was proposed (Kertesz *et al*. 1967).

Only in 2011, Chen and colleagues showed that the heterozygous mutations of the *PRRT2* gene at *16p11.2* locus was responsible for PKD (Chen *et al*., 2011). Several independent groups have identified *PRRT2* as the major causative gene for PKD (Chen *et al*., 2011; Wang *et al*., 2011; Lee *et al*., 2012). PKD is often familial with an autosomal-dominant inheritance with incomplete penetrance (Lee *et al*., 2012). Disease penetrance is estimated at 60-90% leading to unaffected or only mildly affected family members, despite the presence of a known pathogenic mutation or a full manifestation (van Vliet *et al*., 2012). Sporadic PKD cases are also reported in different patients carrying the *c.649dupC* mutation (Li *et al*., 2013). This might be attributed to the incomplete penetrance of *c.649dupC*, or, alternatively, *c.649dupC* might derive from *de novo* mutations.

A hotspot mutation *c.649dupC* has been found in PKD cases from different ethnic origins (Méneret *et al*., 2012; Heron and Dibbens, 2013).

However, *PRRT2* mutations do not account for all PKD cases, especially for those sporadic ones, suggesting the existence of additional gene mutations or possible misdiagnosis due to overlapping clinical manifestations (Lee *et al*., 2012: Li *et al*., 2012, Chen *et al*., 2014).

Bruno and colleagues proposed diagnostic criteria for PKD in 2004. The attacks show an identified kinesigenic trigger, usually lasting for less than a minute, with an average ~30 s. Importantly, PKD attacks do not occur during sleep and never involve loss of consciousness, pain or weakness. The frequency of attacks is variable, usually peaking in puberty, with improvement or even remission in adulthood. Auras are frequent, allowing in some patients a partial control of the attacks (Bruno *et al*. 2004; **Table 1**).

Diagnostic tests such as Electroencephalography (EEG) and Magnetic Resonance Imaging (MRI) do not reveal any distinct abnormalities in PKD patients. The few reported interictal studies point to abnormalities in the cortico-striatopallido-thalamic circuitry, although the diagnostic and pathophysiological implications remain limited (Joo *et al*., 2005; Zhou *et al*.,

2010; Kim *et al*., 2011, 2014). Notably, the question about the origin of PKD attacks (cortical *vs.* subcortical) remains until now unanswered (Ebrahimi-Fakhari *et al*., 2015).

Different non-specific pharmacological approaches are currently used for PKD. Carbamazepine is the drug of choice for PKD. It is used at dosages that are much lower than those used to treat epilepsy (e.g. 50-200 mg/day) to reduce or to suppress the attacks (Bruno *et al*., 2004). Other classical anticonvulsant agents may also be effective, including phenytoin, valproate, oxcarbazepine, lamotrigine, levetiracetam and topiramate (Bruno *et al*., 2004; Strzelczyk *et al*., 2011).

Clinical criteria for PKD
Identified kinesigenic trigger for the attacks
Short duration of attacks (< 1 min)
No loss of consciousness and no pain during attack
Exclusion of other organic diseases and normal neurologic examination
Control of attacks with an antiepileptic drug such as carbamazepine or pH
Age at onset between 1 and 20 years if no family history of PKD. Age criteria might not be as important in the familial cases. Cases with older age of onset have been described in instances where there is a family history of PKD

Table 1. Diagnostic criteria for PKD. Clinical manifestations used to attempt to determinate the PKD pathology (From Bruno *et al*., 2004, *modified*).

1.2.2. PRRT2 and the Benign Familial Infantile Epilepsy

BFIE (OMIM: 605751), once termed benign familial infantile seizures or benign familial infantile convulsions, is a self-limiting seizure disorder of infancy with autosomal-dominant inheritance (Caraballo *et al*., 2002). Patients have non-febrile seizures with onset between the ages of four and twelve months and of age and offset by two years of age (Heron and Dibbens, 2013). Neurological tests and imaging studies (EEG and MRI) are usually normal. This syndrome was originally defined from Watanabe and colleagues in 1987 (Watabe *et al*., 1987). The phenotype was described in

depth in 1992 and named '*benign familial infantile convulsions*' (Vigevano *et al*., 1992). BFIE-related seizures usually occur in clusters of complex-partial or generalized tonic-clonic seizures, and in this context, motor arrest, decreased responsiveness, and automatisms, were reported (Watanabe *et al*., 1987). Watanabe and colleagues observed that the infants showed an apparently normal developmental outcome and that seizures were easily controlled with antiepileptic drugs (Watanabe *et al*., 1987), which is in contrast to what happen in many cases of seizures during infancy (Heron and Dibbens, 2013). Vigevano and colleagues (1992) described other BFIE diagnostic cases in which the epilepsy was familial showing a favourable outcome. Moreover, these patients presented clinical features similar to those seen in benign familial neonatal convulsions, apart from the age of onset (Vigevano *et al*., 1992). It was also observed that the features in these patients overlapped those described by Watanabe in 1987. The therapy with drugs such as phenobarbital, carbamazepine or valproate has been frequently used, and generally, a combination of two or more anticonvulsants was not employed (Caraballo *et al*., 2002). In addition, seizures often remit shortly after the start of anticonvulsants but, because of the benign course of the syndrome and the spontaneous remission of seizures, patients with low seizure frequency do not necessarily have to be treated (Callenbah *et al*., 2002). So it is very important that mutations in *PRRT2* have been identified in the majority of families with BFIE, resulting in 602 patients with PRRT2-associated BFIE reported to date (Ebrahimi-Fakhari *et al*., 2015).

1.2.3. PRRT2 and the Infantile Convulsion and Choreoathetosis

ICCA (OMIM: 602066) is a syndrome in which BFIE and PKD co-occur in the same patient or family as a single autosomal dominant trait (Heron *et al*., 2012, Lee *et al*., 2012). In 1997, Szepetowski and colleagues identified four French families in which BFIE was inherited as an autosomal dominant trait together with variably expressed paroxysmal choreoathetosis (Szepetowski *et al*., 1997). The strong association of both neurological symptoms in the same families defined ICCA as a new syndrome, which can be distinguished as a separate entity, although its convulsive component is similar to the one initially described by Vigevano *et al*. (1992).

In these families the locus of ICCA overlapped with the first locus of PKD on chromosome 16. Moreover, additional families with ICCA and linkage to the same region were characterized (Swoboda *et al*., 2000). To date, more than 200 PKD/IC patients with *PRRT2* mutations have been reported (Cloarec *et al*., 2012).

In conclusion, BFIE, PKD and ICCA form a continuous disease spectrum and the core of PRRT2-associated diseases. The natural evolution from infantile seizures to a paroxysmal movement disorder in adolescents is peculiar. However, both ends of the spectrum share many key features, namely their paroxysmal and stereotypical character, benign nature, excellent response to anticonvulsants and favourable prognosis (Ebrahimi-Fakhari *et al*., 2015).

1.2.4. PRRT2 and the Intellectual Disability

Despite is known a large number of mutations of *PRRT2* gene, a fine correlation between genotype and phenotype is missing until now (Lee *et al*., 2012).

Heterozygous *PRRT2* mutations are mainly reported as *loss-of-function* mutations (Dale *et al*., 2012) in BFIE, ICCA, or PKD, which share a self-limited disorder and good prognosis (Labate *et al*., 2012). In 2011, an Iranian family with five individuals with severe non-syndromic ID was described, carrying a homozygous mutation in the *PRRT2* gene (*c.649dupC*) (Najmabadi *et al*., 2011).

Labate and colleagues in 2012 described few patients carrying homozygous mutations (Labate *et al*., 2012) and then other fifteen patients with homozygous or compound-heterozygous mutations have been reported (Najmabadi *et al*., 2011; Liu *et al*., 2013; Chen *et al*., 2014; Delcourt *et al*., 2015). The patients showed a more severe encephalopathic phenotype, including cognitive and neurological development deficit in addition to the common paroxysmal movement disorder (Labate *et al*., 2012). A great variability within *PRRT2*-linked phenotypes was shown even within the same family. In this context, the members of the family with mutation, showed febrile convulsion, epileptic seizures, PKD or headache (Brueckner *et al*., 2014). These pleiotropic effects probably suggest the

presence of additional genetic or acquired factors, which modulate the clinical expression of *PRRT2* mutations.

Because the *c.649dupC* mutation introduces a premature stop codon that causes truncated polypeptide lacking a transmembrane domain, it is probable that homozygous mutations demolish any binding ability with interactive proteins or ligands such as Synaptosomal-Associated Protein 25 kDa (SNAP-25), and could well explain the very severe phenotype, in particular the mental retardation (Labate *et al*., 2012).

In conclusion, the association of *PRRT2*-linked pathologies with the more severe phenotype of homozygous mutations indicate that the disorders are attributable to *loss-of-function* of the protein and the existence of a gene-dosage effects (Ebrahimi-Fakhari *et al*., 2015; Michetti *et al*., 2017). This further highlights the importance of PRRT2 for synaptic functions and might suggest an additional role during neuronal development.

Mutations	Diagnosis	Additional clinical feature	Reference
c.510dupT & c.647C>G	PKD	Non-convulsive seizures	Liu *et al.*, 2013
c.510dupT & c.647C>G	PKD	PNKD; non-convulsive seizure	Liu *et al.*, 2013
c.439G>C & c.640G>C	PKD	n.a.	Chen *et al.*, 2011
c.649dupC & deletion of PRRT2 on second allele	BFIE	PNKD; episodic ataxia; learning difficulties/mild ID; ADHD; cerebellar atrophy	Delcourt *et al.*, 2015
Homozygous *c.649dupC*	Non-syndromic ID	Five patients of the same kindred, no additional feature reported	Najmabadi *et al.*, 2011
Homozygous *c.649dupC*	PKD/IC	DD/ID; absence seizures; episodic ataxia	Labate et al., 2012
Homozygous *c.649dupC*	PKD/IC	DD/ID; possible absence seizures and other types of seizures; repetitive behaviours	Labate *et al.*, 2012
Homozygous *c.649dupC*	BFIE	PNKD; mild learning disability; ADHD	Delcourt *et al.*, 2015
Homozygous *c.649dupC*	BFIE	PNKD; episodic ataxia; mild ID; behavioural problems and motor tics	Delcourt *et al.*, 2015
Homozygous *c.649dupC*	BFIE	PNKD; episodic ataxia; mild learning disabilities	Delcourt *et al.*, 2015
Homozygous *c.913G>A*	BFIE	Episodic ataxia	Delcourt *et al.*, 2015

Table 2. Reported compound-heterozygous and homozygous *PRRT2* mutations (number *PRRT2* mutations= 15). ADHD (attention-deficit hyperactivity disorder); **DD** (developmental delay); **ID** (intellectual disability) (Ebrahimi-Fakhari *et al*., 2015, *modified*).

1.3. The full-length PRRT2 protein and its role until now

The predicted structure of the PRRT2 protein contains a proline-rich domain within N-terminal region and two putative transmembrane domains divided by few AAs that anchor the protein to the plasma membrane (Chen *et al*., 2011; Méneret *et al*., 2012; Heron and Dibbens, 2013). Owing to this general structure, PRRT2 was assigned to the recently characterized family of dispanins (DSPs) (Sällman *et al*., 2012), which share the two-transmembrane domains topology. DSPs putative topology is characterized by two transmembrane helices in the C-terminal region of 20-30 AAs, separated by an intracellular loop of variable length, an often long N-terminal region (>10 AAs), both of which are oriented towards the extracellular space (Sällman *et al*., 2012). According to this topology, it was suggested that the long PRRT2 N-terminal domain could be oriented outside of the cells, interacting with proteins of the extracellular matrix and/or to the extracellular domains of synaptic proteins, hence working as a synaptic adhesion molecule (Rossi *et al*., 2016). The crucial role of several trans-synaptic interacting proteins in synapse formation, and they role in pathologies that cause synaptopathies when mutated, has been envisaged in epilepsy and/or autism (Südhof, 2008; Cowell, 2014). The predicted primary structure of human PRRT2 identified two transmembrane helices in the C-terminal region of the protein (TM1: AAs 269-289, exon 1; TM2: AAs 318-338, exon 2): a long and putatively N-terminal region (AAs 1-268), including a proline-rich domain (AAs 131-216) and an intracellular *loop* (AAs 290-317) connecting the two transmembrane helices and a very short C-terminal end (Rossi *et al*., 2016). The mouse PRRT2 ortholog is virtually identical to the human protein in the C-terminus, with few differences in the N-terminal region (Chen *et al*., 2011) (**Fig. 3 A**).

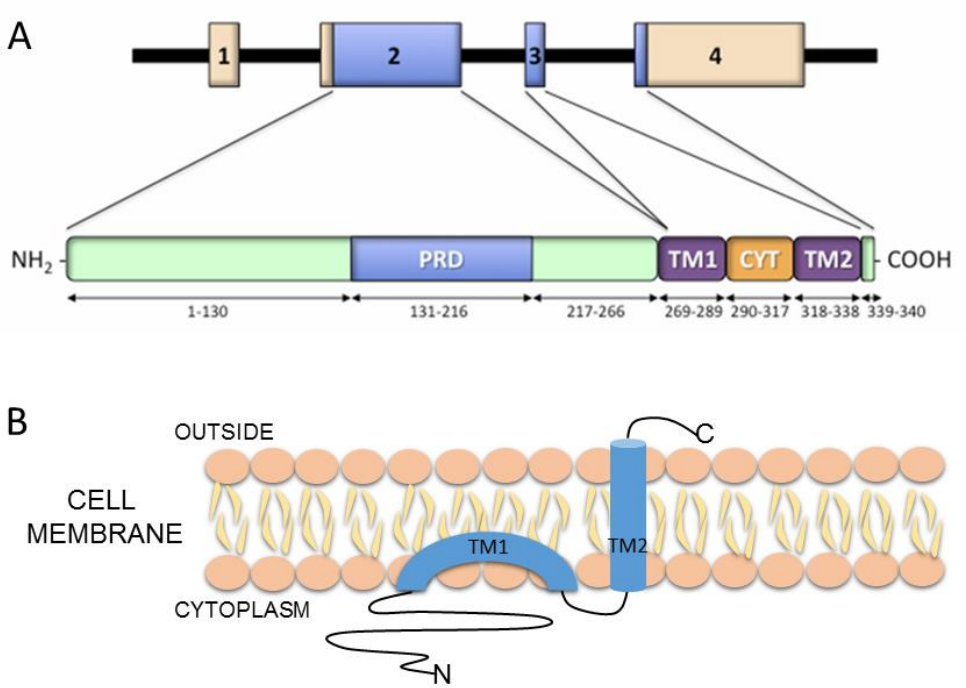

Figure 3. The gene, the protein structure and the putative membrane topology of PRRT2. **A.** the *PRRT2* gene contains four exons (1-4) encoding a protein of 340 AAs. Protein domains are highlighted: TM1 (269-289) and TM2 (318-338) domains, the long N-terminal domain (1-268) containing a proline-rich region (PRD), an intracellular loop (CYT, 290-317) and a COOH-terminal dipeptide (339-340). **B.** membrane topology hypothesized for PRRT2, member of the Dispanin family (DSP) (Chen *et al*. 2011; Sallman-Almen *et al*., 2012, *modified*).

However, different structural features were obtained when the orientation of PRRT2 in the plasma membrane was investigated experimentally. A recent study conducted in our laboratory, revealed, in fact, that the large N-terminal domain was located in the cytosol, and the very short C-terminus in the extracellular side of the plasma membrane (N_{cyt}/C_{exo} orientation) (Rossi *et al*., 2016) (**Fig. 3 B**). This topology resembles that of type 2 transmembrane proteins with a very short C-terminal anchor and suggests that the second C-terminal hydrophobic stretch spans the plasma membrane, the first one is associated with the inner surface of the membrane without crossing it (Rossi *et al*., 2016). This important evidence introduces the hypothesis of a new set of putative protein interactors for PRRT2, with different functions, respect to the previous hypothesized structure. In our laboratory we have recently demonstrated that PRRT2 interacts with a few SH3 domains proteins, specific synaptic and regulatory proteins involved in exo/endocytosis of SVs or in signal transduction (Rossi *et al*., 2016). A previous work described that PRRT2 binds Intersectin 1

(involved in clathrin-mediated endocytosis at nerve terminals, Saheki and De Camilli, 2012), proving the intracellular localization of the N-terminus and its function related to SVs homeostasis. This interaction suggests a direct important role of PRRT2 in the regulation of vesicle trafficking and endocytosis (Rossi *et al*., 2016).

Many studies showed that PRRT2 presents a neuron-specific expression, detecting the highest levels of mRNA of the protein in the cerebellum, basal ganglia and neocortex in humans and rodents (**Fig. 4 A**) (Chen *et al*., 2011; Heron *et al*., 2012; Lee *et al*., 2012, Valente *et al*., 2016a; Michetti *et al*., 2017). Notably, all these regions are putatively involved in the pathogenesis of the *PRRT2*-linked diseases.

PRRT2 mRNA levels are regulated during development in mouse brain: they increase during neural development from postnatal (P) day P0 to P14 and then they are regulated negatively in adulthood (Chen *et al*., 2011). This evidence reflects probably the observation that in many cases PRRT2-dependent diseases in infancy are relatively benign and generally are attenuated in the adulthood (Chen *et al*., 2011). Longitudinal analysis of the murine nervous system revealed low levels of both PRRT2 mRNA and protein during early development, with marked increases postnatally (Chen *et al*., 2011; Ebrahimi-Fakhari *et al*., 2015; Valente *et al*., 2016a). A previous study from our laboratory has shown that, in primary cultures of cortical neurons and hippocampal neurons, PRRT2 was already expressed at early postnatal stages, and its expression increased reaching a plateau at one month of life (10-21 days in vitro, DIV), a period of intense synapse formation and rearrangement *in vitro* (Valente *et al*., 2016a) (**Fig. 4 B**).

Of note, PRRT2 expression was almost undetectable in primary astroglial cultures, showing its neuron-specific expression (Valente *et al*., 2016a).

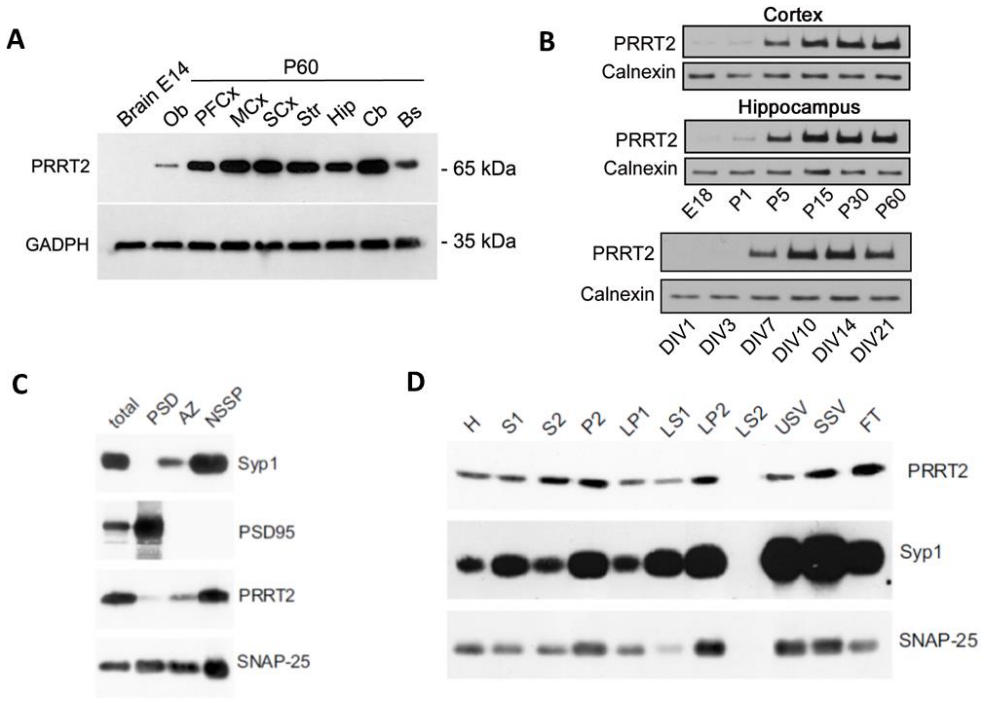

Figure 4. The PRRT2 neuronal expression and its enrichment at presynaptic level. A. Regional expression of PRRT2 in the mouse brain. Western blot analysis of PRRT2 protein levels in mouse brain regions at embryonic (E14) and postnatal (P60) stages of development. **Brain**, Total brain; **Ob**, Olfactory bulb; **PFCx**, Prefrontal cortex; **MCx**, Motor cortex; **SCx**, Somatosensory cortex; **Str**, Striatum, **Hip**, Hippocampus; **Cb**, Cerebellum, **Bs**, Brain stem. GAPDH was used as loading control. **B.** Temporal expression profile of PRRT2 in the developing mouse brain and in primary hippocampal neurons. **C.** Ultrafractionation of brain synaptosomes. Purified synaptosomes from adult mouse brain were subjected to ultrasynaptic fractionation to separate the active zone (**AZ**), postsynaptic density (**PSD**), and non-synaptic synaptosomal density (**NSSP**) made by extrinsic and integral membrane proteins of the nerve terminal. Aliquots of total synaptosomes and of each ultrasynaptic fraction were probed with antibodies against PRRT2, SNAP-25, and protein markers to validate ultrasynaptic compartments such as Synaptophysin-1 (Syp1) and Post-synaptic Density 95 (PSD95, 95 kDa), a post-synaptic marker for glutamatergic synapses. The partition of PSD95, Syp1, and SNAP-25 in the corresponding fractions is shown. Note that PRRT2 preferentially partitioned in the NSSP fraction, similarly to Syp1 and SNAP-25. **D.** Subcellular distribution of endogenous PRRT2 in neurons. Forebrain fractions obtained at various stages of SV purification were analysed by western blotting using antibodies to PRRT2, SNAP-25, and Syp1. **H**, homogenate; **S1**, post-nuclear supernatant; **S2**, supernatant of P2; **P2**, crude synaptosomes; **LP1**, crude synaptic plasma membranes; **LS1**, supernatant of LP1; **LP2**, crude synaptic vesicles; **LS2**, synaptosol; **USV**, highly purified synaptic vesicles; **SSV**, salt-treated highly purified synaptic vesicles; **FT**, flowthrough fraction containing small presynaptic membranes (Valente *et al*., 2016a, *modified*).

In neurons, like other proteins codified by genes involved in epilepsy (Syntaxin-Binding Protein 1, Dynamin 1 and Leucine-Rich Glioma Inactivated 1 genes), PRRT2 shows a distal distribution at synapses. At this level, PRRT2 is co-distributes with other proteins associated with the presynaptic site (Lee *et al*., 2012; Liu *et al*., 2016; Valente *et al*., 2016a).

By use of yeast two-hybrid it has been shown a potential interaction between PRRT2 and SNAP-25 (Stelzl *et al*., 2005). SNAP-25 is one of the most important soluble N-ethylmaleimide sensitive factor of the SNARE (Soluble NSF Attachment Protein Receptor) family, participating in the Ca^{2+} evoked fusion of SVs (Südhof and Rizo, 2011, Lee *et al.*, 2012). This interaction was confirmed in a recent work conducted in our laboratory (Valente *et al*., 2016a). We showed that PRRT2 was co-distributed with SNAP-25 and with other proteins of the presynaptic site when the brain was subjected to subcellular fractionation of the mouse brain (Valente *et al*., 2016a) (**Fig. 4 C**). Interestingly, we also found detectable levels of PRRT2 in association with SVs (**Fig. 4 D**), confirming previous proteomic results obtained with synaptic fractions enriched in docked SVs (Boyken *et al.,* 2013). These results corroborate the data that PRRT2 is located at the presynaptic site suggesting that during the SVs exo-endocytic cycle, PRRT2 cycles between the presynaptic cytoplasm and the SV membranes, as shown for SNAP-25 (Walch-Solimena *et al*., 1995). Although its interaction with SNAP-25 may suggest a link with the machinery of neurotransmitter release (Lee *et al*., 2012; Li *et al*., 2015; Valente *et al*., 2016a), the function of PRRT2 is still poorly understood. A high-resolution proteomics study revealed the presence of PRRT2 among new auxiliary proteins participating in the formation of the AMPA glutamate receptor complex, with a preferential association of PRRT2 with the Glutamate AMPA receptor subunit 1, GLUA1 (Schwenk *et al*., 2014). Moreover, low levels of PRRT2 are also detected in fractions of proteins of post-synaptic densities (Liu *et al*., 2016; Valente *et al*., 2016a). This evidence suggests also a postsynaptic localization of PRRT2 and a potential role of this protein in the homeostatic control of postsynaptic machinery.

Because the cytosolic N-domain of PRRT2 accounts for 80% of the primary structure of the protein (Chen *et al*., 2011, Rossi *et al*., 2016), it opens to the possibility of novel interactions of this protein with others cytosolic elements involved in presynaptic functions. This possibility was explored and corroborated by Valente *et al*. (2016a), demonstrating an important

physiological role for PRRT2 in the regulation of the Ca^{2+}-sensing and SVs fusion machinery. In that study it was demonstrated that PRRT2 interacts not only with SNAP-25, but also with Vesicle-Associated Membrane Protein 2 (VAMP-2), a member of the vesicle-associated membrane protein VAMP/synaptobrevin family and with two forms of synaptotagmin, Synaptotagmin 1 and Synaptotagmin 2 (Syt1/2) (see **Fig. 5**). Notably, all these proteins are intimately implicated in the Ca^{2+}-sensing mechanism involved in the final steps of fast synchronous neurotransmitter release (Lee *et al*., 2012; Boyken *et al*., 2013; Valente *et al*., 2016a).

It was shown that the reduced PRRT2 expression in hippocampal primary neurons led to an abnormal asynchronous/synchronous neurotransmitter release ratio suggesting that the fusion mechanism *per se* is not altered and that a specific defect in coupling Ca^{2+} influx to exocytosis may be involved (Valente *et al*., 2016a). Interestingly, a previous study reported similar results in a mouse strain carrying a Syt2 mutation and manifesting with EA (Pang *et al*., 2006a), one of the clinical phenotypes of PRRT2 in humans.

Finally, in the study of Valente et al. (2016) it was found that *PRRT2* acute silencing caused a diminution of synaptic contacts, and minor changes in synaptic ultrastructure consisting of a small reduction in the SV volume and an increase in the fraction of SVs docked at the release sites (Valente *et al*., 2016a). A similar study, using RNA interference, showed that knocking down *PRRT2* expression in mouse embryos led to a delay in neuronal migration and defects in synaptic development (Liu *et al*., 2016).

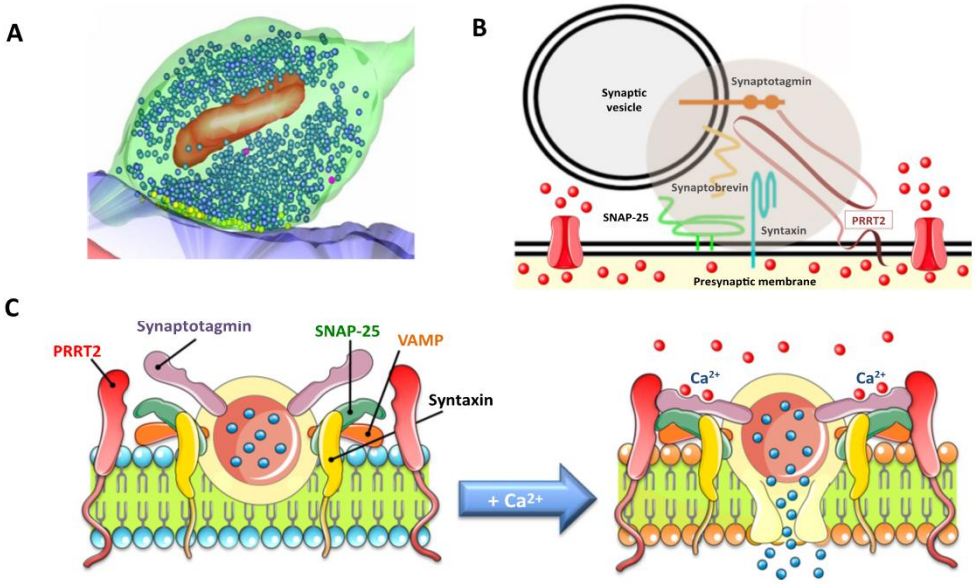

Figure 5. The PRRT2 protein is a key factor of SNARE complex. A. 3D reconstruction of the ultrastructure of a presynaptic terminal from serial sections. **B.** Cartoon of the presynaptic portion of the nerve terminal located at the active zone. PRRT2, associated with the presynaptic plasma membrane, interacts with the other proteins of the SNARE complex (SNAP-25 and VAMP/synaptobrevin) and with the fast Ca^{2+} sensor synaptotagmin. Presynaptic Ca^{2+} channels and Ca^{2+} ions are also represented. **C.** Mechanistic model for the role of PRRT2 in Ca^{2+}-dependent fast SV release. At rest (*left*), PRRT2 is in the proximity of both the Ca^{2+} sensor synaptotagmin and the SNARE complex; upon stimulation (*right*), after increase of concentration of Ca^{2+} ions, PRRT2 interacts with both SNARE proteins and synaptotagmin. As a consequence PRRT2 endows the SNARE complex with Ca^{2+}-sensitivity and increases the probability of synchronous neurotransmitter release (from Valtorta *et al*., 2016).

In order to deeply investigate the role of PRRT2 at synapses, it has been recently characterized in our laboratory a genetically altered mouse in which the *PRRT2* gene has been constitutively inactivated (*PRRT2*-KO). In agreement with the previous report, the expression of PRRT2 protein in various brain area was confirmed (Michetti *et al*., 2017).

The *PRRT2*-KO mice were normal at birth and their viability was not impaired by PRRT2 inactivation. The general health status of *PRRT2*-KO pups were comparable to that of heterozygous and wild-type animals (Michetti *et al*., 2017).

The *PRRT2*-KO mice showed a higher frequency of abnormal events than heterozygous and wild-type mice starting from P8, a crucial window for movement development. In particular, *PRRT2*-KO mice presented loss of equilibrium at P8, with completely balance impairments at P16.

Furthermore, *PRRT2*-KO mice showed bouncing and back walking movements, demonstrating paroxysmal behaviours (Michetti *et al*., 2017). These motor alterations were accompanied by paroxysmal dyskinesias (increase of frequency of racing and jumping) in response to audiogenic stimulations. Pharmacologically, the *PRRT2*-KO mice exhibited an increase of susceptibility to the effects of convulsant drug propentylentetrazole (Michetti *et al*., 2017).

This phenotype persisted in the adult *PRRT2*-KO mice and is similar to the phenotype of patients with EA type 1 described by Graves *et al*. (2014), suffering of brief attacks of unsteadiness and dizziness with persistent myokymia (Graves *et al*., 2014).

Electrophysiological data from granule cells of the dentate gyrus of the hippocampus showed that synaptic transmission was not markedly altered, except for an increase in miniature excitatory postsynaptic currents (mEPSCs), a result consistent with the increased density of VGLUT1-positive synapses described from Michetti *et al*. (2017). In the cerebellum, functional analysis showed a long-lasting facilitation at the synapses of parallel fiber-Purkinjie cells synapses while no evident depression was observed, even at the highest stimulation frequency (Michetti *et al*., 2017). An altered plasticity, together with a sharp decrease of evoked synchronous transmission, probably due to a loss of Ca^{2+} sensitivity of the release machinery, suggested that the absence of PRRT2 induces functional abnormalities due to a global network instability and/or excitation/inhibition imbalance (Michetti *et al*., 2017).

Furthermore, homozygous *PRRT2*-KO mouse recapitulated many of the phenotypic features of the human PRRT2-linked disorders, showing abnormal motor behaviors and a motor/epileptic phenotype in response to environmental stimuli. By contrast, the heterozygous mice did not show any evidence of pathogenic phenotype (Michetti *et al*., 2017).

In a recent work it was demonstrated a direct evidence between PRRT2-associated dyskinesia and specific cerebellar presynaptic deficits (Tan *et al*., 2017). In that study mutant mice with global or cerebellum-specific truncation exhibited severe episodes of aberrant motor behaviours similar to the clinical features of PKD in patients, including dyskinesia and dystonic postures. These manifestations have been confirmed by electron microscopic and electrophysiological analyses of the cerebellar to Purkinje cell inputs. Mutant mice in which *PRRT2* was deleted in

granule cells of the cerebellum exhibited a facilitated transmission at parallel fiber-Purkinjie cells synapses, showing an enhanced firing of Purkinjie cells and a typical paroxysmal behavior (Tan *et al*., 2017).

1.4. Neurological Paroxysmal Disorders and ion channels

Ion channels are the most fundamental elements in excitability of the membrane of cells and are expressed broadly throughout the body (Hille, 2001). Mutations of ion channels in central nervous system (CNS) underlie a broad spectrum of episodic neurological disorders. In this context, PDs and other episodic movement disorders are often proposed to be channelopathies (Bhatia *et al*., 2000; Margari *et al*., 2005; Ryan and Ptácek *et al*., 2010). Here we schematically analyse channelopathies related to different voltage-gated ion channels dysfunctions that are involved in a variety of paroxysmal-like seizures. The major inherited diseases of different voltage-gated ion channels are reported in **Table 3.**

The Voltage-gated K^+ Channels (K_V) belongs to the large family of proteins composed by six transmembrane α helices (S1-S6), with S4 subunit serving as the voltage sensor and a pore-forming loop between S5 and S6 subunits. Moreover, four of such subunits constitute a functional channel (Gutman *et al*., 2005). K_V channels are largely activated during the repolarizing phase of the membrane after the depolarization phase mediate by Na^+ and Ca^{2+} influx (Liu and Bean, 2014).

K_V channels $K_v7.2$ and $K_v7.3$, encoding by K^+ Voltage-gated Channel Subfamily Q Member 2 (*KCNQ2*) and K^+ Voltage-gated Channel Subfamily Q Member 3 (*KCNQ3*) genes, have an important role in limiting network excitability in the neonatal brain (Rogawski *et al*., 2000). *KCNQ2* and *KCNQ3* mutations were found in families with different neurological disorders, such as self-limited epilepsy and/or BFIE (Maljevic and Lerche, 2014).

In 2009, an autosomal recessive disorder characterized by the tetrad of Epilepsy, Ataxia, Sensorineural deafness, and Tubulopathy (a renal salt-wasting), defined EAST syndrome, was firstly described by two independent groups (Bockenhauer *et al*., 2009; Scholl *et al*., 2009). This syndrome is caused by *loss-of-function* mutations in an inwardly-rectifying

K^+ channel subtypes 4.1, which has a pivotal role in glial function, neuronal excitability, and systemic K^+ homeostasis (Scholl *et al*., 2009).

Different cases of episodic EA type 1 showed mutations in *KCNA1* gene, encoding for $K_V1.1$ channels that are expressed in interneurons of the cerebellum (Ryan *et al*., 2010). EA type 1 is inherited in an autosomal dominant manner and $K_V1.1$ mutations lead to a drastic decrease in currents, often at least partly due to improper trafficking (Ryan *et al*., 2010; D'Adamo, 2015).

Moreover, several mutations were found in the K^+ Ca^{2+}-Activated Channel Subfamily M α1 (*KCNMA1*) gene that encodes for α1 subunit of Ca^{2+}-activated K^+ channels belonging to the family of ion channels with a big conductance for K^+ ions, named Big K^+ channels (Du *et al*., 2005). These channels are involved in neuronal excitability, synaptic transmission and in regulation of myogenic tone (Zhang *et al*., 2015). It was reported a mutation in *KCNMA1* gene that cause an autosomal dominant form of early onset of PNKD (Du *et al*., 2005). Patients present a non-kinesigenic phenotype with alcohol as possible trigger and epileptic attacks (Du *et al*., 2005). Moreover, two PNKD patients with mutations in *KCNMA1* gene without epilepsy attacks are described (Zhang *et al*., 2015).

Voltage-gated Ca^{2+} channels (Ca_V) are composed by four or five distinct subunits and the α1 represents the largest subunit, incorporating the conduction pore and other domains (Catterall *et al*., 2005a). This subunit is organized in four homologous domains (I-IV) with six transmembrane segments (S1-S6) in each (Catterall *et al*., 2005a).

Ca_V mediate Ca^{2+} influx in response to membrane depolarization and regulate intracellular processes such as contraction, secretion, neurotransmission, and also gene expression in many different cell types (Catterall *et al*., 2005a). The Ca^{2+} Voltage-gated Channel Subunit A α1 (*CACNA1A*) gene encodes for the pore-forming α1 subunit of the P/Q type Ca_V channels, $Ca_V2.1$. These channels are highly expressed in cerebellar Purkinje cells, in which they mediate neurotransmitter release (Todorov *et al*., 2012). Mutations in $Ca_V2.1$ lead to familial HM type 1, EA type 2, and spinocerebellar ataxia type 6. Familial HM type 1 mutations cause *gain-of-function* effects on these channels, increasing channel activity, synaptic transmission, and susceptibility to cortical spreading depression (Tottene *et al*., 2009; Pietrobon, 2010). EA type 2 mutations induce a *loss-of-channel* function, with a decrease in Ca^{2+} currents through $Ca_V2.1$, often due to

protein instability (Rajakulendran *et al*., 2010; Nachbauer *et al.*, 2014). Spinocerebellar ataxia type 6 mutations cause a toxic *gain-of-function* effect in which mutant $Ca_V2.1$ channels are incompletely degraded forming insoluble aggregates and inclusion bodies within Purkinje cells (Unno *et al*., 2012).

Voltage-gated Na^+ channels (Na_V) are fundamental in the initiation and generation of action potentials (APs) in neurons and other excitable cells, propagating APs along nerves (axons), muscle fibers and the neuronal somato-dendritic compartment (Hille, 2001). Na_V are heteromeric transmembrane proteins that are open in response to an alterations in membrane potential to provide selective permeability for Na^+ ions (Anger *et al*., 2001). In mammalian brain are complexes of a 260 kDa α-subunit with one or two β-subunits (β1-β4) of 33 to 36-kDa in size (Catterall, 2000; Catterall *et al*., 2005b). The α-subunit consists of four internally repeated domains (I-IV), each of which contains six α-helical transmembrane segments (S1-S6). In each domain, the S1 through S4 segments serve as the voltage-sensing module, and one non-helical relatively short reentrant segment, the P-segment, located between S5 and S6, serve as the ion selectivity filter and ion pathway (Catterall *et al*., 2005b; Waszkielewicz *et al*., 2013). Several classical features of Na_V described from Hodgkin and Huxley defined their functions: a) voltage-dependent activation, b) rapid inactivation and c) selective ion conductances (Hodgkin and Huxley, 1952). On the other hand, some channels undergo slow-inactivation, which takes considerably longer time (seconds to minutes) (Kyle and Ilyin 2007).

There are ten mammalian α subunit genes encoding the proteins $Na_V1.1$-$Na_V1.9$ (Namadurai *et al*., 2015). Separate α subunit isoforms are expressed in tissue-specific patterns and exhibit differences in gating behaviour that tailor them for distinct physiological roles (Waxman, 2012). Among others, the subtypes $Na_V1.1$, $Na_V1.2$ and $Na_V1.6$ are abundantly expressed in the CNS and are very important for the integration of information at this level (Gordon *et al*., 1987; Beckh *et al*., 1989; Vacher *et al*., 2008). In this context, excitatory and inhibitory synaptic inputs are integrated in a specific region of the neuron, defined axon initial segment (AIS) (Catterall, 1981). The AIS is a proximal part of the axon where Na^+ channels are grouped and generated the depolarizing phase during an AP. The AIS is a specialized structure of about 20-60 μm in neurons that is localized between axonal and somatodendritic domains. At this level it

operates for the action potential firing and helps to maintain neuron polarity (Jones and Svitkina, 2016).

In excitatory cells, the distal part of the AIS in enriched in $Na_V1.6$ and the proximal part in $Na_V1.2$ (Rasband *et al*., 2010). Functionally, these different subdomains of AIS determine the progressive reduction in the half-activation voltage in the AIS, with increasing distance from the soma (Hu *et al*., 2009). Further molecular model studies supported by simultaneous somatic and axonal recordings showed that distal $Na_V1.6$ promotes AP initiation, whereas proximal $Na_V1.2$ promotes its backpropagation to the soma (Hu *et al*., 2009).

On the other hand, recent studies revealed that $Na_V1.1$ is important for the excitability of GABAergic neurons clustering in the AIS of some types of interneurons (Yu *et al*., 2006; Ogiwara *et al*., 2007). Moreover, several reports showed that $Na_V1.1$ expressed at somato-dendritic level of neurons controls excitability through integration of synaptic impulses regulating the threshold for AP generation and propagation to the dendritic and axonal compartments (Yu *et al*., 2006; Vacher *et al*., 2008).

The abnormal expression and/or function of Na_V channels has been investigated in different pathophysiological conditions of the CNS (Waszkielewicz *et al*., 2013).

In this context, several studies have shown altered levels of mRNA and protein for $Na_V1.1$, $Na_V1.2$, $Na_V1.3$ and $Na_V1.6$ α-subunits and for β-subunits in animal model of epilepsy (Bartolomei *et al*., 1997; Aronica *et al*., 2001; Klein *et al*., 2004; Blumenfeld *et al*. 2009) and in human epileptic brain tissue (Lombardo *et al*., 1996; Whitaker *et al*., 2001). The epileptiform activity can also be associated with changes in Na^+ channel functions. An increase in a small persistent Na^+ current due to an incomplete fast inactivation of this conductance predisposes neurons to hyperexcitability (Crill, 1996; Kearney *et al*., 2001).

Thus, in general, diverse mutations in Na^+ channels expressed in the CNS cause different forms of paroxysmal-related disorders (Erro *et al*., 2017). A heterozygous missense mutation in the neuronal Na_V channel gene *SCN1A* (coding for $Na_V1.1$ α-subunit) was identified in families with familial HM with aura (Dichgans *et al*., 2005), one of the several autosomal dominant paroxysmal disorders (Marini *et al*., 2012). Probably, familial HM mutations may cause a *gain-of-function* of the $Na_V1.1$ channels (Scalmani *et al*., 2006). Some mutations in $Na_V1.1$ cause Generalized Epilepsy with Febrile

Seizure Plus type 2 and Severe Myoclonic Epilepsy of Infancy (or Dravet syndrome) (Catterall *et al*., 2010; Meisler *et al.*, 2010), revealing a *loss-of-function* mechanism. Moreover, several mutations in *SCN2A* gene (coding for $Na_V1.2$ α-subunit) are identified in BFIE (Heron *et al*., 2002; Scalmani *et al*., 2006), inducing a *gain-of-function* that leads to paroxysmal manifestations.

Five major phenotypes of *SCN2A*-benign neonatal infantile, intermediate neonatal infantile, severe neonatal infantile, childhood epilepsy, and isolated autism and intellectual disability phenotypes are described (Howell *et al*., 2015). Furthermore, it has been recently reported choreoathetosis in a child with normal development, *de novo SCN2A* mutation, and a history of neonatal and infantile seizures (George *et al*., 2017).

PKD, BFIE, and ICCA have been reported in patients with *SCN8A* mutations (Gardiner *et al*., 2015; Wang *et al*., 2017), coding for $Na_V1.6$ α-subunit. *SCN8A* mutations have been identified in three families with a total of sixteen affected members, identifying the same cosegregating heterozygous missense mutation (Gardella *et al*., 2016). The paroxysmal nature of the clinical symptoms, such as dystonic/dyskinetic or "shivering" attacks, triggered by stretching, motor initiation, or emotional stimuli have suggested that attacks might in fact be epileptic in nature (Gardella *et al*., 2016). Interestingly, other studies on the phenotypic spectrum of *SCN8A*-related epileptic encephalopathies reported the presence of choreo-dystonia and dystonic dyskinesias in some cases (Larsen *et al*., 2015), supporting the idea that episodic movement disorders can occur with *SCN8A* mutations. Furthermore, functional analyses have suggested that *SCN8A* mutations can lead to either *gain-of-function* (by an increased persistent Na^+ current) or *loss-of-function* effects (by an unstable protein) (Meisler *et al*., 2016).

Different genetic studies have identified the Na_V channels $Na_V1.7$ (encoded by *SCN9A* gene) as a key player in several conditions in which recurrent pain or the inability to sense pain is the prominent symptom (Yang *et al*., 2004; Cox *et al*., 2006). Recently, a novel *p.L1612P* $Na_V1.7$ mutation has been identified as a cause of paroxysmal extreme pain disorder with a unique combination of clinical symptoms and electrophysiological properties (Suter *et al*., 2015). There are several Na^+ channel blockers used in epilepsy therapy and related pathology, such as phenytoin or

carbamazepine that selectively block ion conductance and/or stabilize the inactivated state of these channels (Ragsdale *et al*., 1994, 1996).

Disease	Gene	Channel	Reference
Voltage-gated K^+ channels			
- Benign Familial Infantile Seizure - Self-limited epilepsy	*KCNQ2* *KCNQ3*	$K_V7.2/K_V7.3$	Maljevic and Lerche, 2014
EAST Syndrome	*KCNJ10*	Kir4.1	Scholl *et al.*, 2009
Episodic Ataxia Type 1	*KNCA1*	$K_V1.1$	Ryan *et al.*, 2010 D'Adamo *et al.*, 2015
Early Paroxysmal non-kinesigenic Dyskinesia	*KCNMA1*	K^+ Ca^{2+}-activated channel subfamily M α 1	Du *et al.*, 2005 Zhang *et al.*, 2015
Voltage-gated Ca^{2+} channels			
Hemiplegic Migraine with Aura Type 2	*CACNA1A*	$Ca_V2.1$	Pietrobon, 2010; Tottene *et al.*, 2011
Episodic Ataxia Type 2			Rajakulendran *et al.*, 2010; Nachbauer *et al.*, 2014
Spinocerebellar Ataxia Type 6			Unno *et al.*, 2012
Voltage-gated Na^+ channels			
Hemiplegic Migraine with Aura	*SCN1A*	$Na_V1.1$	Dichgans *et al.*, 2005; Scalmani *et al.*, 2006
- Generalized Epilepsy with Febrile Seizure Plus Type 2 - Dravet Syndrome			Catterall *et al.*, 2000; Meisler *et al.*, 2010
Benign Familial Infantile Epilepsy	*SCN2A*	$Na_V1.2$	Heron *et al.*, 2002; Scalmani *et al.*, 2006
Infantile-Onset Epilepsy			Howell *et al.*, 2015
PKD, BFIE and ICCA	*SCN8A*	$Na_V1.6$	Whang *et al.*, 2013; Gardiner *et al.*, 2015; Gardella *et al.*, 2016
Epileptic Encephalopathies			Larsen *et al.*, 2015
Paroxysmal Extreme Pain Disorder	*SCN9A*	$Na_V1.7$	Cox *et al.*, 2006; Yang *et al.*, 2009; Suter *et al.*, 2015

Table 3. Some significant neurological inherited diseases of voltage-gated K^+, Ca^{2+} and Na^+ channels at CNS. Several PDs affecting neuronal function and ranging in severity (from mild or latent disease to life-threatening or incapacitating conditions) have been linked to mutations in different human Na_V genes (Gardiner *et al*., 2015, *modified*).

1.5. The Induced Pluripotent Stem Cells Technology

In recent years, researchers have begun to explore the Induced Pluripotent Stem Cell (iPSC) technology's full potential for creating disease models from patients with complex genetic defects, thus overcoming major ethical concerns that have plagued human embryonic stem cells (ESCs) ESCs (Yamanaka, 2010). Before the advent of iPSCs technology, several strategies are used to generate such disease models using human ESCs (Prajumwongs *et al*., 2016).

Human ESCs are pluripotent stem cells derived *in vitro* from the inner cell mass of developing embryos (Gokhale and Andrews, 2006). The first human ESCs line was obtained in 1998 from human blastocysts, showing the ability to differentiate into ectoderm, mesoderm and endoderm, the three germ layers (Thomson *et al*., 1998). Therefore, human ESC-derived cells have been widely used for different analysis such as gene targeting, cell therapy, tissue repair, and organ regeneration (Zhao *et al*., 2013).

However, the main disadvantages of the use of human ESCs were the immune rejection, the incorrect tissue regeneration, the tumor formation, and even the ethical considerations about the manipulation of human embryos (Isobe *et al*., 2014; Kim *et al*., 2014). In 2006, Yamanaka and his group opened a completely new venue in stem cell research by showing that the forced expression of only four transcription factors was sufficient to convert mouse fibroblast cells into ESC-like cells (Takahashi and Yamanaka, 2006). These cells, named iPSCs, were considered pluripotent stem cells not derived from embryos but from *in vitro* reprogramming methods in order to mimic ESCs (Takahashi and Yamanaka, 2006). Thus, iPSCs technology became an extremely useful tool for regenerative medicine (Wan *et al*., 2015) and/or *in vitro* modelling of disease (Colman *et al*., 2009). A detailed iPSCs scheme generation is reported in **Fig. 6**.

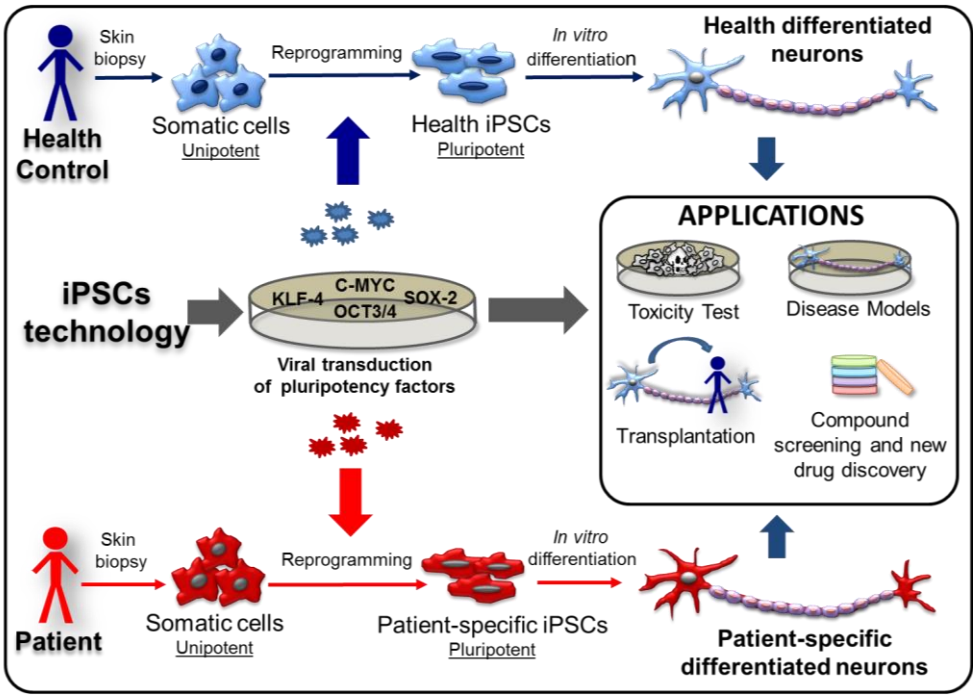

Figure 6. The iPSC technology. Adult somatic cells can be reprogrammed into stem cell by the iPSC approach. By the use of this technique, mammalian somatic cells were reprogrammed to iPSCs by ectopic expression of the pluripotent factors: OCT3/4, SOX2, KLF4, and C-MYC. IPSCs generated in this manner share the main properties of preimplantation embryo-derived ESCs, which include unlimited self-renewal and the potential to differentiate into cells of the three germ layers. IPSC-derived neurons can be obtained from skin biopsies from patients and relative healthy controls. IPSCs, owing to their ESC-like pluripotency, allow the production of a variety of derived cells such as neurons, for applications in regenerative medicine such as transplantation therapy, toxicity tests and also for modelling human diseases and new drug development (Wan *et al*., 2015, *modified*).

The growing interest in iPSCs technique and its clinical applications has led to the debate about the differences between iPSCs and ESCs, in particular if iPSCs are close to the gold standard ESC, and if they are "safe" for clinical use (Bilic and Belmonte, 2012).

The first issue was to understand if the transcriptional profile of good iPSCs quality was similar to ESCs (Bilic and Belmonte, 2012). In previous studies, iPSCs and ESCs were considered nearly identical to their embryo-derived counterparts (Takahashi and Yamanaka, 2006; Maherali *et al*., 2007; Takahashi, 2007; Lowry *et al*., 2008). Later on, it was demonstrated that a small group of genes were continuously differentially expressed in iPSC and ESC lines, using genome-wide analysis (Chin *et al*., 2009). These differences were found in early passage iPSC lines, and were conserved

across various studies and species, suggesting that the two cell types were transcriptionally different (Chin *et al*., 2010). Moreover, Stadtfeld *et al*. (2010) demonstrated that the expression state of a single imprinted gene cluster (*Dlk1-Dio3* gene) distinguished most murine iPSCs from ESCs and allows for the prospective identification of iPSC clones that have the full development potential of ESCs. In human iPSCs, the *Dlk1-Dio3* locus is not silenced, suggesting a different iPSC state/reprogramming. Thus, it became useful to find similar marker in human cells (Bilic and Belmonte, 2012).

The direct comparison of the differentiation potential of iPSCs and ESC presented several difficulties, considering the high variability in the analysis, due to different culture conditions and/or differentiation protocols (Bilic and Belmonte, 2012). A previous study demonstrated that the human iPSCs and ESCs displayed the same neural-differentiation potential, including those with or without integrating transgenes (Hu *et al*., 2010). This indicates that techniques other than simple removal of reprogramming transgenes are needed to improve the differentiation efficiency and potency for iPSCs (Hu *et al*., 2010).

The efficiency of differentiation was lower in iPSCs than ESCs, probably for epigenetic changes or genetical aberration that occur during the process, making iPSCs more refractory to external differentiation signals (Chin *et al*., 2009). Importantly, *in vitro* human ESCs presented various differentiation capacity, as some lines showed a marked propensity for differentiating into specific lineages, making comparison with iPSCs much more difficult (Hu *et al*., 2010; Osafune *et al*., 2008).

Moreover, DNA methylation is an important epigenetic modification of the mammalian genome that has widespread influences on gene expression (Liu *et al*, 2008). When analysed, the DNA methylation pattern was very similar between iPSC and ESC compared with nonpluripotent lines, such as fibroblasts (Guenther *et al*., 2010). A considerable amount of literature has been published on these differentiation properties, using small number of iPSC and ESC cell lines for comparison (Doi *et al*., 2009; Marchetto *et al*., 2009; Ghosh *et al*., 2010; Kim *et al*., 2011; Lister *et al*., 2011; Ohi *et al*., 2011). Several differentially methylated regions were found comparing three iPSC lines and three ESC lines by genome-scale analysis (Doi *et al*., 2009). However, the most interesting finding was that not all the differentially methylated regions belong to the cell-of-origin memory, indicating that iPSCs also accumulate novel aberrant epigenetic state (Doi

et al., 2009; Lister *et al*., 2011). Furthermore, it was found that reprogrammed cells re-organize their chromatin architecture to reflect the less repressive state of stem cells (Hawkins *et al*., 2010). Thus, it was suggested that inhibiting repressive chromatin structure may facilitate reprogramming either through inhibition of the repressive regions or overexpression of demethylases.

Until now, relatively little is known about the differences between ESCs and iPSCs about their non-coding regulatory transcripts, such as microRNA (miRNA) (Tang, 2005). MiRNA expression profiles are known to change depending from the development of tissue and from individual cells differentiation (Krützfeldt *et al*., 2006). Chin *et al.* (2009) showed that there was a difference in the expression profile for 105 miRNAs between ESCs, iPSCs and fibroblasts. Moreover, it was demonstrated that few miRNA were differentially expressed in both pluripotent cell lines (Chin *et al*., 2009; Wilson *et al*., 2009). These findings could be explained with the variation of miRNA profile during development, suggesting a late iPSCs signature (Chin *et al*., 2009).

One of the most important discovery relevant for the generation of iPSCs was the identification of the key pluripotency molecules, named of Yamanaka's factors (Takahashi and Yamanaka, 2006). Before their discovery, other works postulated the existence of factors that could change the cellular fate (Davis *et al*., 1987; Halder *et al*., 1995; Tada *et al*., 2001; Cowan *et al*., 2005).

The original method of reprogramming murine fibroblasts by Yamanaka utilized retroviral transduction of OCT3/4, SOX2, KLF4 and C-MYC (also defined OSKM factors) into mouse embryonic fibroblasts derived from mice. These murine fibroblasts expressed β-galactosidase-neomycin fusion protein at the *Fbx15* locus (Tokuzawa *et al*., 2003) which is specifically expressed in pluripotent stem cells and serves as an excellent marker for pluripotency (Takahashi and Yamanaka, 2006). Thus, drug selection with G418 after transduction of the OSKM factors resulted in reprogramming of 0.02% of the mouse embryonic fibroblasts 14-21 days post-transduction (Takahashi and Yamanaka, 2006).

One year later the generation of mouse iPSCs, in Yamanaka's lab was demonstrated that the same OKMS factors were sufficient also to generate human iPSCs (Takahashi *et al*., 2007). Interestingly, the use of only three of these factors, omitting C-MYC*,* was also reported to achieve successful

iPSC generation, although with reduced reprogramming efficiency (Wernig *et al*., 2007; Nakagawa *et al*., 2008). In the same years, another work showed the generation of human iPSCs by OCT3/4 and SOX2 factors, the same described from Yamanaka's lab, and two different factors, NANOG and LIN28 (Yu *et al*., 2007). At now, both sets of reprogramming compounds are now used. Interestingly, combinations of these two sets have a synergistic effect on the generation of human iPSC (Yu *et al*., 2009; Tanabe *et al*., 2013).

The use of iPSCs technique is now permeating into many sectors of disease research. This approach could be important for several studies of brain diseases where the most restrictive limitation is the tissues inaccessibility. Reprogramming adult somatic cells from patients into iPSCs and then neurons could be important to avoid this problem. In this context, patient sample-derived iPSCs can be used to construct patient-specific disease models to elucidate previously unknown pathogenic mechanisms of disease development and to test new therapeutic strategies (for review, see Zhao *et al*., 2014).

The procedure of neuronal induction is well described by Broccoli *et al*. (2014; 2015). HPSCs were differentiated into aggregate-like embryoid bodies (EBs) and then, the aggregates were growth in a culture medium in serum-free condition in order to promote selectively the survival and growth of neural cells (Broccoli *et al*., 2014). Neural rosettes were readily identified in the differentiated hPSC colonies as rosette-like structures, while in murine-derived cultures the formation of this rosette appeared slower than human-derived cells (Reubinoff *et al*., 2001; Zhang *et al*., 2001). These structures are formed by neural progenitors cells (NPCs), showing a highly polarized morphology. Neural rosettes have a structure that morphologically resembles the early embryonic neural tube (Zhang *et al*., 2001). These findings suggest that they are equivalent to the developing neural tube with respect to structure and function (Broccoli *et al*., 2014). Rosette neural progenitors intertwine to create overlapping cellular layers; however, they remain constrained to the surface where they anchor (Broccoli *et al*., 2014). Then, rosette neural progenitors can be expanded *in vitro* forming a renewable cell population as neurospheres in suspension or also attached to a substrate.

NPCs have the ability to generate most neural cell types, such as cortical neurons, dopaminergic neurons, GABA-ergic neurons, astrocytes and

oligodendrocytes (Begum *et al*., 2015; Du and Parent, 2015) (see **Table 4**). This is a long and multistep process. At the beginning, neurons show a very immature morphology and acquire functional properties only after several weeks in culture (Broccoli *et al*., 2014). To promote a specific neural line, different factors of differentiation and growth were added in culture medium (Bardy *et al*., 2015). It was observed that neurons present mature functional and synaptic properties after 8-12 weeks in culture (Ricciardi *et al*., 2012). Moreover, some different way to improve neural maturation *in vitro* are described, such as culture supplementation with neurotrophins and cAMP that decreases cell death mechanisms (Soldner *et al*., 2009) and the co-culture of neurons with primary rat feeder layer (or astrocytes) (Broccoli *et al*., 2014).

Finally, mature neurons derived from iPSC technology should be functionally evaluated by taking into account the electrophysiological properties of the newly generated neurons.

Cell type	Reference
Cortical-like excitatory neurons	Chambers *et al*., 2009: Shi *et al*., 2012
Dentate granule cell-like neurons	Yu *et al*., 2014
Cortical-like inhibitory interneurons	Liu *et al*., 2013; Maroof *et al*., 2013
Motor neurons	Hu and Zhang, 2009; Karumbayaram *et al*., 2009
Dopaminergic neurons	Swistowski *et al*., 2010; Kriks *et al*., 2011
Astrocytes	Krencik and Zhang, 2011; Juopperi *et al*., 2012
Oligodendrocytes	Hu *et al*., 2009
Brain microvascular endothelial cells	Lippmann *et al*., 2012

Table 4. Main neural and other brain-related cell types differentiated from iPSCs. The ability to neurally differentiate iPSCs allows one to study the development of patient-derived cells over time as they mature and manifest neurological disease phenotypes. These "*disease-in-a-dish*" models provide the unique opportunity to understand the progression of pathology and gain insight into the prevention of clinical disease onset. (Du and Parent, 2015, *modified*).

2. OBJECTIVES AND APPROACHES

The main purpose of this research project has been to perform a thorough investigation of the possible molecular basis of *PRRT2*-associated paroxysmal disorders. The aim of this work was the further characterization of the PRRT2 function in the modulation of electrophysiological properties of neuronal cells. To this end, we have used different experimental approaches.

First, we have studied the *PRRT2*-KO mouse model in which the *PRRT2* gene was constitutively inactivated *in vitro*. We have investigated the electrical phenotypes of primary hippocampal neurons, obtained from mouse *PRRT2*-silenced embryos in comparison to WT neurons. The functional properties of *PRRT2* silenced neurons at single-cell and network levels in terms of synaptic properties and excitability have been addressed.

Second, we generated and characterized iPS cell lines from patients carrying a mutated *PRRT2*, which as allowed to investigate mature human neuronal cells as PRRT2-disease model. We have studied IPSCs and differentiated into functional neurons that carry the common *PRRT2* mutation *c.649dupC*. The iPSCs were generated from fibroblasts of patients from a consanguineous Italian family carrying the *c.649dupC* mutation in heterozygosity or homozygosity. We used iPSCs generated from sex- and age-matched normal donors as controls. All clones generated and characterized are summarized in **Table 5**.

Finally, we used HEK-293 stably expressing various clones of voltage-gated sodium channels as model system to deeply investigate the modulation of PRRT2 on electrophysiological properties of neuronal cells. This study should clarify the functional interactions of PRRT2 with key actors of cellular excitability, and address the functional mechanism that impairs the normal functionality of the neurons.

Individual	Genotype	Phenotype	Age at Onset	Number of Clones ID)
Control 1 (C1)	Wild type	➢ None	None	3: C1.25 C1.28 C1.32
Control 2 (C2)	Wild type	➢ None	None	1: C2.6
Patient 1 (P1)	Het c.649dupC	➢ Infantile seizures	4 months	3: P1.30 P1.35 P1.45
Patient 2 (P2)	Hom c.649dupC	➢ Infantile seizure ➢ Absences ➢ Paroxysmal kinesigenic dyskinesia ➢ Intellectual disability	3 months	2: P2.5 P2.18
Patient 3 (P3)	Hom c.649dupC	➢ Infantile seizures ➢ Absences ➢ Paroxysmal kinesigenic dyskinesia ➢ Episodic ataxia ➢ Intellectual disability	4 months	1: P3.30

Table 5. Genotype-phenotype correlation of iPSC clones generated from fibroblasts of patients carrying *c.649dupC* mutation in PRRT2. All clones were siblings of a consanguineous Italian family segregating the common PRRT2 mutation *c.649dupC* (P1-P3). IPSC clones from two unrelated healthy individuals (C1 and C2) were also generated and used as control. For each individual, the number of clones (ID) of the respective iPSC clones is reported.

3. RESULTS

3.1. Constitutive PRRT2 deletion strongly decreases excitatory spontaneous and evoked transmission, strengthening inhibitory synaptic transmission

In order to evaluate the functional effects of PRRT2 deletion *in vitro*, we analyzed spontaneous and evoked synaptic transmission in low density and autaptic cultures of primary neurons from E18 embryonic hippocampus, respectively. Electrophysiological recordings of miniature excitatory (mEPSCs) and inhibitory (mIPSCs) postsynaptic currents were performed at the soma of voltage-clamped neurons (V_h= -70 mV), plated as low-density network (**Fig. 7 A, B**, respectively). Because miniature events reflect the spontaneous exocytosis of neurotransmitter-loaded vesicles in the absence of APs (Fatt and Katz, 1952), we have conducted the electrophysiological recordings in the presence of tetrodotoxin (TTX, 1 μM)

in the extracellular solution in order to block spontaneous firing activity. Notably, the mEPSCs frequency was significantly lower in *PRRT2*-KO cultures than the frequency recorded in WT hippocampal neurons (**Fig. 7 A, B**, *left panels*). Statistical analysis of mEPSCs amplitude, kinetics (80% decay, rise) and unitary charge (area) was not significantly different from WT excitatory control synapses (**Fig. 7 C**). Conversely, no differences were observed in the analysis of mIPSCs parameters studied in *PRRT2*-KO and WT inhibitory synapses (**Fig. 7 D**).

We next analyzed evoked synaptic transmission in glutamatergic and GABA-ergic hippocampal neurons plated as autaptic cells (**Fig. 8 A, B**). Postsynaptic currents (PSCs) were discriminated for their kinetics and sensitivity to the specific blockers of AMPA or $GABA_A$ receptors for excitatory and inhibitory transmission, respectively (**Fig. 8 B**). Voltage-clamp recordings, obtained with paired-pulse stimulation at different interpulse intervals (from 20 ms to 10 s, **Fig. 8 B**, *inset*), revealed a significantly decrease in the amplitude of the first (I_1) excitatory evoked PSC (eEPSC) in *PRRT2*-KO condition (**Fig. 8 C**, *left*), compared to WT. By contrast, we observed a significant increase in the I_1 of the inhibitory evoked PSC (eIPSC) amplitude (**Fig. 8 D**, *left*). The values of paired-pulse ratio (PPR) were measured as a function of interstimulus interval (ISI), which represent an indirect measure of release probability (Pr) (Fioravante and Regher, 2011). *PRRT2*-KO excitatory synapses showed a two-fold increase in paired-pulse facilitation at ISI of 20 and 50 ms, while the inhibitory synapses displayed a stronger depression than WT inhibitory synapses at the same values ISIs (**Fig. 8 C,** *right* and **Fig. 8 D,** *right*).

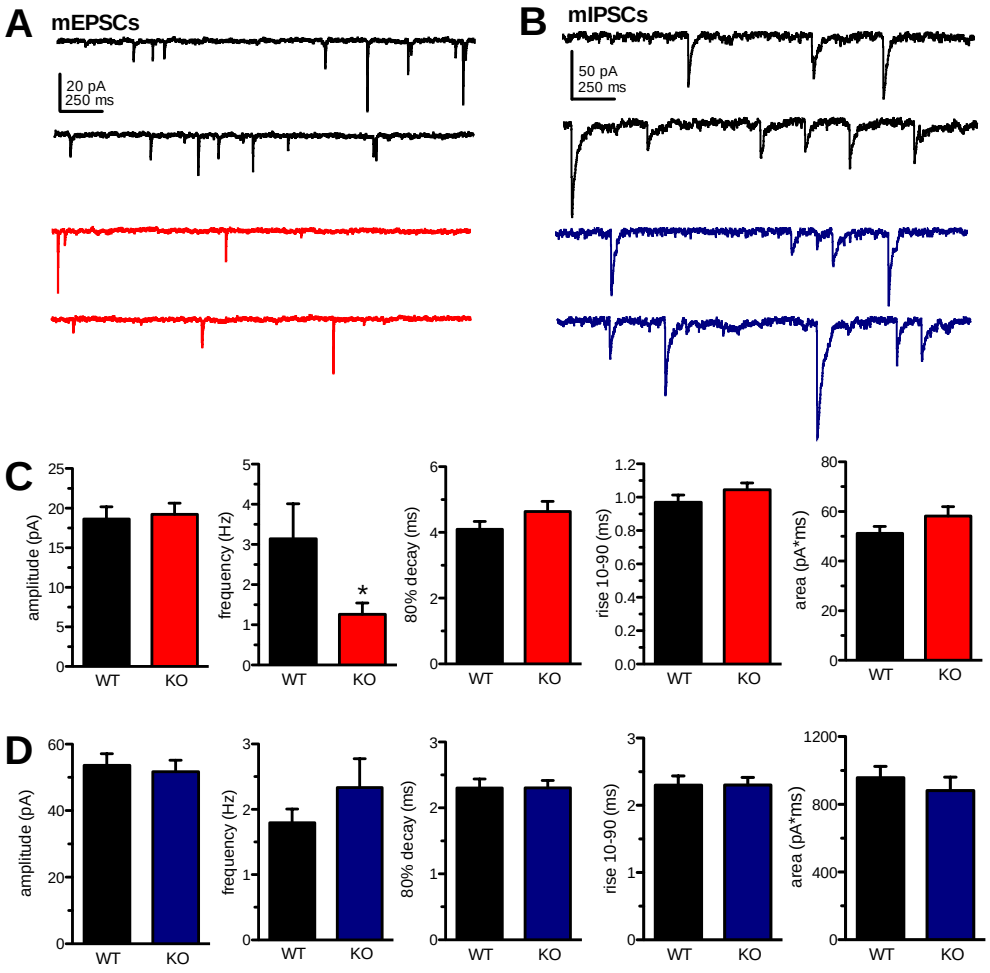

Figure 7. PRRT2 deletion decreases spontaneous excitatory transmission. A, B. Representative recordings traces of mEPSCs (A) and mIPSCs (B) from WT (black) and PRRT2-KO (EPSCs, red; IPSCs, blue) hippocampal low-density neuronal networks. **C, D**. Analysis of mEPSCs (C) and mIPSCs (D). From *left* to *right*, the mean ±sem values of amplitude, frequency, 10%-90% rise time, 80% decay and charge are shown. All parameters were obtained from at least 50-100 events recorded from WT (n=31) and *PRRT2*-KO cells (n=34) for mEPSCs and from WT (n=25) and *PRRT2*-KO (n=26) cells for mIPSCs from at least n=3 independent cell culture preparations. *p < 0.05, unpaired Student's t-test.

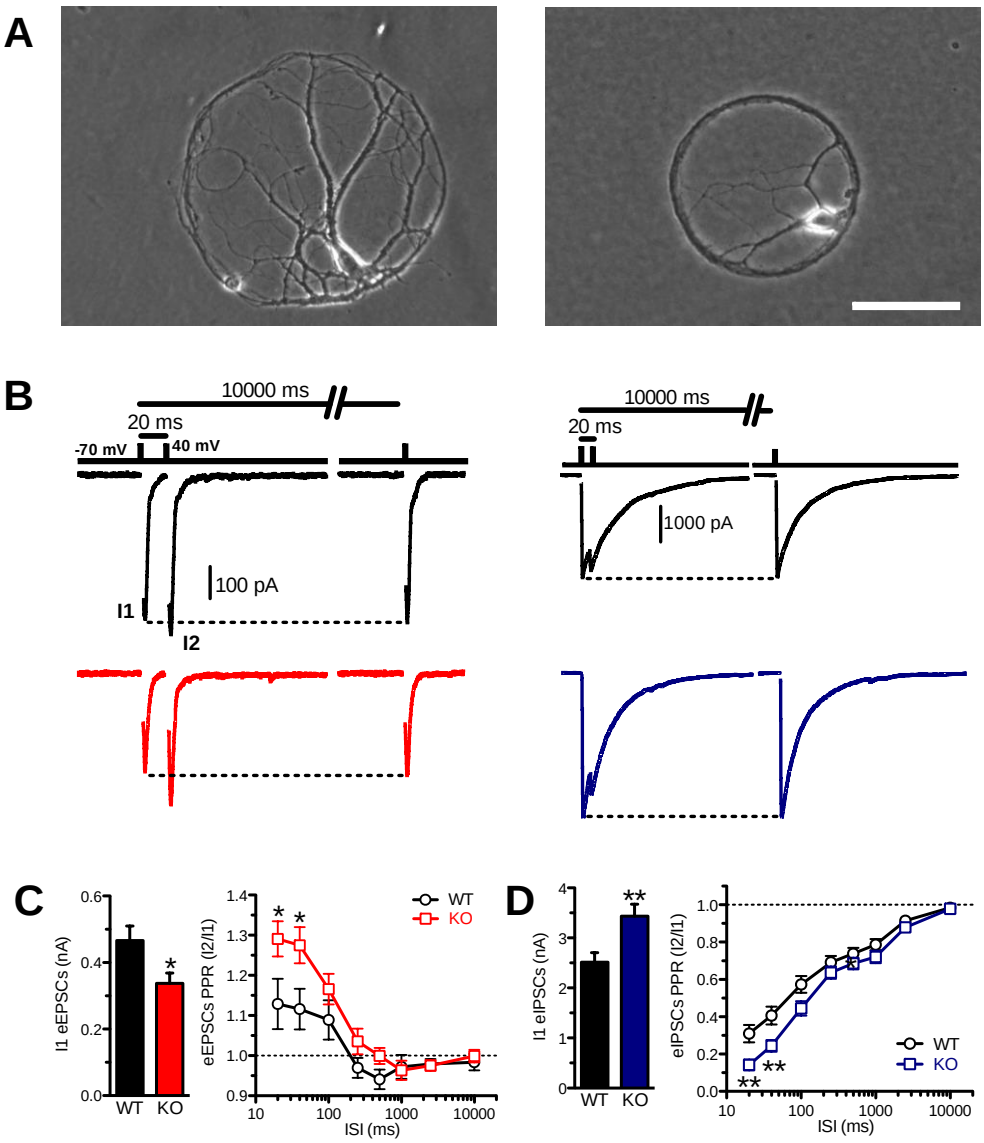

Figure 8. PRRT2 deletion decreases evoked excitatory transmission and increases evoked inhibitory transmission. A. Phase-contrast micrographs of typical glutamatergic (*left*) and GABA-ergic (*right*) hippocampal autaptic neuron. The identity of the two types of autaptic cells was confirmed by retrospective biophysical and pharmacological analysis of evoked currents. Scale bar, 100 µm. **B.** Representative eEPSCs (*left*) and eIPSCs (*right*) traces evoked in excitatory and inhibitory autaptic cells from WT (black traces) or *PRRT2*-KO (red/blue traces for EPSCs and IPSCs, respectively) mice. Currents were elicited at V_h = -70mV and stimulating it with two 0.5 ms steps to 40 mV separated by the indicated ISIs and applied at a frequency of 0.1 Hz. **C.** eEPSC amplitude (*left*) and PPR as a function of ISIs ranging from 20 to 10,000 ms (*right*) for WT (black bar/symbols) and *PRRT2*-KO (red bar/symbols) neurons. Data were obtained from n=53 WT and n=54 *PRRT2*-KO glutamatergic neurons. **D.** eIPSC amplitude (*left*) and PPR as a function of ISIs ranging from 20 to 10,000 ms (*right*) for WT (black bar/symbols) and *PRRT2*-KO (blue bar/symbols) neurons. Data were obtained from n=32 WT and n=34 *PRRT2*-KO GABA-ergic neurons. In all traces, the stimulation artefacts were blanked for clarity. Data are shown as means ±sem. *p < 0.05, **p < 0.01 unpaired Student's t-test/Mann-Whitney's U-test.

3.2. Excitatory and inhibitory *PRRT2*-KO neurons respond differently to high-frequency stimulation

The effects of PRRT2 deletion on the excitatory and inhibitory synapses and by modulation of the PPR led us to study the short-term plasticity (STP) properties of these synapses. We have conducted this study using short (2 s) stimulation trains with increasing frequency (from 5 to 40 Hz). These protocols promote Ca^{2+} rise in the nerve terminal and the progressive depletion of the Readily Releasable Pool (RRP) (Fioravante and Regehr, 2011). The results were similar to those obtained analyzed PPR. Excitatory synapses of *PRRT2*-KO neurons displayed a larger facilitation than WT synapses in the high frequency range and a milder depression in the low frequency range (**Fig. 9 A, B**). By contrast, inhibitory *PRRT2*-KO synapses showed a faster depression in response to 20 and 40 Hz trains without change in the response to trains of 5 and 10 Hz (**Fig. 9 C, D**).

These findings suggest that PRRT2 deletion has a presynaptic effect most likely on the Pr. Thus, a protocol of stimulation consisting of a train of 40 Hz, which is used to promote a full RRP depletion, was used to study the quantal parameters of release in both excitatory and inhibitory synapses using the cumulative PSC amplitude analysis (**Fig. 10 A, D**). The same changes in the current amplitude of synchronous release observed in excitatory and inhibitory *PRRT2*-KO synapses were attributable to opposite changes in the initial Pr, without any detectable effect on the RRP_{syn} total current (**Fig. 10 C, F;** *middle panels*).

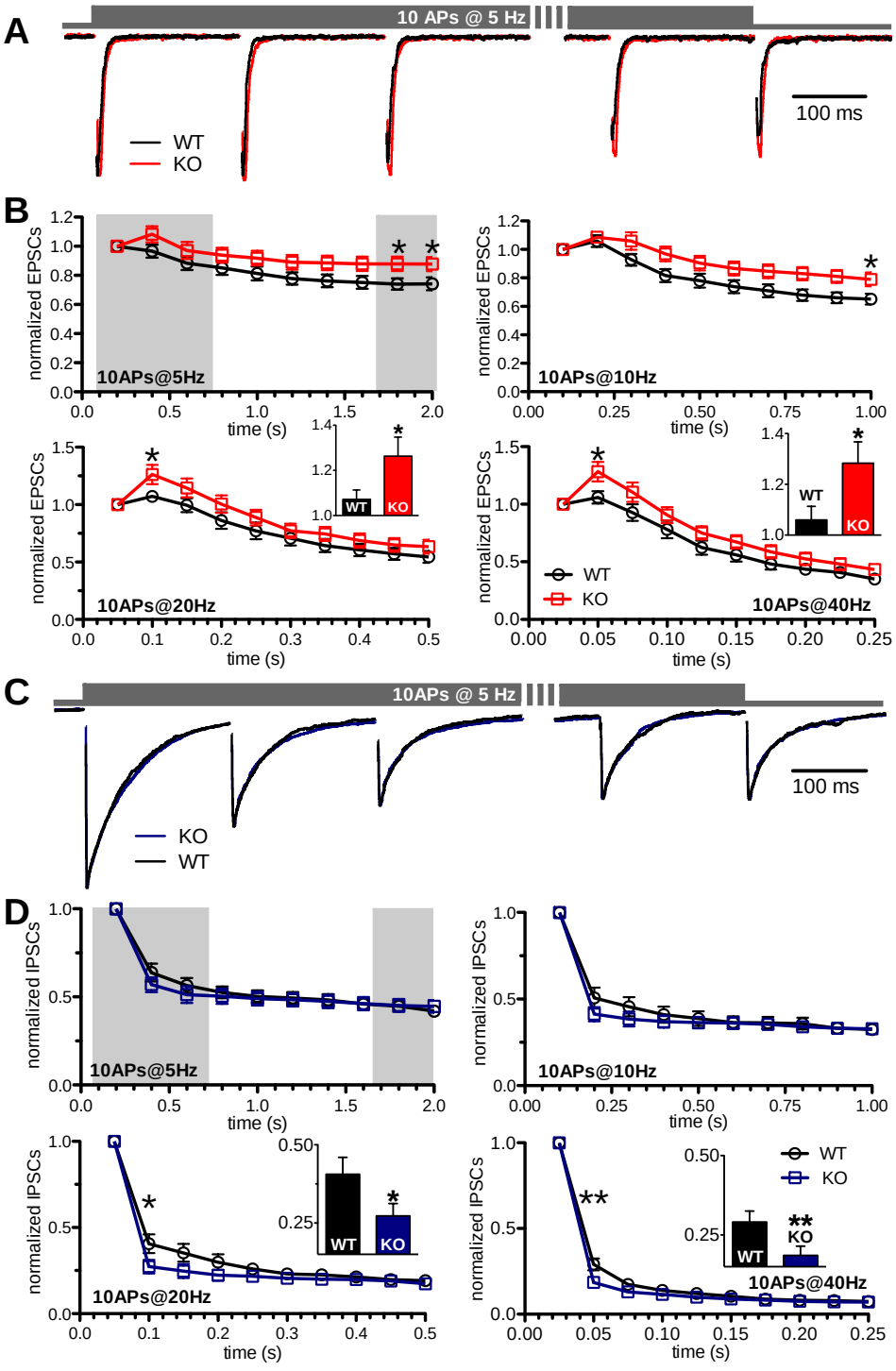

Figure 9. PRRT2 deletion enhances facilitation of glutamatergic synapses and produces a more profound synaptic depression compared with GABA-ergic synapses. A, C. Representative recordings of eEPSCs (A) and eIPSCs (C) evoked by 2 s tetanic stimulation at 5 Hz administered to WT (black traces) or *PRRT2*-KO (red/blue traces for EPSCs and IPSCs, respectively) autaptic hippocampal cultures. **B, D**. Mean ±sem of normalized values of eEPSC (B) and eIPSC (D) amplitude showing the time course of synaptic facilitation and/or depression evoked in WT (black traces) or *PRRT2*-KO (red and blue traces for EPSCs and IPSCs, respectively) autaptic hippocampal neurons in response to 2 s

tetanic stimulations at 5, 10, 20 and 40 Hz. The shaded areas in the 5 Hz panels refer to the representative traces shown in A and C. The *insets* in the 20 and 40 Hz panels report the mean ±sem of the extent of facilitation (B) or depression (D) representing the second stimulus in the train. Data were obtained from: 5 Hz (WT, n=16; *PRRT2*-KO, n=18), 10 Hz (WT, n=21; *PRRT2*-KO, n=20), 20 Hz (WT, n=21; *PRRT2*-KO, n=20) and 40 Hz (WT, n=22; *PRRT2*-KO, n=21). *p < 0.05, unpaired Student's t-test/Mann-Whitney's U-test.

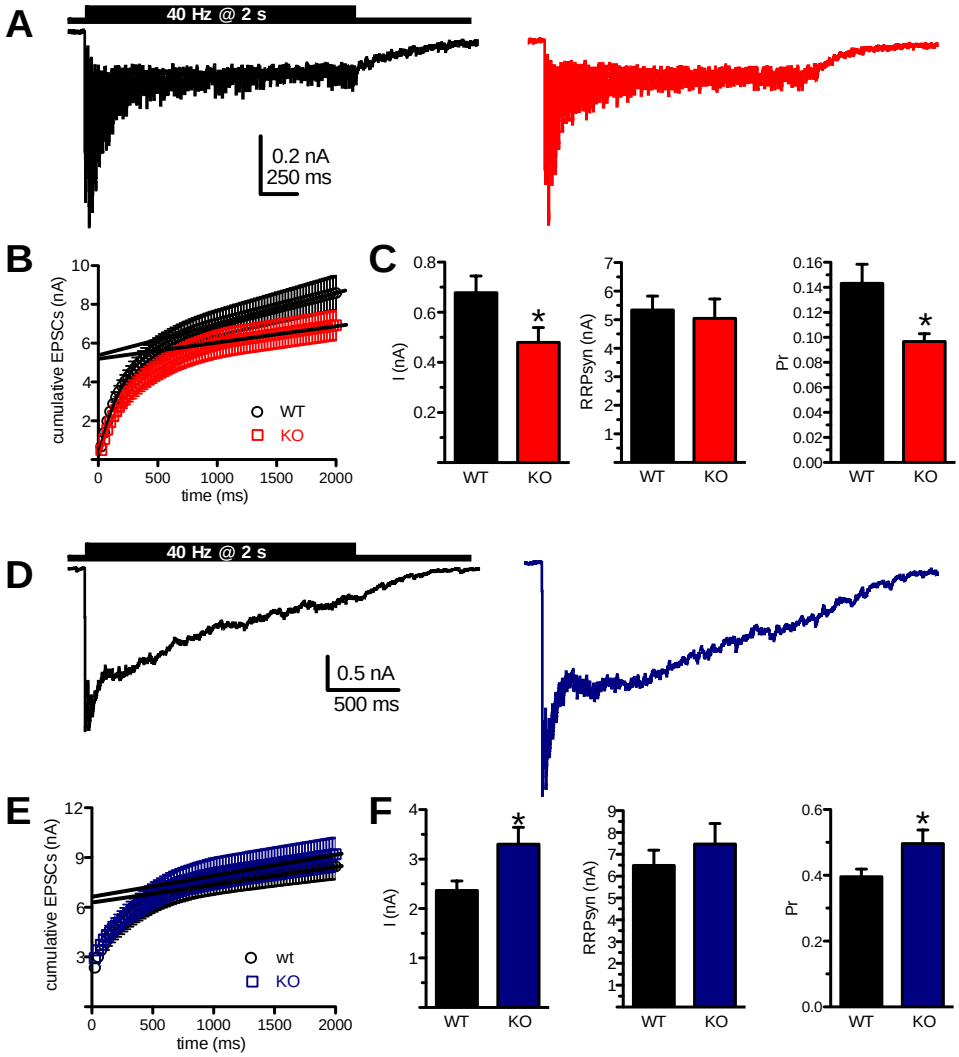

Figure 10. Constitutive PRRT2 deletion shows opposite effects on release probability in excitatory and inhibitory *PRRT2*-KO neurons. A, D. Representative recordings of eEPSCs (A) and eIPSCs (D) evoked by 2 s tetanic stimulation at 40 Hz administered to WT (black traces) and *PRRT2*-KO (red/blue traces for EPSCs and IPSCs, respectively) autaptic hippocampal neurons. **B, E**. Cumulative amplitude profiles of eEPSCs for WT (n=22) and *PRRT2*-KO (n=21) neurons subjected to 40 Hz stimulation for 2 s. Data points in the 1- to 2-s range were fitted by linear regression and back-extrapolated to time 0 (solid lines) to estimate the RRP_{syn}. **C, F**. Mean ±sem amplitude of the first eEPSC in the train used to perform quantal analysis (*left*), RRP syn size (*middle*) and Pr (*right*) estimated in WT and *PRRT2*-KO autaptic neurons (WT, n=22; *PRRT2*-KO, n=21). *p < 0.05, unpaired Student's t-test/Mann-Whitney's U-test.

3.3. Primary *PRRT2*-silenced networks display a state of spontaneous hyperactivity and robust synchronization in bursting events

Since we observed the alterations in both excitatory and inhibitory synaptic transmission at single-cell level, we then investigated the functional consequences of these changes at the network level. To address this issue we plated the primary hippocampal neurons onto multi-electrode array (MEA) chips (**Fig. 11 A,** *left*). By this approach, we monitored spontaneous activity of *PRRT2*-KO and WT primary hippocampal neurons at high density, in time periods ranging from early synapse formation (14 DIV) to that of mature synaptic connections (21 DIV). **Fig. 11 A** (*right*) showed raster plots of the spiking activity recorded from representative *PRRT2*-KO and WT networks. Basal activity from representative networks of both genotypes was characterized by the occurrence of isolated spikes, single-channel bursts and synchronous array-wide bursts (raster plots and *inset*, **Fig. 11 A**), lasting from few hundreds ms up to 1 s (Van Pelt *et al*., 2004, Chiappalone *et al*. 2007; Vajda *et al*. 2008). Periodic population bursts activity in primary neuronal cultures is a sign of global network synchronization that closely depends from synaptic connectivity and basal intrinsic excitability (Maeda *et al*. 1995, Penn *et al*. 2016; Suresh *et al*. 2016). Under our experimental conditions, we reported that only 55.1% of the WT cultures (29 cultures out of 49) versus 86.9% of the KO (40 out of 46) generated networks bursts (**Fig. 11 A**, *right panel*). The main activity parameters, evaluated at a mature stage of *in vitro* development, showed an increased network mean firing rate in the network of *PRRT2*-KO cultures compared to WT cultures (**Fig. 11 B**). We observed a hyperactivated *PRRT2*-KO, in line with the increased synaptic facilitation of excitatory transmission that strongly impairs activity dynamics in reverberant networks (Abbott and Regehr, 2004). The average network bursting rate and the intraburst firing rate in *PRRT2*-KO neurons were significanty higher than that in WT neurons, with a decrease in the bursts duration (**Fig. 11 B**). Moreover, the value of bursts percentage (the fraction of total spikes within bursts) was significantly higher than in WT cultures. The synchrony index, representing the degree of synchronization of bursting activity throughout each networks (Paiva *et al*., 2010), was markedly increased in *PRRT2*-silenced cultures with respect to WT condition. These data confirm that

mature *PRRT2*-KO networks express a more pronounced synchronization in their bursts behaviours (**Fig. 11 B**). We hypothesized that the shorter network bursts observed in silenced cultures could be due to the increased inhibitory network activity described in the analysis of synaptic properties, or to a faster depletion of synaptic resources during high-frequency synchronized activity (Cohen and Segal, 2011).

Furthermore, to test whether the described changes of inhibitory transmission could have an impact on the spontaneous hyperactivity of *PRRT2*-KO networks, the effect of an acute treatment with bicuculline of mature cultures (BIC, 30 µm, blocking $GABA_A$ receptors) was investigated (Chiappalone *et al*., 2009; Lignani *et al*., 2013). In both WT and silenced neurons, raster plots showed that BIC treatment increased bursting activity, while random spiking was completely abolished (**Fig. 11 C**). Moreover, in WT networks, BIC induced an increase in the values of firing rate, bursting rate and burst duration, while it decreased the value of intra-burst firing rate (**Fig. 11 C**). The same qualitative changes were observed in *PRRT2*-KO networks, but quantitatively more pronounced (**Fig. 11 C**). To compare the effect of the BIC treatment across genotypes, the values of individual network activity parameters were normalized to the corresponding values before drug administration (BIC/base ratio; *right panels* in **Fig. 11 C**). The BIC/base ratios for firing rate, bursting rate, burst percentage were significantly higher for *PRRT2*-KO networks than for WT networks. The enhancement of the differences between the two conditions under BIC is in line with the strengthened inhibitory tone observed in whole-cell patch-clamp recordings in silenced neurons.

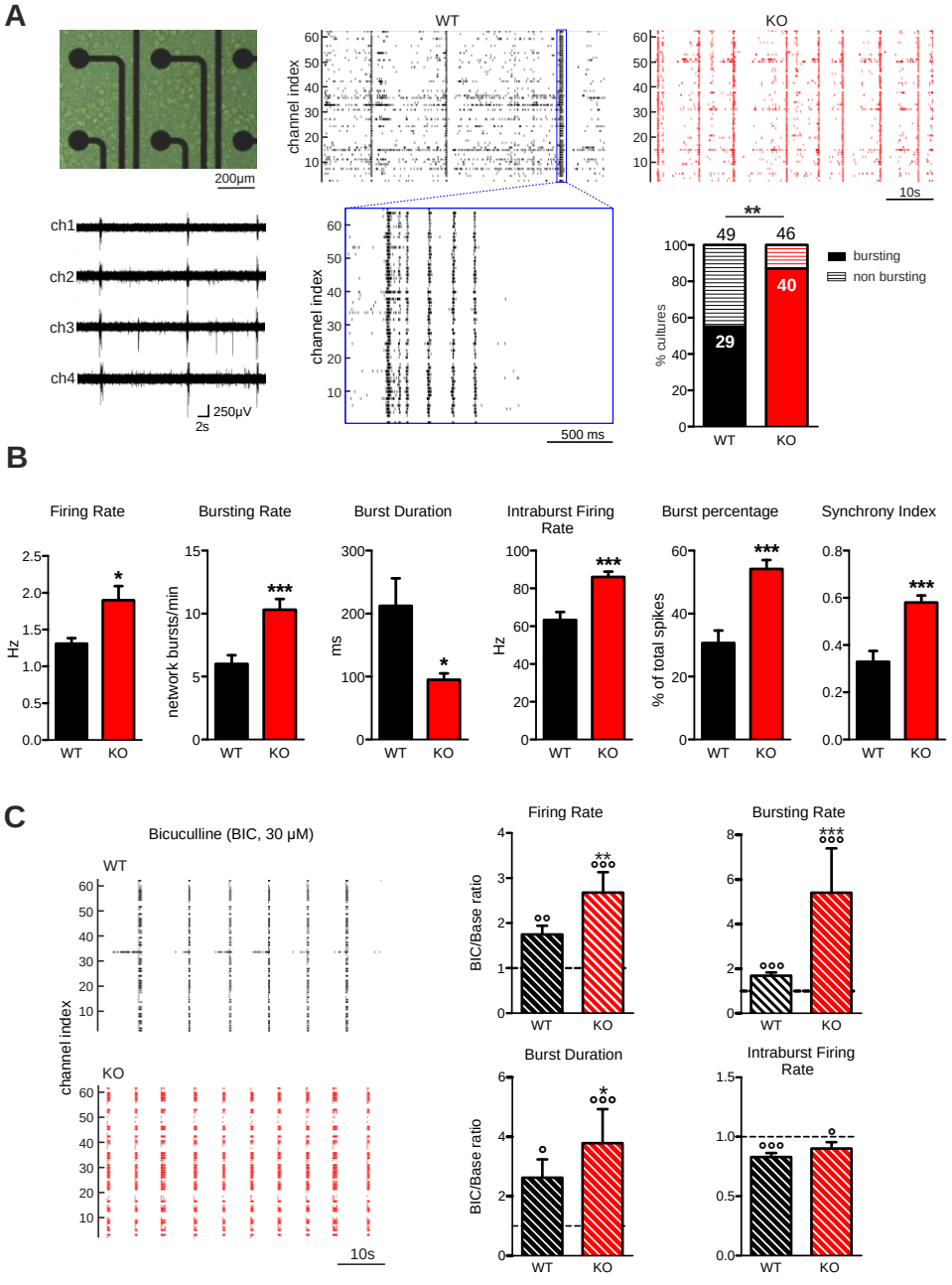

Figure 11. *PRRT2*-KO hippocampal networks display heightened excitability under basal conditions and under blockade of $GABA_A$-mediated inhibitory transmission. A. Phase contrast micrograph of WT network over a MEA at 14 DIV and spiking activity recorded from four adjacent microelectrodes are showed in the top and bottom *left* panels, respectively. Electrophysiological spontaneous activity from WT or *PRRT2*-KO primary hippocampal networks was recorded between the second and the third week in vitro (14-21 DIV). On the last day of the experiments, networks were challenged with bicuculline (BIC, 30 µM), the $GABA_A$ receptor blocker. In the panels on the right, raster plots of spiking activity recorded over 60 s from WT and *PRRT2*-KO cultures. Each row is an electrode of the array and marks represent APs. The magnification shows spontaneous population bursting generated by a mature WT culture (*inset*). Collective bursts lasted few hundreds of milliseconds and were separated by longer periods of scarce firing activity as highlighted in the panel *inset*. The bar plot shows the fraction of networks generating population bursts, expressed as a percentage of total cultures for each

genotype. **B:** Main firing and bursting parameters measured for WT (black) and *PRRT2*-KO (red bars) cultures at 14 and 21 DIV. From *left* to *right*: firing rate, network bursting rate, network burst duration, intra-burst firing rate, burst percentage and synchrony index measured for each experimental group during the third week *in vitro* (n=4 independent preparations for each genotype, 49 and 46 independent experiments for WT and *PRRT2*-KO, respectively). **C**. Left: Raster plots of the activity recorded from WT and *PRRT2*-KO cultures in the presence of BIC (30 μM) over 60 s. *Right*: Statistical analysis of the effect of BIC treatment on firing rate, network bursting rate, network burst duration and intra-burst firing rate expressed as ratios between individual values of each network parameter under BIC and the corresponding values under basal conditions (BIC/base ratio) (n=3 independent preparations for each genotype, 32 and 31 independent experiments for WT and *PRRT2*-KO, respectively). Data are plotted as means ±sem for WT (black) and *PRRT2*-KO (red bars) cultures. Unpaired Student's t-test/Mann-Whitney's U-test was used to compare the activity parameters (Fig. 11 B) and the BIC/Base ratios (Fig. 11 C) across genotype (*$p < 0.05$; **$p < 0.01$, ***$p < 0.001$). The effects of BIC within genotype were analyzed by either Wilcoxon or paired Student's t-test (°$p < 0.05$; °°$p < 0.01$; °°°$p < 0.001$).

3.4. *PRRT2* silencing is associated with an increase of intrinsic excitability of hippocampal excitatory neurons

MEA analysis showed a general hyperactivity of *PRRT2*-KO networks compared to WT. In order to get insights in the underlying mechanism, we performed electrophysiological analysis at single-cell level on excitatory pyramidal neurons in low-density hippocampal network. These cells were visually inspected and retrospectively determined (Pozzi *et al*., 2013). The macroscopic Na^+ and K^+ currents were studied by voltage steps of increasing amplitude and ramp protocol (**Fig. 12 A,** protocols are showed as *inset*). Analysis of the density-voltage relationship (JNa^+/V) of Na^+ current showed a significant increment of JNa^+ in *PRRT2*-KO hippocampal neurons compared to WT (**Fig. 12 B**). This effect was not accompanied by changes of the K^+ current density (JK^+) of both phenotypes measured at +120 mV (**Fig. 12 C**).

We next studied the spontaneous and evoked firing activity under current clamp condition. The spontaneous firing of *PRRT2*-KO neurons clamped near the threshold (V_h =-40 mV) by injection of a constant depolarizing current was significantly higher than that observed in WT neurons analysed under the same conditions (**Fig. 12 D, E**). Next, we also depolarized the neuronal membrane potential with subsequent current steps injection of 5 pA to evoke the firing activity. Mutant neurons showed a higher evoked

firing activity compared to WT neurons, as depicted from the analysis of mean firing rate calculated as the ratio of the number of APs evoked by the minimal current injected to the time interval in seconds between the first and the last evoked AP (**Fig. 12 F, G**). It is well known that neurons present the ability to show adaptation to current steps stimulation, which increases their firing frequencies (Awiszus *et al*., 1988). Thus, we finally evaluated the adaptation of excitatory hippocampal neurons injecting 5 ms supra-threshold current steps, administered at frequencies from 10 to 120 Hz (**Fig. 12 H**). For each stimulation frequency tested, the percentage of evoked APs over the total number of stimuli was calculated in both phenotypes. The two neuronal populations were able to fire the 100% of APs up to 40 Hz. Interestingly, over this frequency, WT neurons displayed a progressively increasing amount of failures, while *PRRT2*-KO neurons were able to sustain higher stimulation frequencies (from 80 to 120 Hz) with a significantly higher probability of success (**Fig. 12 I**).

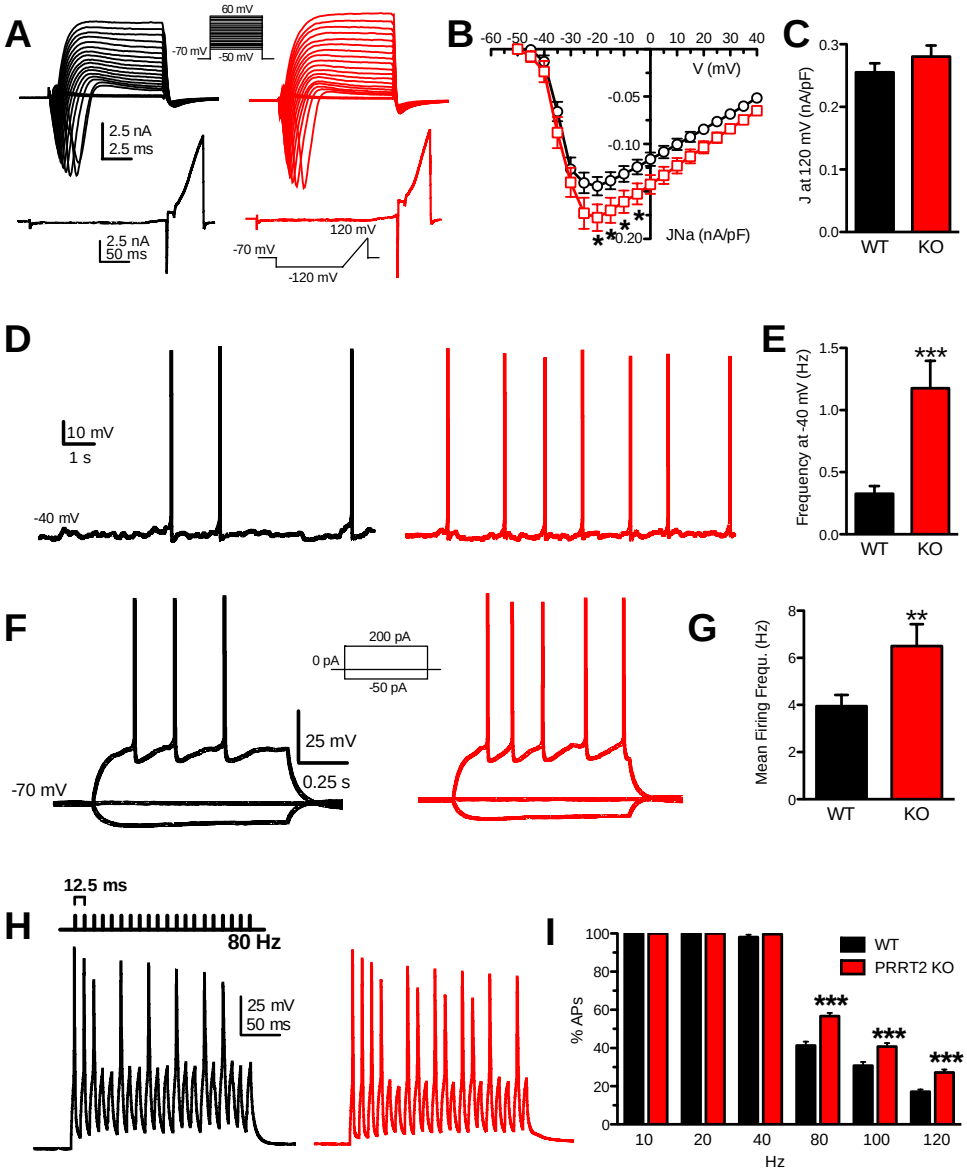

Figure 12. *PRRT2*-KO excitatory neurons show an increased intrinsic excitability. A, B. Representative whole-cell macroscopic currents (A) evoked by a family of 10 mV depolarizing voltage steps or a ramp protocol (*insets*) and (B) current density vs voltage relationship, calculated using the protocol shown in panel A. Excitatory hippocampal WT neurons (n=58) are showed with black symbols/traces; *PRRT2*-KO neurons (n=54) with red symbols/traces. **C**. J at +120 mV for WT/*PRRT2*-KO genotypes calculated using the ramp protocol (lower part of panel A) (WT, n=58; *PRRT2*-KO, n=54). **D, E**. Representative voltage trace recordings (D) of spontaneous APs generated by WT and *PRRT2*-KO neurons during the injection of a constant depolarizing current to maintain the membrane potential at the threshold ($V_h \cong -40$ mV) and mean ±sem of spontaneous firing frequency (E) recorded using the protocol shown in D (WT, n=21; *PRRT2*-KO, n=22). **F, G**. (F) Representative current-clamp recordings of action potentials evoked by the injection of -50, 0 and +200 pA steps of 1 s duration (*inset*) and statistical analysis of mean ±sem firing frequency (G) observed in WT (n=56) and *PRRT2*-KO (n=60) neurons. **H, I**. Representative current-clamp traces of action potentials activated by 20 current steps (5 ms) at 80 Hz (H) and mean ±sem of the

probability to evoke action potentials in WT (n=59) and *PRRT2*-KO (n=63) neurons (I) at increasing frequencies of current injection. The percentage of the amount of injected current was reported as the minimal current able to evoke 100% of APs at 10 Hz. *p < 0.05, **p < 0.01, ***p < 0.001, unpaired Student's t-test/Mann-Whitney's U-test.

3.5. IPSCs are generated and characterized from fibroblasts of patients carrying the *PRRT2 c.649dupC* mutation

The results of the electrophysiological characterization showed that *PRRT2*-KO neurons have a sustained increase of single-cell and network excitability compared to WT cells. In an attempt to understand the molecular basis of the PRRT2-associated dysfunctions, we generated and characterized iPSCs from fibroblasts of patients from a consanguineous Italian family (Labate *et al*., 2012), carrying the *c.649dupC* common *loss-of-function* mutations in heterozygosity (Patient P1) or homozygosity (Patients P2 and P3, siblings of P1). As control we have used iPSCs generated from sex- and age-matched normal donors (C1 and C2). P1 generally presented a self-limiting seizure of childhood, whereas P2 and P3 showed a more severe phenotype with co-occurrence of other forms of PDs (see **Table 4**). To generate iPSCs, fibroblast cells were transfected with retroviral reprogramming factors (OCT3/4, SOX2, KLF4 and C-MYC, see Introduction and Materials and Methods).

In order to assure high quality of iPSC clones, expression analyses for known pluripotency marker expression by qRT-PCR and immunofluorescence were performed. By analysis of qRT-PCR experiments, we confirmed that iPSCs expressed pluripotent stem cells markers. As a negative control, fibroblast culture that showed any expression of these pluripotency markers was used (**Fig. 13 A**, opens bars in the graphs). A second step in the cell characterization includes the determination of iPSC clone's ability to differentiate into cells of the three germ layers: endoderm, mesoderm and ectoderm (**Fig. 13 E-G**). To perform this test, cells were differentiated into the type of germ layers using defined medium containing the necessary differentiating factors and then we evaluated the expression of germ layer markers. This assay confirmed the pluripotency of the generated iPSCs. Only the iPSC clones that passed this test of staminality were used subsequently for differentiation into

neurons. The neuronal differentiation *in vitro* goes through to different steps (**Fig. 14 A**). In the first phase, iPSC clones produce EBs that consist of three-dimensional aggregates formed in suspension like “neurosphere”. Then, upon dissociation and plating onto substrate, these cells generate adherent neural rosette upon exposure to small-molecules that inhibit the Bone Morphogenetic Protein and the Transforming Growth Factor-β signaling. By the inhibition of these two antineurogenic factors, the production of proteins that interfere with the transcriptional activities of proneural proteins in neural progenitor cells is blocked, inducing the generation of neuronal rosette.

In this study, rosettes were co-cultured with embryonic rat cortical neurons (see Materials and Methods) used as feeder layer. This feeder layer were important to induce normal neuronal differentiation of our cells. It was also found that adding common neural modulating molecules, such as retinoic acid, BDNF and GDNF to the neuronal differentiation medium in the last phase of the treatment, greatly enhanced neuronal differentiation and maturation, which resulted in the generation of a stable population of self-renewal NPCs. After 25-30 days of co-culture, neurons derived from iPSCs cells reached a mature state with neuronal-like morphology.

Gene expression profiling showed that NPC-differentiation markers were upregulated in all NPC populations compared to the parental iPSCs, whereas specific pluripotency genes where downregulated (**Fig. 14 B**). Moreover, immunofluorescence analysis indicated that NPCs were positive for the neural cell markers SOX1, SOX2, NESTIN and the dorsal telencephalic marker PAX6. These data clearly indicate that our cells have a clear cortical progenitor fate (**Fig. 14 C, D**).

IPSCs-derived neurons were positive for typical markers of neuronal differentiation: Neuronal Nuclei (NeuN) and Microtubule-Associated Protein 2 (MAP2). NeuN is a neuron-specific protein that has a role in regulating neural cell differentiation and nervous system development (Kim *et al*., 2009) and MAP2 is a neuron-specific cytoskeletal protein involved in determining and stabilizing dendritic shape during neuronal development (Geisert *et al*., 1990) (**Fig. 14 E, G**). The percentage of $NeuN^+$ cells was very similar across all the clones tested (**Fig. 14 F**). IPSC-derived neurons expressed also VGLUT1 and GABA, two markers of excitatory and inhibitory cells, respectively (**Fig. 14 H, I**). This evidence supports the notion that under our conditions both type of neurons are present, forming a

mixed network. Furthermore, we studied the iPSC-derived neurons concerning the expression of Na_V channels, which are essential to shape the excitability of mature neurons. To this end, we used a specific antibody against α-subunits of Na_V channels. We observed that all genotypes of human neurons expressed this subunit at the AIS (**Fig. 14 J**). At a functional level, whole-cell voltage-clamp recordings showed the presence of inward currents with fast activation and inactivation kinetics fully blocked by TTX in all genotypes (**Fig. 14 K,** *left*). The TTX blockade was evident at every potential tested (**Fig. 14 K,** *right*).

Taken together, these data suggest that mature functional neurons were obtained under our conditions *in vitro*.

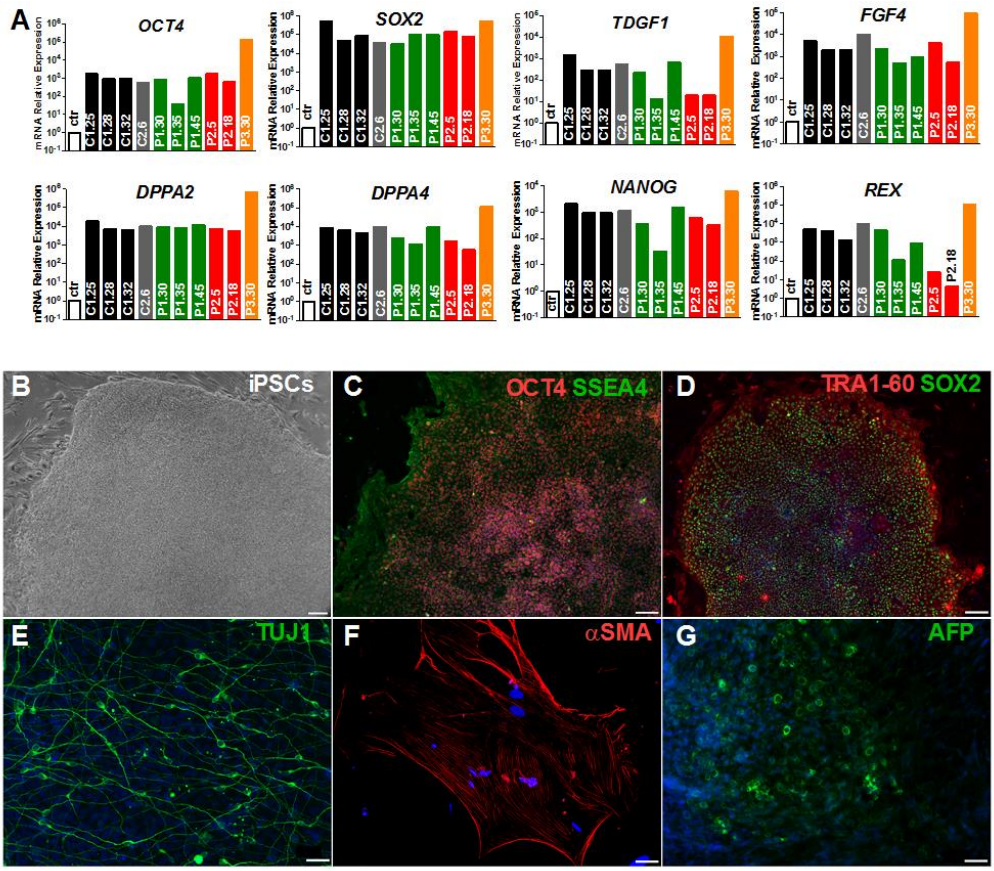

Figure 13. Validation of iPSC lines generated from fibroblasts of patients carrying *c.649dupC* mutation in *PRRT2* gene A. Quantification by RT-qPCR analysis of the expression levels of different pluripotency markers in the different clones obtained from heterozygous Patient 1 (P1.30, P1.35 and P1.45, green bars), from homozygous Patient 2 (P2.5, P2.18, red bars) and Patient 3 (P3.30, orange bar) and from two unrelated non-carrier individuals (C1.25, C1.28, C1.32, black bars; C2.6, grey bar). Data are means ±sem (n=3) of relative expression using non-infected fibroblasts from a control (Ctr) as reference (open bars). **B**.

Morphology of an iPSC clone at the undifferentiated state. Scale bar, 50 µm. **C-D**. Representative immunofluorescence images showing the expression of pluripotency markers (OCT4, SSEA4, TRA1-60 and SOX2) in iPSC lines (nuclei were stained with DAPI; Scale bar, 100 µm). **E-G**. IPSC clones generate cells of the three germ layers: ectodermal (TUJ1), mesodermal (α-SMA) and endodermal (AFP) markers (nuclei were stained with DAPI; scale bar, 50 µm).

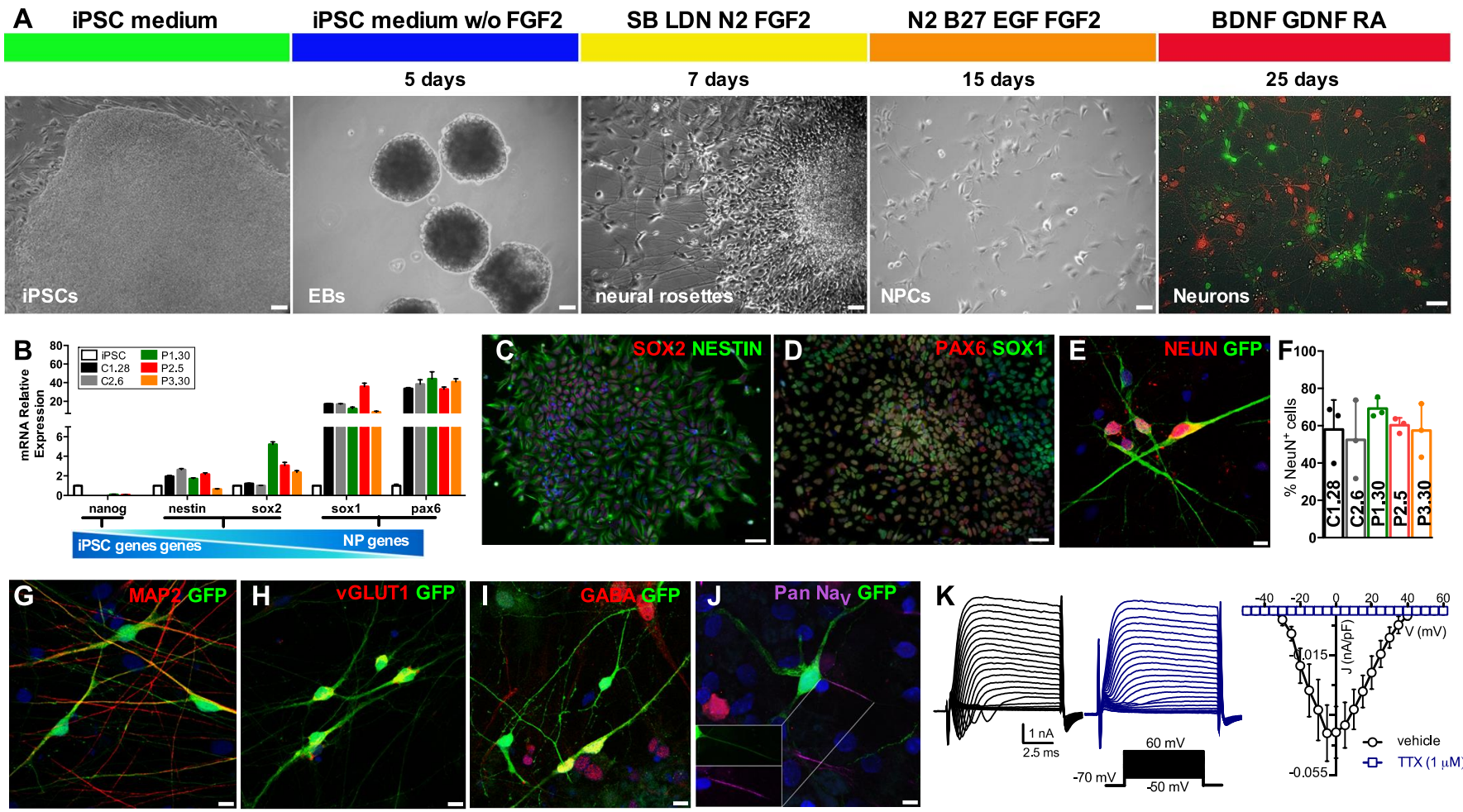
A
iPSC medium
iPSC medium w/o FGF2
SB LDN N2 FGF2
N2 B27 EGF FGF2
BDNF GDNF RA
5 days
7 days
15 days
25 days
iPSCs
EBs
neural rosettes
NPCs
Neurons
B
mRNA Relative Expression
iPSC
C1.28
C2.6
P1.30
P2.5
P3.30
nanog
nestin
sox2
sox1
pax6
iPSC genes genes
NP genes
C
SOX2 NESTIN
D
PAX6 SOX1
E
NEUN GFP
F
% NeuN+ cells
C1.28
C2.6
P1.30
P2.5
P3.30
G
MAP2 GFP
H
vGLUT1 GFP
I
GABA GFP
J
Pan NaV GFP
K
1 nA
2.5 ms
60 mV
-70 mV
-50 mV
V (mV)
J (nA/pF)
vehicle
TTX (1 μM)

Figure 14. Neuronal differentiation and characterization of iPSC-derived neurons. A. Scheme for the generation of iPSCs and representative images at different steps of the neuronal differentiation. From the *left*: representative iPSC colony, embryoid bodies (EBs), neural rosettes, NPCs and representative live image of iPSCs-derived neurons (GFP^+, green), co-cultured with cortical rat neurons ($TdTomato^+$). Scale bar, 50 µm. **B.** Quantification by RT-Q PCR analysis of the NPC gene expression profile. NPC-specific markers *SOX1* and *PAX6* are upregulated in NPCs, as compared to iPSCs. *NESTIN* and *SOX2,* participating in self renewal and neural differentiation, are expressed by both cell types. The pluripotency specific gene *NANOG* is strongly downregulated in NPCs. Data are means ±sem of relative expression using iPSCs as reference. **C, D.** Representative immunofluorescence images of neuronal rosettes showing expression of NPC markers (**C**: SOX2, red; NESTIN, green; **D**: PAX6, red; SOX1, green). **E, G.** Representative immunofluorescence images of the immunoreactivity of iPSC-derived neurons for mature neuronal markers NeuN (quantified in F) and MAP2 (G) after four weeks of differentiation. Scale bar, 10 µm. **F.** Data are expressed as means ± SD of n=3 independent experiments (at least 50 cells each experiment). One clone for each genotype is shown. Not significant, Kruskal-Wallis/Dunn's test. **H, I.** Representative immunofluorescence images of VGLUT1- and GABA-positive cells. Scale bar, 10 µm. **J.** Representative immunofluorescence of iPSC-derived neurons expressing voltage-gated Na^+ channels. The *inset* shows colocalization of GFP and $PanNa_V$ at the AIS. Nuclei were stained with DAPI. Scale bar, 5 µm. **K.** *Left:* Representative whole-cells currents elicited by depolarizing C1.28 neurons with a family of 10-ms depolarizing voltage steps (*inset*) in the absence (black) or presence of TTX (1 µm, blue). *Right:* Current density *vs* voltage relationship for C1.28 neurons exposed to either vehicle or TTX (1 µm; n=9).

3.6. Homozygous iPSC-derived neurons display increased Na^+ current densities

In the next set of experiments we have studied in detail the functional properties of the generated neurons. To this end we characterized the electrophysiological properties of all the produced clones of human neurons obtained from the heterozygous patient P1 (P1.30), the two homozygous patients P2 and P3 (P2.5 and P3.30) and the two healthy controls C1 and C2 (C1.28 and C2.6). Single-cell neuronal excitability was studied by measuring the macroscopic Na^+ and K^+ conductance evoked by a family of voltage-steps and by ramp protocol (**Fig. 15 A**). Before functional characterization, the level of PRRT2 mRNA in these clones has been quantified. The analysis of PRRT2 mRNA expression by qRT-PCR in the various neuronal preparations showed that the homozygous clones had very low levels of PRRT2 mRNA with respect to the healthy controls, while the heterozygous clone expressed intermediate levels (**Fig. 15 B**).

Functional analysis indicated that both homozygous clones displayed greatly increased fast-inactivating inward currents in response to voltage-steps and ramp stimulations, while the peak outward currents recorded at +120 mV, were comparable in all genotypes tested. These results were evident also from the inspection of the Na^+ current density (JNa^+)-voltage relationship and of the bar-graph of maximal JNa^+ (**Fig. 15 C, D;** *left*). The increase in JNa^+ at -5 mV in either homozygous clone (P2.5 and P3.30) was significantly higher than that recorded in either control clone, as well as in the heterozygous clone, which was not significantly different from controls (**Fig. 15 E,** *left*). At variance, no significant differences were observed in the JK^+ measured at +120 mV across all genotypes (**Fig. 15 D, E;** *right*).

We also tested supplementary iPSC clones, derived from the same healthy individual C1 (C1.25, C1.32) and patients P1 and P2 (P1.35, P2.18) that, compared to control neurons, displayed significant increase in JNa^+ in homozygous neurons, but not in heterozygous (**Fig. 16 A, B**). The statistical analysis of JK^+ at +120 mV showed no differences between each genotypes (**Fig. 16 C**).

Taken together, these data show that iPSC-derived neurons obtained from fibroblasts of two homozygous *PRRT2* patients display an increase in voltage-gated Na^+ current compared to control and heterozygous neurons.

These results are very interesting because, whereas the common heterozygous *PRRT2* mutations are associated with relatively mild and pleiotropic phenotypes, the very rare homozygous mutations hitting both alleles cause severe syndromic forms, cause all the isolated paroxysmal phenotypes with ataxia, PKD, severe epilepsy and are often associated with intellectual disability (Labate *et al*., 2012; Liu *et al*, 2016).

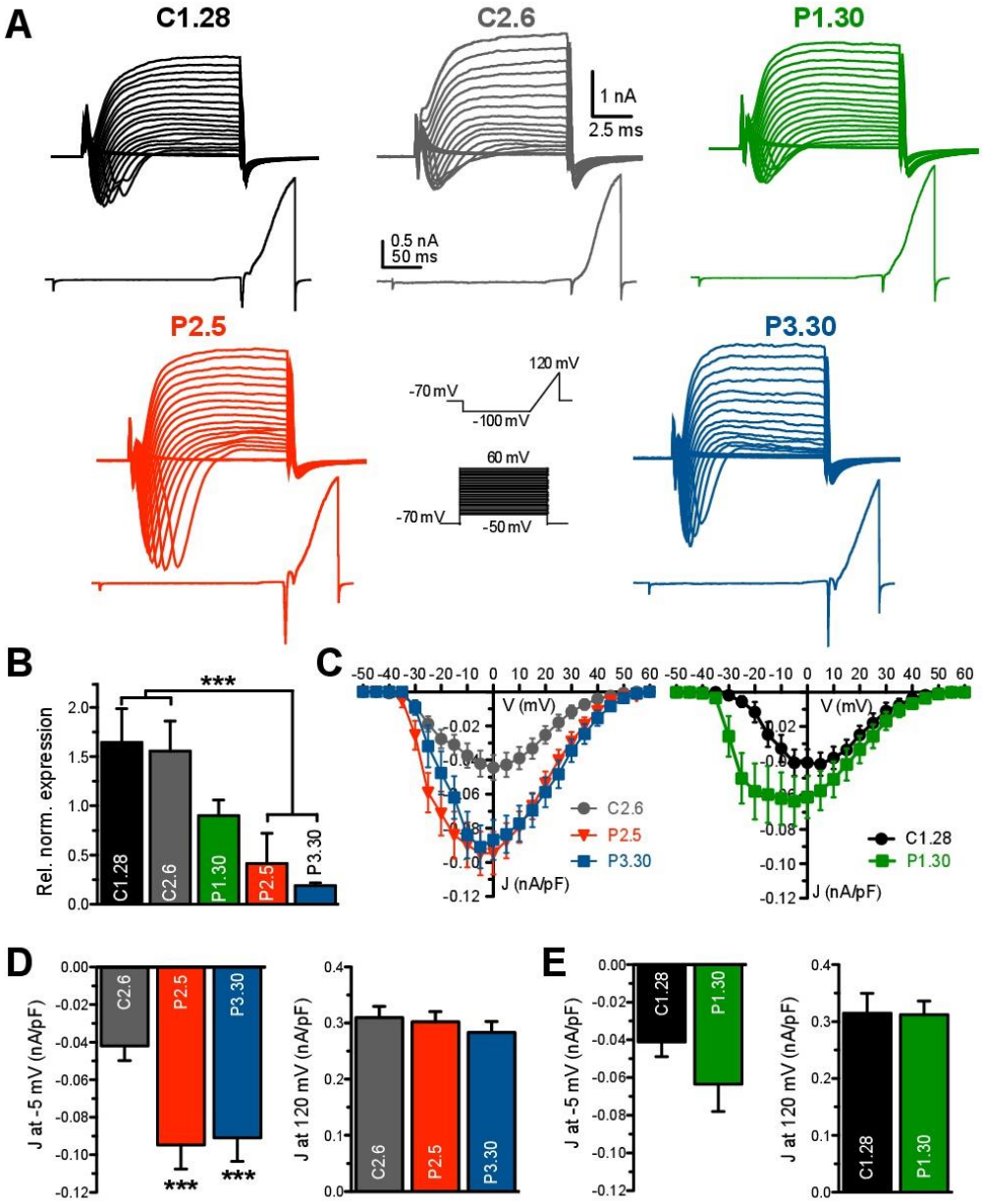

Figure 15. Patient iPSC-derived neurons show an increase of Na^+ channels current. A. Representative whole-cell families currents recorded in C1.28, C2.6 (from controls), P1.30 (from heterozygous Patient 1) and in P2.5 and P3.30 clones (from homozygous Patient 2 and 3). Currents were elicited using a family of depolarizing 10 ms voltage steps or a ramp protocol (*inset*). Cells were clamped at -70 mV before stimulation. **B.** Amount of PRRT2 mRNA expression tested by qRT-PCR in iPSC-derived neurons (25 days of differentiation). Results are expressed as means ±sem of n=3 independent experiments. *p< 0.05; Kruskal-Wallis/Dunn's tests. **C.** Current density vs voltage relationship for C2.6, P2.5 and P3.30 (*left*) and C1.28, P1.30 (*right*) iPSC-derived neurons, calculated using the protocol shown in panel A. Neurons were grouped in two distinct panels for clarity. **D, E.** Statistical analysis of the current density (as shown in panel C) at -5 mV (*left*) and at +120 mV (*right*) for clones C2.6, P2.5, P3.30 (D), C1.28 and P1.30 (E). The current density at +120 mV was calculated by the ramp protocol represented in panel A (as *inset*).

Data are shown as means ±sem (n=20 for C1.28, n=34 for C2.6, n=29 for P1.30, n=32 for P2.5 and n=19 for P3.30). ***p<0.001 Kruskal-Wallis/Dunn's tests.

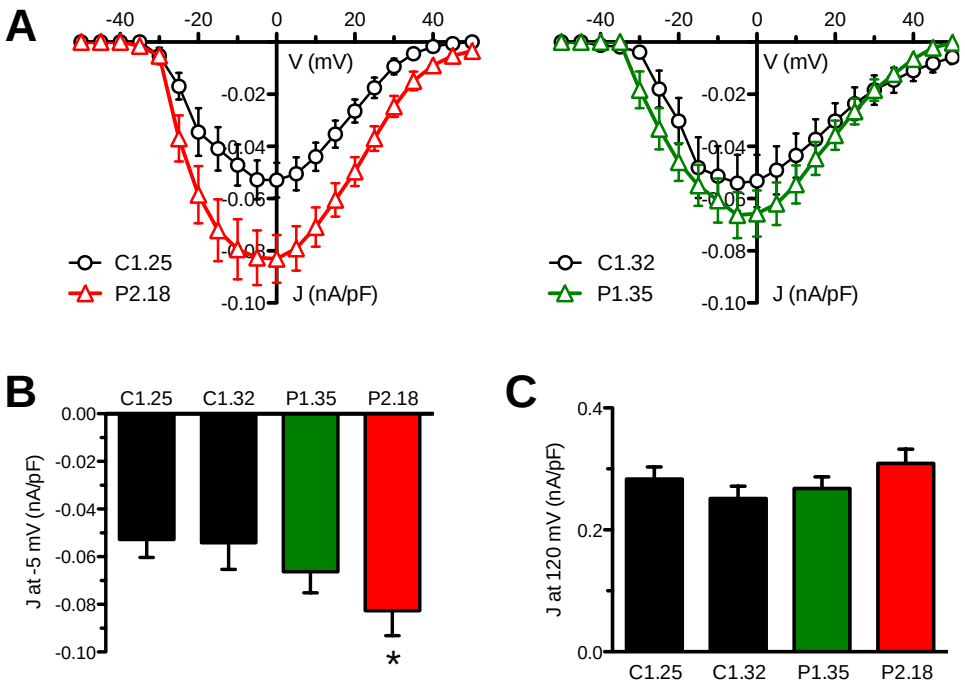

Figure 16. Homozygous neurons derived from different iPSC clones show the same increase in Na^+ current. A. Current density vs voltage relationship for C1.25 and P2.18 (*left* panel) and C1.32 and P1.35 (*right* panel) iPSC-derived neurons, analysed using the protocol shown in Fig. 15 A (*inset*). **B.** Statistical analysis of the current density at -5 mV (*left*) and at +120 mV (*right*) for clones reported in panels A-B. The current density calculated at +120 mV was analysed by the ramp protocol reported in Fig. 15 A (*inset*). Data are shown as mean ±sem. *p<0.05 vs C1.28, ##p<0.01, ###p<0.001 vs C2.6; Kruskal-Wallis/ Dunn's tests.

3.7. Homozygous iPSC-derived neurons have an altered intrinsic excitability rescued by the reintroduction of human wild-type form of PRRT2

Since the homozygous reprogrammed neurons showed an increase of voltage-gated Na^+ conductance, and because this conductance plays a central role in the control of cellular excitability, we next investigated further this genotype in order to study the intrinsic excitability properties.

To verify whether the observed phenotypic changes were due to the lack of PRRT2 protein, its expression was rescued in the homozygous neurons by

infection with lentivirus encoding Cherry-tagged WT human PRRT2. The P2.5-derived neurons were alternatively transduced with the PRRT2-Cherry or with the Cherry-alone virus as a control (MOCK), while control C1.28-derived neurons were only infected with Cherry-alone virus. Exogenous PRRT2 was correctly expressed in P2.5-derived neurons and the mRNA levels of PRRT2, determined by qRT-PCR, were greatly increased (**Fig. 17 A, B**).

Electrophysiological analysis confirmed the sustained increase of the JNa^+ in the MOCK-transduced P2.5 neurons observed before, whereas the re-expression of PRRT2-WT decreased it compared to the MOCK-transduced control (C1.28), suggesting a dose-dependent modulation of Na_V channels activity operated by PRRT2 (**Fig. 17 C, D**).

Because Na_V channels play a critical role in the initiation and propagation of APs in neurons, we next analysed the firing properties of both types of human-derived neurons. These properties were studied by delivering constant current pulses (1 s of duration) of increasing amplitude (5 pA steps) and then studying the resulting APs activated (**Fig. 17 E**). We observed that homozygous iPSC-derived neurons responded to the injection of a depolarizing current with APs firing whose frequency did not differ from control neurons. In contrast, re-expression of PRRT2 WT in homozygous neurons significantly decreased the evoked firing activity (**Fig. 17 E, F**). Homozygous iPSC-neurons exhibited a decreased input resistance and threshold for AP generation, and an increase of AP peak, amplitude and maximal slope of the rising phase of AP (**Fig. 17 G**). Of note, all these changes observed in homozygous neurons were fully normalized when WT form of human PRRT2 was reintroduced (**Fig. 17 G**). In summary, these experiments demonstrate, for the first time, that iPSC-derived neurons obtained from fibroblasts of two homozygous *PRRT2* patients display increased excitability and increased voltage-gated Na^+ current. They also show that iPSC-derived neurons from the heterozygous sibling exhibited electrical features that parallels the mild and age-dependent clinical manifestations. Finally, we show that the phenotype of homozygous iPSC-derived neurons is totally rescued by re-expression of WT human PRRT2.

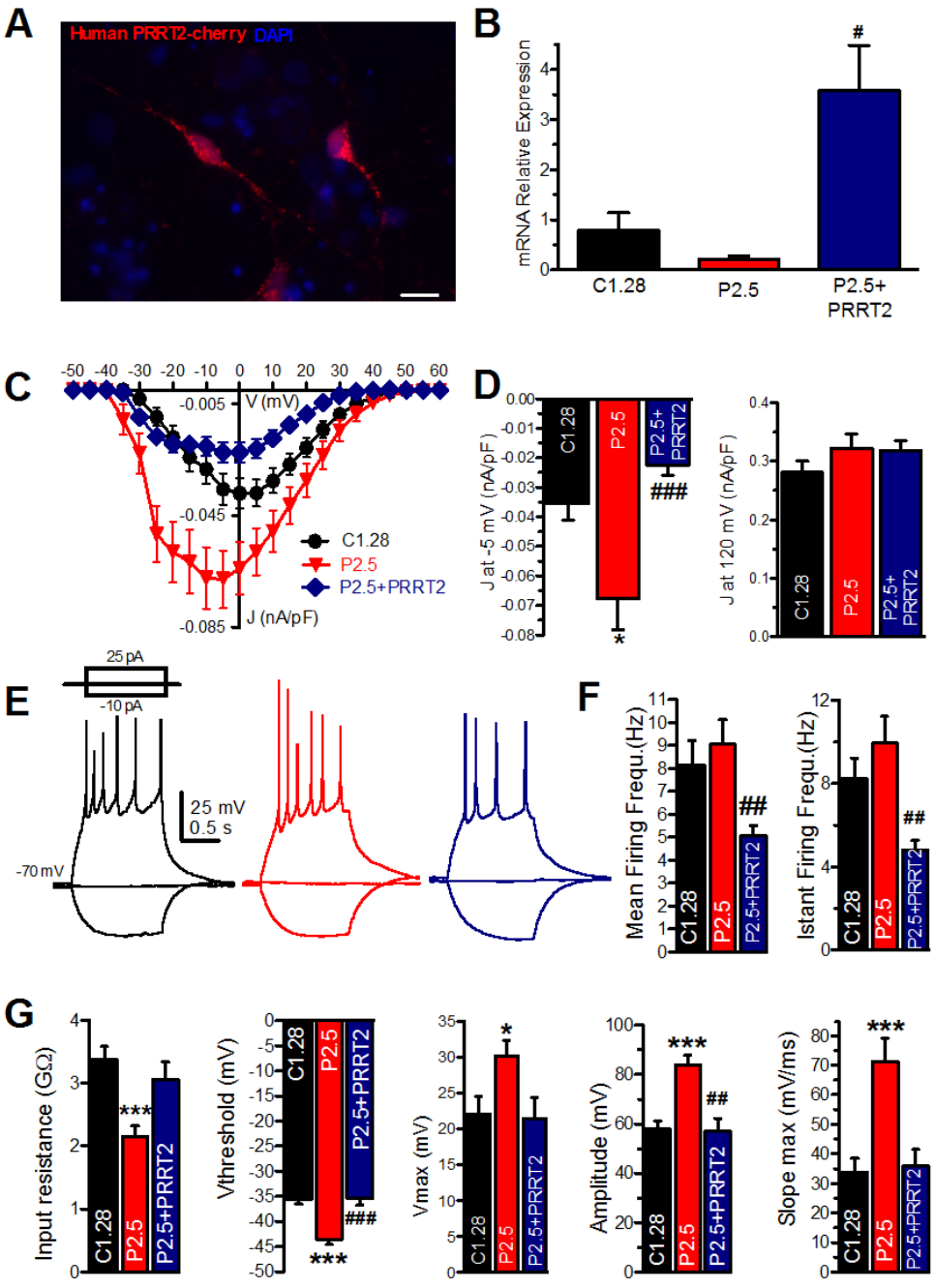

Figure 17. **Homozygous iPSC-derived neurons have an altered excitability that is rescued by the reintroduction of human WT form of PRRT2. A.** Representative image of fluorescence of homozygous P2.5 neurons infected with a Cherry lentivirus (red) used as reporter of PRRT2 expression. Scale bar, 20 µm. **B.** Expression of PRRT2 mRNA in MOCK-transduced C1.28 (black), MOCK-transduced P2.5 (red) and PRRT2-rescued P2.5 (blue) iPSC-derived neurons (25 days of differentiation). Results are expressed as means ±sem of n=3 independent experiments. **C.** Current density vs voltage relationship for the MOCK-transduced C1.28 and P2.5 iPSC-derived neurons and P2.5 cells in which PRRT2 expression was rescued (P2.5+ PRRT2). **D.** Statistical analysis of the J at -5 mV (*left*, for all conditions plotted in C) and at +120 mV. Data are expressed as means ±sem (n=35 for C1.28, n=31 for P2.5, n=26 for P2.5+PRRT2). **E.** Representative current-clamp recordings of APs evoked by the injections of 5 pA step current (1-s duration; protocol shown in the *inset*) for C1.28, P2.5 and P2.5+PRRT2 iPSC

neurons **F.** Mean and Instantaneous firing frequency of analysed conditions expressed as means ±sem. **G.** Input Resistance, Voltage Threshold of action potentials activation, Maximal voltage (Vmax), Amplitude and Maximal slope (slope max) of action potentials calculated for the first action potential evoked by minimal injection of current from all studied conditions. Data are shown as means ±sem (n=28 for C1.28, n=33 for P2.5, n=19 for P2.5+ PRRT2). In panels **B**, **D**, **F**, **G**: *p<0.05, **p<0.01, ***p<0.001 vs MOCK-transfected C1.28; #p<0.05, ##p<0.01, ###p<0.001 vs MOCK-transfected P2.5; Kruskal-Wallis/Dunn'stests.

3.8. PRRT2 modulates $Na_V1.2$ and $Na_V1.6$ channel conductance when expressed in HEK-293 cells

Excitability properties of neurons derive from the integration of excitatory and inhibitory synaptic inputs at the AIS of the neuronal cells. At this level, clusters of distinct Na_V channel subtypes generate APs (Kole *et al*., 2008). It has been reported that glutamatergic neurons display an abundant expression of subtypes $Na_V1.2$ and $Na_V1.6$ at the proximal and distal part of AIS respectively, while $Na_V1.1$ is particularly abundant in the AIS of GABA-ergic neurons (Mantegazza and Catterall, 2012). With the aim to unveil the mechanistic insights that underlie the increase of JNa^+ and the rise of intrinsic cellular excitability observed in iPSC-derived neurons, we performed whole-cell patch-clamp experiments on HEK-293 stably expressing the different subtypes of human Na_V channels 1.1, 1.2 and 1.6.

HEK-293 cells stably expressing $Na_V1.1$, $Na_V1.2$ or $Na_V1.6$ channels were transfected with the human form of full-length protein PRRT2 and with empty vector (MOCK), used as control. Strikingly, in the absence of channel inactivation (V_h= -120 mV), PRRT2 expression significantly reduced the Na^+ current amplitude (**Fig. 18 A**) and density (**Fig. 18 B**) in $Na_V1.2$ and $Na_V1.6$ but not in $Na_V1.1$ expressing cells. The fast inactivating voltage-gated Na^+ currents were studied by delivering 100 ms steps from -80 to +65 mV (V_h = -120 mV) with 5 mV increments (**Fig. 18 A**, *inset*), and were used to obtain the JNa^+/V relationship under all conditions tested.

The decrease of Na^+ current recorded mediated by $Na_V1.2$ and $Na_V1.6$ channels, when PRRT2 was expressed, was not accompanied by any significant variation of the normalized conductance-voltage (G/Gmax-V) curves, suggesting that PRRT2 does not affect the voltage-dependent activation of these channels (**Fig. 18 C**). In contrast, the voltage-dependence of fast inactivation was shifted to more negative potentials in

the presence of PRRT2 in both $Na_V1.2$ and $Na_V1.6$, but was unaffected in $Na_V1.1$-expressing cell lines (**Fig. 18 D**). The inactivation was more negative in HEK-293 $Na_V1.2$ and $Na_V1.6$ in the presence of PRRT2 of about 10 mV and 6 mV, respectively (**Fig. 18 D**, *right panels*).

These results indicate that a sustained negative modulation of the current density occurs when PRRT2 is co-expressed with $Na_V1.2$ or $Na_V1.6$ but not when PRRT2 is co-expressed with $Na_V1.1$. This negative modulation by PRRT2 is accompanied by changes in the voltage-dependence of inactivation which render these channels less excitable under resting conditions.

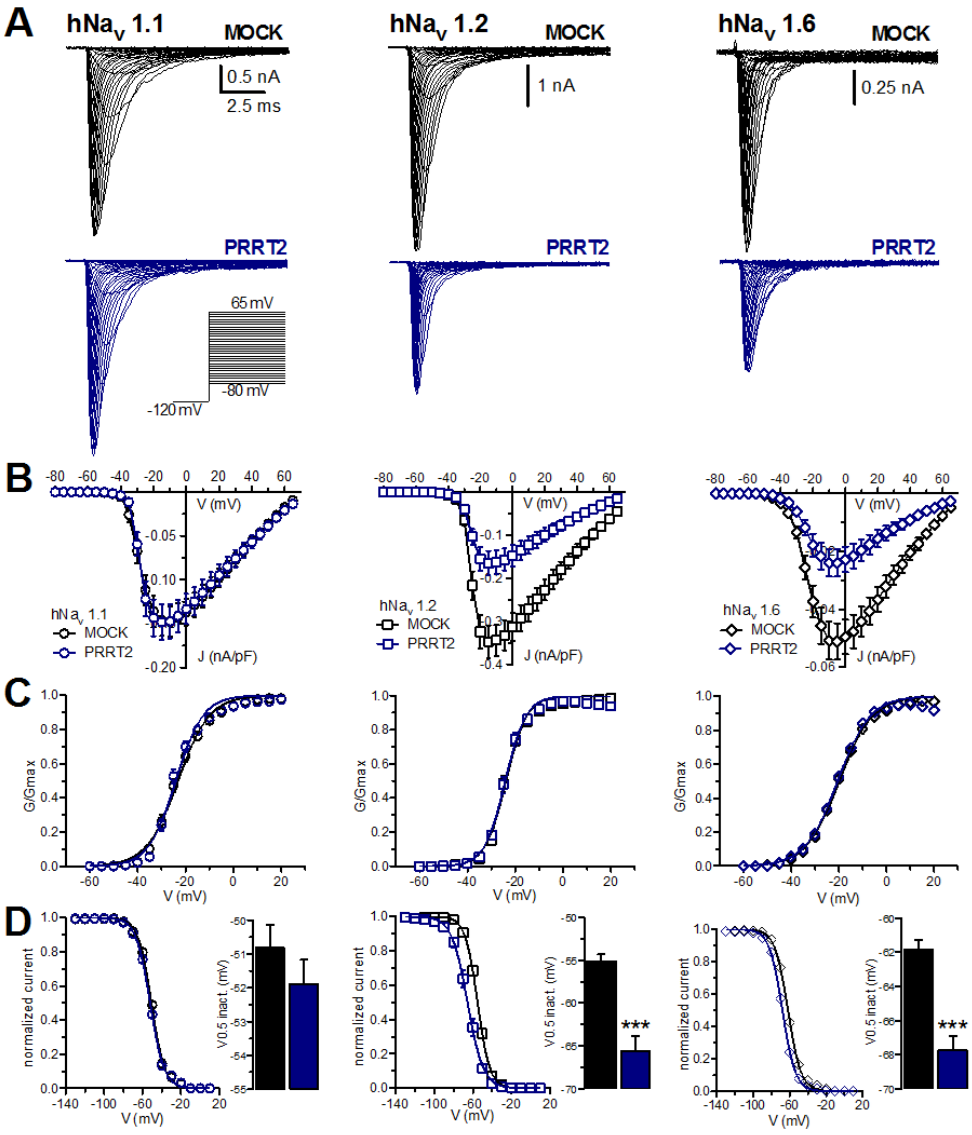

Figure 18. PRRT2 expression decreases the Na^+ current density of $Na_V1.2$ and $Na_V1.6$, but not of $Na_V1.1$, stably expressed in HEK-293 cells. A.

Representative traces of whole-cell recordings on HEK-293 clones stably expressing $Na_V1.1$ (*left*), 1.2 (*middle*) and 1.6 (*right*) and transiently transfected with empty vector (MOCK, black) or PRRT2 (blue). Currents were activated by 5 mV steps depolarization from -80 to 65 mV (V_h= -120 mV, *inset*). **B.** Current density vs voltage relationship for all conditions described in panel A. **C.** Voltage-dependence of activation for the three subtypes of Na_V channels co-expressed with MOCK or PRRT2. The lines are the best-fitted Boltzmann curves with the following mean values of half maximal voltage activation ($V_{0.5}$) and slope (k): $Na_V1.2$, MOCK, $V_{0.5}$: -23.89±0.19 mV, k: 4.39±0.16 (n=22), PRRT2 $V_{0.5}$: -24.16±0.21; k: 4.37±0.19 (n=20); $Na_V1.6$, MOCK, $V_{0.5}$: -19.81±0.14 mV, k: 6.99±0.12 (n=27), PRRT2 $V_{0.5}$: -20.46±0.17, k: 6.83±0.15 (n=29). **D.** Steady-state inactivation curves for all conditions tested. The lines are the best-fitted Boltzmann curves and the half-maximal voltages for inactivation ($V_{0.5}$ inact.) was graphed on the right. Data are means ±sem ($Na_V1.2$: MOCK, n=22 and PRRT2, n=18; $Na_V1.6$: MOCK, n=24 and PRRT2, n=21). ***p<0.001; unpaired Student's t-test or Mann-Whitney U-test.

3.9. PRRT2 specifically interacts with $Na_V1.2$ and 1.6 α-subunits and regulates their surface expression

The electrophysiological results obtained in *PRRT2*-KO neurons, in iPSC-derived neurons from homozygous patients and in HEK-293 cells heterogously expressing Na_V channels, suggest a possible interaction between PRRT2 and $Na_V1.2$/$Na_V1.6$ α-subunits. To address this hypothesis, a possible interaction between the human form of full-length PRRT2 protein and the $Na_V1.2$/$Na_V1.6$ α-subunits was tested.

To test this possibility, PRRT2 was fused with the HA-tag and the interactions with the Na_V channel subtypes expressed in HEK-293 were evaluated by pull-down assays. The unrelated bacterial alkaline phosphatase (BAP) protein was used as control (**Fig. 19 A**). Co-immunoprecipitation assays showed that PRRT2 pulled down the $Na_V1.2$/$Na_V1.6$ α-subunit, with any precipitation of $Na_V1.1$ (**Fig. 19 A**). These data were in agreement with the patch-clamp experiments in HEK-293 cell lines expressing different subtypes of Na_V. These results combined with the effect on the *PRRT2*-KO neurons and on the iPSC-derived neurons, suggest that PRRT2 could be also a modulator of other properties of Na_V channels, such as channel trafficking, membrane exposure and/or stability.

In order to discriminate between these possibilities, we performed surface biotinylation assays in HEK-293 cell lines expressing the various Na_V subtypes transfected with either *PRRT2*-HA or an empty vector as control

(**Fig. 19 B**, *left panel*). We observed that whereas the total levels of each Na_V α-subunit were unmodified between MOCK- and PRRT2-transfected cells, the cell surface abundance of $Na_V1.2$/$Na_V1.6$ was significantly decreased in the presence of PRRT2 with respect to control, a result that was paralleled by a quantitative similar increase in the intracellular fraction (**Fig. 19 B**, *right panel*). By contrast, no effect on surface was detected about the surface expression of $Na_V1.1$.

Altogether, these results show that PRRT2 interacts with $Na_V1.2$ and 1.6 channels exerting a negative modulation on the expression increase of both subtypes of Na_V. At this point, data also indicate that the JNa^+ and the hyperexcitability observed in mouse neurons and in *PRRT2*-KO human neurons were correlated to the modulation of functional $Na_V1.2$ and $Na_V1.6$ channels. These results strongly suggest that PRRT2 could regulate neuronal excitability also through the control of the expression at the plasma membrane of relevant voltage-gated Na^+ channels.

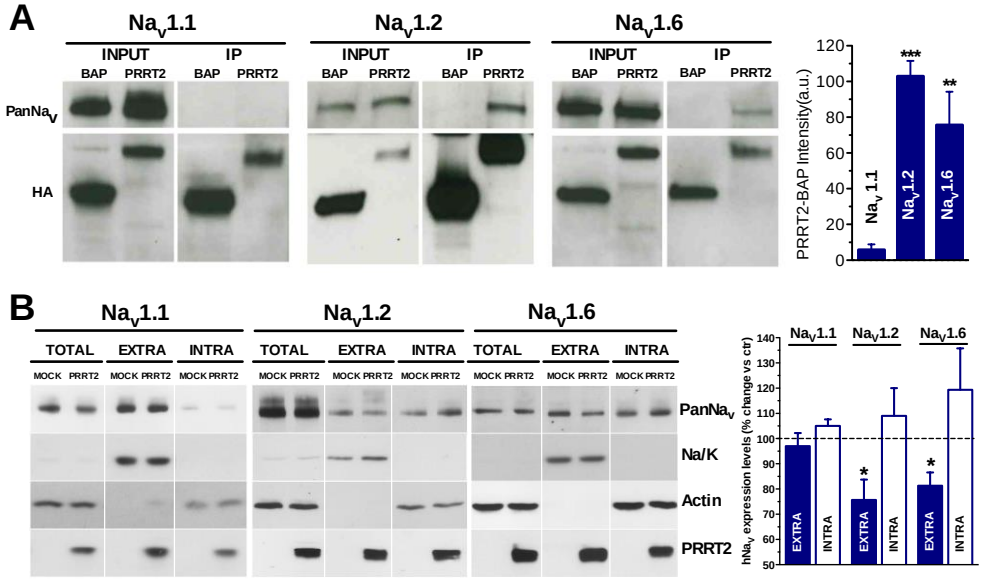

Figure 19. PRRT2 interacts specifically with $Na_V1.2$ and 1.6 and modulates their surface expression. A. *Left*: Representative immunoblots of $Na_V1.1$, $Na_V1.2$ and $Na_V1.6$ co-immunoprecipitated by PRRT2. Either HA-tagged PRRT2 (PRRT2) or bacterial alkaline phosphatase (BAP) was expressed in HEK-293 cells that express human $Na_V1.1$, $Na_V1.2$ or $Na_V1.6$. Cells lysates (INPUT, 10 µg) and samples immunoprecipitated by anti-HA beads (IP) were analyzed by Western blotting with anti-PanNa_V and anti-HA antibodies. *Right*: Quantification of the PanNa_V signal in PRRT2 immunoprecipitates normalized to the BAP values. Means ±sem of n=3 independent experiments. **p<0.01; ***p<0.001 vs $Na_V1.1$; ANOVA/Dunnett's tests vs $Na_V1.1$. **B.** Left: Representative immunoblots of cell

surface biotinylation performed in HEK-293 cells expressing $Na_V1.1$, $Na_V1.2$ and $Na_V1.6$ and transfected with *PRRT2*-HA or empty vector (MOCK). Total lysates (TOTAL), biotinylated (cell surface, EXTRA) and non-biotinylated (intracellular, INTRA) fractions were analyzed by Western blotting. Membranes were probed with antibodies to $PanNa_V$, PRRT2, Na^+/K^+-ATPase (Na^+/K^+) and actin, the latters used as markers of cell surface fraction and intracellular fraction, respectively. *Right*: Cell surface and intracellular $PanNa_V$ immunoreactivities are expressed in percent of the respective MOCK value after normalization to Na^+/K^+-ATPase (for EXTRA fraction) and actin (for INTRA fraction). Means ±sem of n=3 independent experiments. *$p<0.05$; paired Student's t-test.

4. DISCUSSION

Previous studies demonstrated that PRRT2 has a potential role in maintaining the pre-synaptic structure and function (Valente *et al*., 2016a). Furthermore, it was suggested that PRRT2 is likely involved in regulating synaptic vesicle fusion and the ensuing release of neurotransmitters (Lee *et al*., 2012, Stelzl *et al*., 2005, Tan *et al*., 2017, Valente *et al*., 2016).

Even though it is well known that the expression of PRRT2 is neuron-specific although its functions in the regulations of neuronal networks it is still largely unknown. Recent studies have indicated that *PRRT2* is the major gene at the basis of a broad spectrum of rare infantile neurological disorders (Gardiner *et al*., 2012). It has been shown that heterozygous and homozygous mutations of PRRT2 cause impaired or *loss-of-function* expressions of the protein and recapitulate the all paroxysmal phenotypes (Labate *et al*., 2012; Delcourt *et al*., 2015).

Several studies have investigated the role of PRRT2 in synaptic transmission, both *in vitro* and *in vivo* (Liu *et al*., 2016; Valente *et al*., 2016a; Michetti *et al*., 2017; Tan *et al*., 2017). PRRT2 is expressed at both glutamatergic and GABA-ergic neurons, although it appears more reliably targeted at excitatory synapses. A recent work from our laboratory has found that an acute downregulation of the PRRT2 gene led to synaptic alterations, such as the decrease of synaptic glutamatergic density, but without altering its ultrastructure (Valente *et al*., 2016a). This effect was accompanied by an increase in the number of docked SVs, as a result of a decreased probability of SVs release in excitatory synapses. In addition, a decrease of glutamatergic synchronous release was observed during synaptic transmission after acute deletion of PRRT2 by RNA interference (Valente *et al*., 2016a). These data were explained by the tenet that PRRT2 was functionally linked to the Ca^{2+}-sensitive machinery involved in the neurotransmitter release.

A similar study demonstrated that *knocking-down* PRRT2 expression *in vivo* by using *in utero* electroporation of shRNA into cortical neurons resulted in a delay in neuronal migration during embryonic development and a marked decrease in synaptic density after birth (Liu *et al*., 2016).

A recent behavioral study reported that *PRRT2*-KO mice exhibit the same symptoms as patients with *PRRT2* diseases (Michetti *et al*., 2017). Those

mice were characterized by wild running and jumping in response to intense sensory stimuli and increased sensitivity to the epileptogenic action of convulsants.

All of these data suggest that the alteration of PRRT2 functionality leads to an imbalance between inhibitory and excitatory transmission. Therefore, the main objective of this doctoral work was to analyze the modulatory role of PRRT2 on the electrical properties of neurons by using different complementary approaches. So, we generated a human model of PRRT2-linked diseases based on the generation of iPSC-derived neurons obtained from fibroblasts of a consanguineous patients, carrying the *c.649dupC* common *loss-of-function* mutations in heterozygosity or homozygosity (Labate *et al*., 2012). The latter approach has allowed to compare the human KO phenotype with the cellular and network features of mouse *PRRT2*-KO neurons.

4.1. Constitutive deletion of *PRRT2* alters synaptic connectivity

In this work we have analyzed the electrical properties of primary hippocampal neurons in which we constitutively deleted *PRRT2* in order to create a model for the study of the paroxysmal phenotype *in vitro*. Data from previous works highlighted a possible role of PRRT2 in synaptic formation and rearrangement of synaptic connections (Liu *et al*., 2016; Valente *et al*., 2016a). We evaluated the effect of *PRRT2* silencing on the spontaneous neurotransmitter release at both excitatory and inhibitory synapses. We observed that the phenotype of spontaneous release was similar to that observed upon acute silencing of *PRRT2* in neurons (Valente *et al*., 2016a). In hippocampal neurons without *PRRT2* we observed a decreased spontaneous frequency of mEPSCs while other parameters of spontaneous release such as amplitude, rise, decay and area were fully preserved. This suggests an impairment of spontaneous release at single synaptic sites. Since this effect was associated with decreased synaptic density in excitatory neurons, these results indicate that the absence of *PRRT2* causes structural alterations of the synapses (Valente *et al*., 2016a).

Of note, the lack of PRRT2 in excitatory synapses induced a decrease in the probability of release and a slowdown of the release kinetics. Although this effect caused a decreased amplitude of evoked excitatory post-synaptic current and charge of synchronous glutamate release in response to single stimuli, it also led to a markedly strengthening of the facilitation and decreased depression during high frequency activity (see, e.g., Millar *et al*., 2002). A possible explanation of the decreased Pr of RRP may be that residual Ca^{2+} and the local Ca^{2+} influx decreases the probability of release by altering the binding to different Ca^{2+} sensors in *PRRT2*-KO neurons, and hence impairing the SVs fusion process. The result of a reduced Ca^{2+}-sensitivity of release in the absence of PRRT2 suggests that defects caused by PRRT2 silencing reside in the dysregulation of the Ca^{2+}-sensing apparatus, as previously reported for the interaction of PRRT2 with SNAP-25 and Syt1/Syt2 (Valente *et al*., 2016a).

Interestingly, a completely different effect was found in GABA-ergic neurons. While spontaneous release was not significantly different between *PRRT2*-KO and WT conditions in GABA-ergic neurons stimulated with a paired-pulse stimulus, we have observed that the inhibitory strength increase due to a parallel increase in Pr. This alteration may reflect an adaptive mechanism of plasticity in GABA-ergic transmission in response to chronic *PRRT2* deletion (see, e.g., Scharfman and Brooks-Kayal, 2014). Moreover, this effect was associated with a more profound depression of inhibitory transmission in response to both paired stimuli and high frequency trains.

These results demonstrate that STP studied at excitatory and inhibitory synapses is affected in opposite way upon *PRRT2* deletion. These opposite effects support the concept that an alteration of excitation/inhibition imbalance in the STP frequency domain might cause a state of hyperexcitability/instability in neuronal KO networks. This tenet is supported by the view that in general the network dynamics are highly dependent on the STP of excitatory and inhibitory synapses, rather than on their basal transmission properties (Abbott and Regehr, 2004; Fioravante and Regehr, 2011).

From these results, we can conclude that PRRT2 seems to participate in the changes of the synaptic homeostasis, affecting glutamatergic synapses whereas GABA-ergic synapses are subjected to adaptive changes in the absence of this protein.

4.2. *PRRT2* deletion induces network instability and hyperactivity

PRRT2-linked disorders are associated to different symptoms that can be due to network instability as result of an alteration of neuronal basal electrical and synaptic activities in specific cortical/subcortical areas that are normal at rest, but can be imbalanced after external stimulations. In this study, we have observed that *PRRT2*-KO hippocampal networks display clear signs of hyperexcitability, resulting in enhanced network synchronization and short-term responsiveness to external stimuli.

The displacement of information in the brain relies on a functional balance between excitatory and inhibitory networks. Moreover, in response to perturbing conditions that alter network activity, compensatory mechanisms are recruited to restore the initial circuit set point (Gao and Wehr, 2015). These responses include modulation of excitatory and inhibitory postsynaptic strength, alterations in presynaptic neurotransmitter release probability, and adjustment of intrinsic membrane excitability (Turrigiano *et al*., 2011). Under these conditions, the extent of network firing activity depends from the excitatory/inhibitory balance properties, and hence from the STP properties of glutamatergic and GABA-ergic synapses. As STP of excitatory synapses acts as a high band-pass filter that propagates high frequency activities and prevents the transmission of random low frequency (Abbott and Regehr, 2004), the enhanced facilitation of excitatory transmission of *PRRT2*-KO networks during collective high-frequency events may be responsible for network hyperactivity and hyper-synchronization.

In this study we also report that *PRRT2*-KO hippocampal neurons have an increase of evoked firing properties, a result that was accompanied by an increase of Na^+ current density in KO cells. This finding could be relevant to explain the enhancement of network bursting behavior observed in KO network analysed by MEA technology because slow intrinsic neuronal properties drive single neurons oscillations and determine their entrainment in synchronized collective discharge (Suresh *et al*., 2016).

The increase of single cell firing properties together with the enhanced bursting activities in the network evoked from spontaneous foci more evident in response to localized electrical stimulation that, in *PRRT2*-KO networks, induced a short-lived status of high probability in the discharge of

APs. The increase of STP recorded in *PRRT2*-KO networks also indicates a possible role of this protein in the homeostatic control of neuronal network. Interestingly, the larger evoked response of PRRT2 networks is temporally localized in a brief post-stimulus window followed by a subsequent wave of strong synaptic inhibition. This increase of inhibitory strength after constitutive inactivation of *PRRT2* may suggest the presence of a compensatory mechanism that controls and reduces the effect on network hyperexcitability. It is well known that PRRT2 is highly expressed in different brain areas, including the cerebellum, which is involved in processing sensory information of motor skills (Michetti *et al*., 2017). The data indicate a network instability when *PRRT2* is chronically inactivated, which could explain the motor impairment of patients with *PRRT2*-related disorders associated to aberrant and paroxystic movements.

4.3. From *PRRT2*-KO to iPSC-derived human neurons

While *PRRT2*-KO model reproduced the phenotype of human *PRRT2* mutations, patient iPSC-derived neurons provides an applicable platform to mimic the human pathogenic process (Takahashi and Yamanaka, 2006) and recapitulates the disease in a petri dish, therefore facilitating the investigation of disease-specific phenotypes *in vitro (*Stadtfeld and Hochedlinger*,* 2010*)*.

IPSC technology, used to create a disease model for *PRRT2* mutations, has been recently applied in two studies. In the first work, iPSC lines were generated from epithelial cells in urine samples of single PKD patient with the same mutation reported in our study, a *c.649dupC* heterozygous mutation (Zhang *et al*., 2015). In this work, PKD-iPSCs did not show any significant changes in ion currents that underlie the excitability properties of neurons, i.e. Na_V and K_V conductances.

In the second study, multiple PKD-iPSC lines from two familial PKD patients with two different nonsense mutations (*c.487C>T* and *c.573dupT*) were generated (Li *et al*., 2016). PKD-iPSCs exhibited defects in neural conversion via a step-wise neural induction method, with an extremely low efficiency in generating NPCs compared to control-iPSCs.

In the present work, we obtained iPSC-derived functional mature neurons, exhibiting similar efficiency across genotypes. We demonstrated for the first

time that cells obtained from fibroblasts of two homozygous *PRRT2* patients presented a significant increase in JNa^+ and firing activity. Conversely, the heterozygous siblings exhibited a phenotype that paralleled the mild form of the clinical manifestations (Liu *et al*., 2016), in accord to the previous results from Zhang *et al*. (2015). Moreover, homozygous iPSC-derived neurons showed an altered intrinsic excitability rescued by the reintroduction of human WT form of *PRRT2*. This capacity of PRRT2 to restore JNa^+ and firing activity to a level comparable to that of control, may suggest that PRRT2 would influence the functionality of the Na_V channels. Interestingly, a recent electrophysiological study has shown that mutated forms of different Na_V α-subunits cause an induction of an increased persistent Na^+ current in neuronal and muscle disorders of excitability (Jarecki *et al*., 2010). This cellular phenotype of hyperexcitability of iPSC-derived neurons is recapitulated in hippocampal primary neurons from the *PRRT2*-KO mouse that also display a marked hyperexcitability at both single cell and network levels. The excitability properties of neuronal cells depend on the integration of the excitatory and inhibitory inputs at the neuronal trigger zone called AIS. At this level distinct clusters of different subtypes of Na_V channels generate the potential response producing APs. Interestingly, the distal part of the AIS of glutamatergic neurons, has an abundant expression of $Na_V1.6$, while the proximal part has more $Na_V1.2$, which are the same channel subtypes that were inhibited by PRRT2 when recombinantly expressed in HEK-293 cells. On the contrary, the $Na_V1.1$ subtype, which is not affected by PRRT2 under conditions, plays a major role in the AIS of GABA-ergic neurons (Ogiwara *et al*., 2007; Debanne *et al*., 2011; Catterall, 2014). This is an agreement with the results on *PRRT2*-KO neurons, showing that PRRT2 may alter more glutamatergic than GABA-ergic synapses and indicate that the latter are not altered from the adaptive changes when PRRT2 is absent.

Our data show that this selective negative modulation of $Na_V1.2$ and $Na_V1.6$ mediated by PRRT2 is caused by changing in interfering with the total amount of channels in the plasma membrane as demonstrated by the increased voltage-activated Na^+ conductance, and by the increase of cellular excitability when PRRT2 was absent. The mechanisms that underlie this effect may depend on disturbed trafficking in favor of internalization. Moreover, PRRT2 also modulates the biophysical properties of subtypes $Na_V1.2$/$Na_V1.6$ channels. The results indicate that the voltage-

dependence of fast inactivation was shifted to more negative values and the recovery from inactivation was slowed-down in the presence of PRRT2 decreasing the amount of Na_V channels that can be activated under resting conditions. Altogether, the data of this work clearly show that PRRT2 alter the biophysical properties of $Na_V1.2$/$Na_V1.6$, leading to a less excitability of the neurons, but only when correctly expressed. PRRT2 negatively modulates $Na_V1.2$/$Na_V1.6$ by decreasing their abundance in the plasma membrane promoting their internalization.

4.4. Possible physiological and pathophysiological role of PRRT2 in Paroxysmal Disorders

In this study we have demonstrated that PRRT2 interacts with Na_V channels that play a fundamental role in generation and conductance of action potentials (Mantegazza *et al*., 2012). This specific interaction between PRRT2 and Na_V channels and its effect on neuronal excitability indicate that in a physiological conditions PRRT2 has an additional role which implements its effect in the regulation of neurotransmitter release (Valente *et al*., 2016a). The observed interactions of PRRT2 with $Na_V1.2$/$Na_V1.6$ channels, which are major regulators of the excitability of excitatory neurons, represent a plausible basis for the phenotype of PRRT2-linked disorders. Several considerations support the pathophysiological relevance of these findings. Firstly, the behavioral phenotype of the *PRRT2*-KO mouse (Michetti *et al*., 2017) closely resembles the paroxysmal phenotype of mice with mutations in voltage-dependent channels (Becker *et al*., 2009). Secondly, several studies reported mutations in different Na_V channels that cause a spectrum of epileptic and dyskinetic syndromes negative for *PRRT2* mutations (Heron *et al*., 2002; Scalmani *et al*., 2006; Gardella *et al*., 2016). The co-segregating heterozygous missense mutation (*c.4447G>A*) described in sixteen members of three families (Gardella *et al*., 2016) hits the inactivation gate of the $Na_V1.6$ α-subunit, suggesting an impaired channel inactivation that is consistent with the here described effects of PRRT2 on the $Na_V1.6$ channels. Moreover, affected individuals with PRRT2-related paroxysmal manifestations respond well to low doses of Na^+ channel

blockers, such as carbamazepine or phenytoin (Chen *et al*., 2011). Furthermore, patients with the same *PRRT2* mutations may present variable phenotypes, indicating a pleiotropy in clinical manifestations (Brueckner *et al*., 2014) and comorbid conditions (Ebrahimi-Fakahari *et al*., 2015; Gardiner *et al*., 2015). This pleiotropy has been found also in different channelopathies (Dichgans *et al*., 2005), suggesting that the differential expression of Na^+ channels subtypes modulate the broad phenotypic expression of *PRRT2* mutations.

5. CONCLUSIONS

The study presented in this thesis demonstrates that the lack of PRRT2 leads to neuronal hyperexcitability through the upregulation of Na_V channels in homozygous *PRRT2*-KO human and mouse neurons. In *PRRT2*-KO animal model, chronic absence of PRRT2 markedly alters neuronal network dynamics, making it more excitable and instable. We observed the same altered intrinsic excitability in human neurons obtained from iPSCs of patients carrying the most common mutation of the *PRRT2* gene. Previous functional studies showed that *PRRT2* is a gene with pleiotropic functions in the control of neuronal excitability and synaptic transmission. The research presented in this thesis reveals additional mechanistic insights on PRRT2 regulation on neuronal activity. The results show that PRRT2 operates as negative modulator of $Na_V1.2$ and $Na_V1.6$ channels which are selectively expressed in excitatory neurons. Given the predominant paroxysmal character of pathologies depending of PRRT2 mutations, the imbalance in excitatory and inhibitory activity by lack of negative modulation of Na_V channels at excitatory neurons appears as the key pathogenetic mechanism.

6. MATERIALS AND METHODS

6.1. Animals

PRRT2-KO mice were generated by EUCOMM/KOMP using a targeting strategy based on the "knockout-first" allele (Michetti *et al*., 2017). Mutant animals in a C57BL/6N background were propagated as heterozygous colonies in the IIT SPF facility. Genotyping was performed by PCR as previously described (Michetti *et al*., 2017) to identify WT and KO embryos used in the experiments. All experiments were carried out in accordance with the guidelines established by the European Communities Council (Directive 2010/63/EU of March 4th, 2014) and were approved by the Italian Ministry of Health (authorization n. 73/2014-PR and n. 1276/2015-PR).

6.2. Cell culture procedures

Low-density hippocampal neurons: primary cultures of hippocampal neurons were prepared from WT and *PRRT2*-KO mice as previously described (Baldelli *et al*., 2007; Chiappalone *et al*., 2009) with slight modifications. Animals were sacrificed by CO_2 inhalation, and 17/18-day embryos (E17-18) were removed immediately by cesarean section. In brief, hippocampi or cerebral cortices were dissociated by enzymatic digestion in 0.125% trypsin for 20 min at 37 °C and then triturated with a fire-polished Pasteur pipette. No antimitotic drugs were added to prevent glia proliferation.

Autaptic hippocampal neurons: Primary cultures of hippocampal autapses were prepared as described previously (Valente *et al*. 2016b) with slight modifications. Dissociated neurons were plated at very low density (20 cells/mm^2) on microdots (40-300 μm in diameter) obtained by spraying a mixture of poly-L-lysine (0.1 mg/mL) and collagen (0.25 mg/mL) on Petri dishes or glass coverslip, previously pretreated with 0.15% agarose. Under this culture conditions, each coverslip showed about 10 isolated single autaptic neurons grown on polylysine microdots. Electrophysiological recordings were conducted on single and isolated autaptic neurons between 10 and 15 DIV.

HEK-293 cells: Stably expressing human $Na_V1.1$, $Na_V1.2$ or $Na_V1.6$ HEK-293 cell lines, were kind gifts from Drs. Enzo Wanke and Marzia Lecchi (University of Milano-Bicocca, Italy). HEK-293 cells were maintained in DMEM/F12 (1:1) Glutamax supplemented with 10% fetal bovine serum, 100 units/ml penicillin, 100 µg/ml streptomycin and 500 µg/ml G418 for selection of Na_V channels stably transfected cells. Cell lines were transfected according to manufacturer's instructions at 80% confluency using Lipofectamine 2000. All reagents were purchased from Thermo Fisher Scientific.

6.3. Generation and maintenance of iPSC lines

IPSCs were generated from dermal fibroblasts obtained from skin biopsies of three siblings of a consanguineous family segregating the common *PRRT2* mutation *c.649dupC*. Skin biopsies were performed upon informed consent at the Department of Medical Sciences, Institute of Neurology, University "Magna Graecia", Catanzaro, Italy, using the punch biopsy procedure and fibroblasts were cultured in RPMI (GIBCO) supplemented with 20% (v/v) FBS, 2 mM L-Glutamine and 1% Penicillin/Streptomycin. For control iPSC lines (FF0201992 and FF0631984), fibroblasts of age-matched normal male donors were obtained from the "Cell Line and DNA Biobank from Patients affected by Genetic Diseases" (Institute Giannina Gaslini, Genova, Italy), that is member of the Telethon Network of Genetic Biobanks (project no. GTB12001).

Cells at low passages (2-3) were reprogrammed using the Sendai virus non-integrated CytoTune™-iPS reprogramming Kit (Thermo Fisher Scientific) according to manufacturer's instructions. CytoTune™-iPS reprogramming Kit uses vectors based on a modified, non-transmissible form of Sendai virus to safely and effectively deliver and express key genetic factors necessary for reprogramming somatic cells into iPSCs. The reprogramming vectors include the four Yamanaka's factors, OCT3/4, SOX2, KLF4, and C-MYC, shown to be sufficient for efficient reprogramming.

Colonies appeared after 25 days. At least 20 single colonies for each genotype were isolated by manual picking, maintained on Geltrex-coated (Thermo Fisher Scientific) plates on a layer of mitotically inactivated murine

embryonic CF-1 fibroblasts (GlobalStem) in human ESC culture medium consisting of DMEM/F12 Glutamax supplemented with 20% knockout serum replacement, 1% non-essential AAs, 1% penicillin/streptomycin, 0.55 mM β-mercaptoethanol and 10 ng/ml recombinant human fibroblast growth factor-2 (FGF-2) (all from Thermo Fisher Scientific). Cultures were fed daily and passaged using collagenase IV every 3-5 days. Each clones was expanded separately as cell lines, which are named in deidentified codes. At passage 15, clones were tested for pluripotency marker expression by qRT-PCR and immunofluorescence. For *in vitro* differentiation into cells of all three germ layers, confluent undifferentiated iPSC were incubated in 1 mg/ ml collagenase IV (Thermo Fisher Scientific) for 1 h at 37 °C and transferred to 100 mm low attachment plates in EB medium (hESC without FGF2).

6.4. Differentiation of iPSC clones into neurons

For neuronal differentiation, embryoid bodies were generated from iPSCs clones, cultured for five days in suspension in embryoid body medium and then collected and plated into a Geltrex-coated 6-well plates for additional seven days to form neural tube-like rosettes. After seven days, the emerging neural rosettes were picked manually, completely dissociated with Accutase at 37°C for ten minutes and then transferred to Geltrex-coated plates in NPC medium consisting of DMEM/F12 supplemented with N2 (1:100), B27 (1:500; GIBCO), epidermal growth factor (20 ng/ml) and FGF-2 (20 ng/ml). NPCs were expanded and fed every other day. To obtain terminally differentiated neurons, NPCs were infected with a lentiviral vector containing Green Fluorescent Protein (GFP)-expressing lentiviruses in co-culture with E18 rat primary cortical neurons at seven DIV, previously infected with TdTomato-Lentivirus, in order to discriminate human cells from rat cells. The differentiation lasted 25-45 days in Neurobasal-A medium supplemented with 2mM L-glutamine, N2, B27, BDNF and GDNF and retinoic acid. For iPSCs, three germ layer cells and NPCs, staining was performed with PSC 4-MARKER ICC Kit, 3-GERM LAYER ICC Kit and NSC ICC Kit respectively (all from Thermo Fisher Scientific) according to manufacturer’s instructions.

6.5. Analysis of network activity of primary hippocampal cultures on MEAs

Planar MultiElectrode Arrays (768-GL1-30Au200 from Axion BioSystems) were used to record the electrical activity of WT and *PRRT2*-KO primary hippocampal networks. MEA plates are composed of 12 wells, each containing an array of 64 nano-porous gold electrodes (30 µm electrode diameter; 200 µm center-to-center spacing). To enhance hydrophilicity, wells were treated overnight with poly-L-lysine (0.1 mg/ml, Sigma-Aldrich) in 100 mM borate buffer pH 8.5 and rinsed three times with sterile deionized water to remove the excess of poly-L-lysine. Afterwards, neurons were plated on MEAs at a density of 80,000 per well. Neuronal cultures were maintained in 1.5 ml cell culture medium (Neurobasal medium, 1% Glutamax, 2% B27, 1% Penicillin-streptomycin) and half-volume replacement of the medium was performed twice weekly, at least 24 h before the electrophysiological experiments. Spiking activity from hippocampal networks was recorded using the Axion BioSystems hardware (Maestro amplifier and Middle-man data acquisition interface) and software (Axion Integrated Studio, version 2.1). After 1,200 x amplification, raw data were digitized at 12.5 kHz/channel and stored on a hard disk for subsequent off-line analysis.

Recordings were collected between the second and the third week *in vitro* from a total of 95 cultures (46 from *PRRT2*-KO and 49 for WT, four independent preparations). Spontaneous activity was recorded for 15 min at 37 °C under ambient atmospheric conditions, starting ten minutes after the transfer from the incubator to the Maestro apparatus to ensure stabilization of the electrical signal. On the last day of recording, the spontaneous activity was monitored for 20-30 min before applying low-frequency electrical stimulation. One electrode of the array was chosen as stimulation site based on visual inspection of the evoked responses, to ensure maximal activation of the network. The stimulus pulse was biphasic (1.5 V peak-to-peak amplitude, 500 µs duration, 50% duty cycle) and was delivered at 0.2 Hz (Wagenaar et al., 2004). Only the electrodes recording spontaneous spiking activity was chosen as stimulation sites. After the stimulation session, BIC was directly added to the culture medium at the final concentration of 30 µM (Keefer and Gramowski 2001; Gramowski *et al*. 2004). After five minutes equilibration period, recordings were carried on

for further 20 min. A total number of 63 cultures (32 for WT and 31 for KO) from three independent preparations were treated with BIC.

When stimulating currents/voltages are delivered through one electrode of the array at a constant frequency, the network responds by generating a rich repertoire of reverberating electrical activities, lasting 100-200 ms (Shahaf and Marom, 2001). To analyze the neuronal activity evoked by electrical stimulation, we represented the impulse response of each site of the experimental preparation by means of a post-stimulus time histogram (PSTH). We summated over time (5-ms bin) the spiking responses to the 50 stimuli in the train over a 200-ms period after the stimulus to generate a cumulative histogram that was afterwards normalized by the total number of stimuli and the bin size (Rieke *et al*., 1997). Evoked activity was analyzed using Neuroexplorer (Nex Technologies). Only active channels (i.e., having a PSTH > 1 in the whole stimulation session) were considered for statistical analysis.

6.6. Electrophysiological experiments

Whole-cell patch-clamp recordings were made, as previously described (Baldelli *et al*. 2007; Valente *et al*. 2012). Patch pipettes, prepared from thin borosilicate glass (Hilgenberg) were pulled and fire polished to a final resistance of 2-4 MΩ when filled with standard internal solution. Whole-cell currents were recorded using an EPC-10 amplifier (HEKA Electronic). Voltage-clamp recordings of voltage-gated Na^+ currents and current-clamp recordings investigating single cell firing rates were acquired at 20 kHz and low-pass filtered at 4 kHz, while the AP shape was sampled at 50 kHz and low-pass filtered at 10 kHz. Recordings with leak currents >200 pA or series resistance >20 MΩ were discarded. Data acquisition was performed using PatchMaster program (HEKA Elektronic). Series resistance was compensated 80% (2 μs response time) and the compensation was readjusted before each stimulation. The shown potentials were not corrected for the measured liquid junction potential of 9 mV. All recordings were performed at 22-24 °C. The whole-cell patch-clamp recordings were performed on autaptic neurons grown on micro islands, on low-density primary neurons and on cultures of IPSCs, as previously described

(Valente *et al*., 2012). Measures were conducted on single and isolated autaptic cells between 10 and 15 DIV.

Evoked excitatory and inhibitory postsynaptic currents (eEPSCs/eIPSCs) were recorded using an EPC-10 amplifier (HEKA Electronic). For whole-cells recordings, cells were maintained in a standard external solution containing (in mM): 140 NaCl, 2 $CaCl_2$, 1 $MgCl_2$, 4 KCl, 10 glucose, 10 HEPES (pH 7.3 with NaOH). To record eEPSCs, where otherwise not indicated, D-(-)-2-amino-5-phosphonopentanoic acid (D-AP5; 50 μM; Tocris) and bicuculline (BIC, 30 μM, Tocris) were added to the Tyrode solution to block N-methyl-D-aspartate (NMDA) and $GABA_A$ receptors, respectively. To record eIPSCs, 6-cyano-7-nitroquinoxaline-2, 3-dione (CNQX; 10 μM) and CGP 58845 (CGP; 10 μM) were added to the external solution to block non-NMDA and $GABA_B$ receptors, respectively. The standard internal solution was (in mM): 126 KGluconate, 4 NaCl, 1 $MgSO_4$, 0.02 $CaCl_2$, 0.1 BAPTA, 15 glucose, 5 HEPES, 3 ATP, 0.1 GTP (pH 7.2 with KOH). For experiments in which eIPSCs were studied, the following internal solution was used (in mM): 140 KCl, 4 NaCl, 1 $MgSO_4$, 0.1 EGTA, 15 Glucose, 5 HEPES, 3 ATP, 0.1 GTP (pH 7.2 with KOH). Unclamped APs were evoked by a brief depolarization of the cell body to +40 mV for 0.5 ms at 0.1 Hz using a V_h =-70 mV. Evoked PSCs were acquired at 10-20 kHz sample frequency and filtered at 1/5 of the acquisition rate with an 8-pole low-pass Bessel filter. Recordings with leak currents >100 pA or series resistance >20 MΩ were discarded. Data acquisition was performed using PatchMaster programs (HEKA Elektronic). EPSCs were inspected visually, and only those that were not contaminated by spontaneous activity were considered. Macroscopic currents were elicited using a family of depolarizing 10 ms-voltage steps from -50 to 60 mV and a ramp protocol consisting of a voltage step of 200 ms from the holding potential to -100 mV followed by 100-ms linear ramp up to 120 mV. In both protocols cells were clamped at a V_h of -70 mV before stimulation.

HEK-293 stably expressing human $Na_V1.1$, $Na_V1.2$ and $Na_V1.6$ were transfected with 2 µg of *PRRT2*-HA plasmid or empty vector *pKH3* (mock) with Lipofectamine 2000, following the manufacturer's recommendations. To identify transfected cells, a co-transfection with a second plasmid containing the Tomato fluorescent protein reporter (Clontech) was done. Voltage-clamp recordings of voltage-gated Na^+ currents were performed using the following Extracellular Solutions (in mM): 140 NaCl, 3 KCl, 1

MgCl2, 1 CaCl2, 10 HEPES, 10 Mannitol (pH 7.3 with NaOH); and as Intracellular (in mM): 140 CsCl, 10 NaCl, 2 EGTA, 10 HEPES (pH 7.3 with CsOH). Linear capacity and leakage currents of recordings were eliminated by P/N leak subtraction procedure.

Whole-cell family currents of fast inactivating Na_V channels were evoked by 5 mV steps depolarization from -80 to 65 mV and cells were held at -120 mV. Steady-state inactivation curves were constructed by recording the peak currents amplitude evoked by 20-ms test pulses to -10 mV after 500-ms prepulses to potentials over the range of -130 to 10 mV. Time-dependent rate of recovery from inactivation was calculated by prepulsing the cell with a 20-ms step to -20 mV to inactivate the channels and then bringing back the potential to -100 mV for increasing recovery durations (0.5, 1, 2, 4, 8, 32, 64, 128, 148 ms) before the test pulse of -20 mV. Linear capacity and leakage currents were eliminated by P/N leak subtraction procedure.

6.7. Analysis of electrophysiological data

Spontaneous and asynchronous release. Miniature excitatory (mEPSC) and inhibitory (mIPSC) postsynaptic currents were both collected from low-density plated neurons incubated in the presence of tetrodotoxin (TTX, 1 μM; Tocris) to block spontaneous APs. mEPSC were recorded in the presence of D-AP5 (50 μM), CGP (10 μM) and BIC (30 μM), while mIPSC were recorded with D-AP5 (50 μM), CGP (10 μM) and CNQX (10 μM) in the extracellular solution. mPSC analysis was performed using the Mini analysis program (Synaptosoft). The amplitude and frequency of mPSCs were calculated using a peak detector function with appropriate threshold amplitude and threshold area. The delayed asynchronous release of excitatory autapses was evoked by a tetanic stimulation lasting 2 s at 40 Hz. Asynchronous release was estimated by measuring the charge (pA*ms) of the spontaneous PSCs that follow the stimulation train, in 9 consecutive time-windows lasting 1 s each.

Short-term plasticity. In order to analyze the paired-pulse ratio (PPR), two brief depolarizing pulses were applied to autaptic neurons with variable interpulse intervals ranging from 20 to 10,000 ms. For each couple of PSCs, PPR was calculated as the I_2/I_1 ratio, where I_1 and I_2 are the

amplitudes of the PSCs evoked by the conditioning (1) and test (2) stimuli, respectively. To correctly evaluate the amplitude of I_2, the baseline of I_2 was defined as the final value of the decay phase of I_1 and the amplitude of I_2 was calculated by subtracting the residual amplitude of I_1 from the peak value of I_2. In the analysis of synaptic responses during tetanic stimulation, the interpulse interval was shorter than the time needed for a PSC to return to baseline, so PSCs overlapped partially. Thus, to correctly estimate the PSC amplitude, the baseline of each event was calculated as the final value of the decay phase of the preceding ePSC and the amplitude of PSC (n) was calculated by subtracting the residual amplitude of PSC (n-1) from its peak value.

Cumulative PSC amplitude analysis. The size of the RRP of synchronous release (RRP_{syn}) and the probability that any given SV in the RRP will be released (Pr) were calculated using the cumulative amplitude analysis (Schneggenburger *et al*., 2002). The cumulative amplitude plot was determined by summing up peak EPSC amplitudes during 40 repetitive stimuli applied at 40 Hz. This analysis considers that depression during the steady-state phase is limited by a constant recycling of SVs with an equilibrium existing between released and recycled SVs and that Pr during the train approaches the 1 value (Schneggenburger *et al*., 1999). The number of data points for the linear fitting of the steady-state phase was evaluated by calculating the best fit including the maximal number of data points starting from the last data point (i.e., from the 40th eEPSC). The cumulative amplitude profiles of the last 15-20 data points were fitted by linear regression and back-extrapolated to time 0. The intercept with the Y-axis gave the RRP_{syn} and the ratio between the amplitude of the first PSC (I_1) and the RRP_{syn} yielded the Pr.

Analysis of firing activity. The rheobase was calculated as the minimum depolarizing current needed to elicit at least one action potential. Input resistance was recorded using the Ohm's low in the linear region of the voltage-current relationship determined after injection of hyperpolarizing and depolarizing current steps (-10, -10, 10, 20 pA). For each recorded cell, the plot of the time derivative of voltage (dV/dt) versus voltage (phase-plane plot) was constructed from the first AP elicited by the minimal current injection. This plot was used to extract threshold potential, maximum rising slope and peak potential (V max). Amplitude of APs was calculated as the difference between the V max and the threshold value.

The instantaneous firing frequency and the mean firing frequency were determined at the minimal value of injected current able to evoked two or more APs. The instantaneous firing frequency was estimated as the reciprocal value of the time difference between the first two evoked APs. The mean firing frequency was calculated as the ratio of the number of APs evoked by the minimal current injection to the time interval (s) between the first and the last evoked action potential (Valente *et al*., 2016b). Firing activity was also studied using trains of 5 ms-steps applied at various frequencies (10-120 Hz). The current value used to evoke APs with this protocol was selected as the minimal current able to evoke an AP for each step of the train at 10 Hz (100% of probability) and increased by 100 pA.

Analysis of Na^+ currents. The current density (J) was obtained by dividing the peak current by the cell capacitance (nA/pF). The rheobase was calculated as the minimum depolarizing current needed to elicit at least one AP. Input resistance was calculated using the Ohm's law in the linear region of the voltage-current relationship determined after injection of hyperpolarizing and depolarizing current steps (-10, -10, 10, 20 pA). For each recorded cell, the plot of the time derivative of voltage (dV/dt) versus time (phase-plane plot) was constructed from the first action potential elicited by the minimal current injection. This plot was used to extract threshold potential, maximum rising slope and peak potential (V_{max}). Amplitude of action potentials was calculated as the difference between the V_{max} and the threshold potential. The instantaneous firing frequency and the mean firing frequency were determined at the minimal value of injected current able to evoked two or more action potentials and is valued as previously described (Valente *et al*., 2016b). The conductance-voltage relationship curves were obtained by converting the maximal current values, evoked with the voltage step protocols, to conductance using the relation $G_{Na} = I_{Na}/(V-V_R)$, where G_{Na} is the Na^+ conductance, I_{Na} is the peak Na^+ current, V is the command pulse potential, and V_R is the theoretical reversal potential of Na^+ current. The normalized activation and inactivation curves for each cell were fitted to the Boltzmann equation in the form: $Y=1/\{1+\exp[(V-V_{0.5})/k]\}$, where Y is the normalized G_{Na} or I_{Na}, V the is the command pulse potential, $V_{0.5}$ is the voltage required to activate the half-maximal conductance or inactivation, and k is the slope of curve. The macroscopic currents, the shape of action potentials, firing activity and Na^+ currents were analyzed using the pClamp software (Axon), PatchMaster

program (HEKA Elektronic), OriginPro 8 (OriginLab Corp.) and the Prism software (GraphPad Software, Inc.).

6.8. Biochemical assays

Pull-down and co-immunoprecipitation. HEK-293 cells stably expressing $Na_V1.1$ or $Na_V1.2$ or $Na_V1.6$ subtypes were transfected with *PRRT2*-HA and BAP-HA as control; after 24 h cells were harvested in lysis buffer (1% Triton X-100, 150 mM NaCl, 50 mM Tris-HCl pH 7.4, with protease inhibitors cocktail). For pull-down assays, 20 µl of monoclonal anti-HA-Agarose affinity resin (Sigma-Aldrich) was incubated with cell extract according to manufacturer's instructions for 2 h at 4 °C. After extensive washes in lysis buffer and detergent-free lysis buffer, samples were resolved by SDS-PAGE and subjected to western blotting with polyclonal anti-HA and anti-PanNa_V antibodies. For immunoprecipitation, 5 µg of mouse anti-PanNa_V or mouse control IgGs were precoated with Protein G Sepharose (GE Healthcare) overnight and incubated with a mouse membrane fraction in lysis buffer. After extensive washes in lysis buffer and detergent-free lysis buffer, samples were resolved by SDS-PAGE and subjected to western blotting with anti-PRRT2 and anti-PanNa_V antibodies.

Surface biotinylation. HEK-293 cells stably expressing $Na_V1.1$ or $Na_V1.2$ or $Na_V1.6$ subtypes were transfected with *PRRT2-HA* plasmids or empty vector *pKH3* as a control. Briefly, cells were incubated with 1 mg/ml of EZ-Link™Sulfo-NHS-SS-Biotin in cold phosphate-buffered saline (PBS) for 40 min at 4°C, constantly moving. Free biotin was quenched, twice, with 100mM Tris in cold PBS, and once with cold PBS to remove biotin excess. The cells were then harvested with lysis buffer for 30 minutes. Whole-cell lysates were centrifuged at 16,000 x g at 4 °C for 15 min. 1 mg of the supernatant was incubated with 100 µl of NeutrAvidin conjugated agarose beads for 3 h at 4°C, and the remaining supernatant was kept as input. The beads were subsequently washed five times with lysis buffer before elution. All reagents were purchased from Thermo Fisher Scientific.

6.9. Immunofluorescence

For iPSCs, three germ layer cells and NPCs, stainings were performed with PSC 4-MARKER ICC Kit, 3-GERM LAYER ICC Kit and NSC ICC Kit respectively (all from Thermo Fisher Scientific) according to manufacturer's instructions. For iPSC-derived neurons, primary cortical neurons and HeLa cells, immunofluorescence was performed (see Corradi *et al.*, 2014). PRRT2 staining was performed as described in Liu *et al*. (2016). All images were taken by a Leica TCS SP8 confocal microscope or by a Zeiss AxioImager M2 microscope and analyzed with ImageJ.

6.10. qRT-PCR and Western blotting

qRT-PCR was performed in a real-time thermal cycler (CFX-96, Bio-Rad) using SsoFast EvaGreen Supermix (Bio-Rad). Total mRNA was extracted with RNAeasy mini or micro kit (Qiagen) according to the manufacturer's instructions, and reverse transcribed using the iScript cDNA Synthesis Kit (Bio-Rad). Relative expression was calculated using the $2^{-\Delta\Delta Ct}$ method (Pfaffl, 2001) by normalizing data to the geometric mean of three housekeeping transcripts (GAPDH, PPIA, RPL13A) using the CFX Manager 3.0 software (Bio-Rad). For western blotting analysis, protein concentration of the samples was determined using the BCA or Bradford assay and equivalent amounts of protein were subjected to SDS-PAGE on polyacrylamide gels and blotted onto nitrocellulose membranes. Blotted membranes were blocked for 1 h in 5% milk in Tris-buffered saline (10 mM Tris, 150 mM NaCl, pH 8.0) plus 0.1% Triton X-100 and incubated overnight at 4°C with the appropriate primary antibody. Membranes were washed and incubated for 1 h at room temperature with peroxidase-conjugated secondary antibodies. Bands were revealed with the ECL chemiluminescence detection system (Thermo Fisher Scientific).

6.11. Statistical Analysis

Data are expressed as means ±sem for number of independently differentiated clones (n). The non-parametric Mann-Whitney's U-test was used in order to compare two sample groups that were not normally distributed. To compare more than two normally distributed sample groups, one-way ANOVA, followed by post-hoc multiple comparison tests was used. Statistical analysis was performed using Prism (GraphPad Software, Inc.) software.

7. REFERENCES

Abbott LF, Regehr WG (2004). Synaptic computation. *Nature*. Oct 14; **431**(7010):796-803.

Alam Z, Coombes N, Waring RH, Williams AC, Steventon GB (1998). Plasma levels of neuroexcitatory amino acids in patients with migraine or tension headache. *J. Neurol. Sci*. **156**, 102-106.

Anger T, Madge DJ, Mulla M, Riddall D (2001). Medicinal chemistry of neuronal voltage-gated sodium channel blockers. *J Med Chem*.Jan 18; **44**(2): 115-37.

Aronica E, Yankaya B, Troost D, van Vliet EA, Lopes da Silva FH, Gorter JA (2001). Induction of neonatal sodium channel II and III α-isoform mRNAs in neurons and microglia after status epilepticus in the rat hippocampus. *Eur J Neurosci*. Mar; **13**(6):1261-6.

Awiszus F (1988). Continuous functions determined by spike trains of a neuron subject to stimulation. *Biol Cybern*; **58**(5): 321-7.

Baldelli P, Fassio A, Valtorta F, Benfenati F (2007) Lack of synapsin I reduces the readily releasable pool of synaptic vesicles at central inhibitory synapses. *J Neurosci* **27**: 13520-13531.

Bardy C, van den Hurk M, Eames T, Marchand C, Hernandez RV, Kellogg M, Gorris M, Galet B, Palomares V, Brown J, Bang AG, Mertens J, Böhnke L, Boyer L, Simon S, Gage FH (2015). Neuronal medium that supports basic synaptic functions and activity of human neurons in vitro. *Proc Natl Acad Sci U S A*. May 19; **112**(20): E2725-34.

Bartolomei F, Gastaldi M, Massacrier A, Planells R, Nicolas S, Cau P (1997). Changes in the mRNAs encoding subtypes I, II and III sodium channel α-subunits following kainate-induced seizures in rat brain. *J Neurocytol*.Oct; **26**(10) 667-78.

Bateup HS, Denefrio CL, Johnson CA, Saulnier JL, Sabatini BL (2013). Temporal dynamics of a homeostatic pathway controlling neural network activity. *Frontiers in Molecular Neuroscience*, **6**: 28.

Becker EB, Oliver PL, Glitsch MD, Banks GT, Achilli F, Hardy A, Nolan PM,Fisher EM, Davies KE (2009). A point mutation in TRPC3 causes abnormal Purkinje cell development and cerebellar ataxia in moonwalker mice. *Proc Natl Acad Sci U S A*. Apr; **21**; 106(16): 6706-11.

Becker F, Schubert J, Striano P, Anttonen AK, Liukkonen E, Gaily E, Gerloff C, Müller S, Heußinger N, Kellinghaus C, Robbiano A, Polvi A, Zittel S, von Oertzen TJ, Rostasy K, Schöls L, Warner T, Münchau A, Lehesjoki AE, Zara F, Lerche H, Weber YG (2013). PRRT2-related disorders: further PKD and ICCA cases and review of the literature. *J Neurol*. May; **260**(5): 1234-44.

Beckh S, Noda M, Lübbert H, Numa S (1989). Differential regulation of three sodium channel messenger RNAs in the rat central nervous system during development. *EMBO J*. Dec 1; **8**(12): 3611-6.

Bekkers JM, Stevens CF (1991) Excitatory and inhibitory autaptic currents in isolated hippocampal neurons maintained in cell culture. *Proc Natl Acad Sci USA* **88**: 7834-7838.

Begum AN, Guoynes C, Cho J, Hao J, Lutfy K, Hong Y (2015). Rapid generation of sub-type, region-specific neurons and neural networks from human pluripotent stem cell-derived neurospheres. *Stem Cell Res.* Nov; **15**(3): 731-41.

Berg AT, Berkovic SF, Brodie MJ, Buchhalter J, Cross JH, van Emde Boas W, Engel J, French J, Glauser TA, Mathern GW, Moshé SL, Nordli D, Plouin P, Scheffer IE (2010). Revised terminology and concepts for organization of seizures and epilepsies: report of the ILAE commission on classification and terminology, 2005–2009. *Epilepsia*; **51:** 676-85.

Bhatia K (2011). Paroxysmal dyskinesias. *Mov Disord*. May; **26**(6): 1157-65.

Bhatia K, Griggs R and Ptàĉek L (2000). Episodic movement disorders as channelopathies, *mov. Dis*. **15**-3.

Bilic J, Izpisua Belmonte JC (2012). Concise review: Induced pluripotent stem cells versus embryonic stem cells: close enough or yet too far apart? *Stem Cells.* Jan; **30**(1): 33-41.

Blumenfeld H, Lampert A, Klein JP, Mission J, Chen MC, Rivera M, Dib-Hajj S, Brennan AR, Hains BC, Waxman SG (2009). Role of hippocampal sodium channel Nav1.6 in kindling epileptogenesis. Epilepsia.Jan; **50**(1): 44-55.

Bockenhauer D, Feather S, Stanescu HC, Bandulik S, Zdebik AA, Reichold M, Tobin J, Lieberer E, Sterner C, Landoure G, Arora R, Sirimanna T, Thompson D, Cross JH, van't Hoff W, Al Masri O, Tullus K, Yeung S, Anikster Y, Klootwijk E, Hubank M, Dillon MJ, Heitzmann D, Arcos-Burgos M, Knepper MA, Dobbie A, Gahl WA, Warth R, Sheridan EK (2009). Epilepsy, Ataxia, Sensorineural Deafness, Tubulopathy, and *KCNJ10* Mutations. *N Engl J Med;* **360**: 1960-1970.

Boyken J, Grønborg M, Riedel D, Urlaub H, Jahn R, Chua J (2013). Molecular profiling of synaptic vesicle docking sites reveals novel proteins but few differences between glutamatergic and GABA-ergic synapses. *Neuron*. **78:** 285-297.

Brigidi GS, Bamji SX (2011). Cadherin-catenin adhesion complexes at the synapse. *Curr. Opin. Neurobiol*. **21:** 208-14.

Broccoli V, Rubio A, Taverna S, Yekhlef L (2015). Overcoming the hurdles for a reproducible generation of human functionally mature reprogrammed neurons. *Experimental Biology and Medicine*; **240**(6): 787-794.

Broccoli V, Giannelli SG, Mazzara PG (2014). Modeling physiological and pathological human neurogenesis in the dish. *Front Neurosci*. Jul 24; **8**: 183.

Brueckner F, Kohl B, Puest B, Gassner S, Osseforth J, Lindenau M, Stodieck S, Biskup S, Lohmann E (2014). Unusual variability of PRRT2 linked phenotypes within a family. *Eur J Paediatr Neurol*. Jul; **18**(4): 540-2.

Bruno MK, Hallett M, Gwinn-Hardy K, Sorenson B, Considine E, Tucker S, Lynch DR, Mathews KD, Swoboda KJ, Harris J, Soong B-W, Ashizawa T, Jankovic J, Renner D, Fu Y-H, Ptacek LJ (2004). Clinical evaluation of idiopathic paroxysmal kinesigenic dyskinesia. *Neurology*; **63:** 2280-7.

Callenbach PM, de Coo RF, Vein AA, Arts WF, Oosterwijk J, Hageman G, ten Houten R, Terwindt GM, Lindhout D, Frants RR, Brouwer OF (2002). Benign familial infantile convulsions: a clinical study of seven Dutch families. *Eur J Paediatr Neuro*; **6**(5): 269-83.

Caraballo RH, Cersósimo RO, Amartino H, Szepetowski P, Fejerman N (2002). Benign familial infantile seizures: further delineation of the syndrome. *J Child Neurol*. Sep; **17**(9): 696-9.

Catterall WA (2014). Structure and function of voltage-gated sodium channels at atomic resolution. *Exp Physiol*. Jan; **99**(1): 35-51.

Catterall WA, Perez-Reyes E, Snutch TP, Striessnig J (2005a). International Union of Pharmacology. XLVIII. Nomenclature and structure-function relationships of voltage-gated calcium channels*. Pharmacol Rev*. Dec; **57**(4): 411-25.

Catterall WA, Goldin AL, Waxman SG (2005b). International Union of Pharmacology.XLVII. Nomenclature and structure-function relationships of voltage-gated sodium channels. *Pharmacol Rev*. Dec; **57**(4): 397-409.

Catterall WA (1981). Inhibition of voltage-sensitive sodium channels in neuroblastoma cells by antiarrhythmic drugs. *Mol Pharmacol*. Sep; **20**(2): 356-62.

Cedar H, Bergman Y (2009). Linking DNA methylation and histone modification: patterns and paradigms. *Nat Rev Genet.* May; **10**(5): 295-304.

Chen J, Zhou L, Pan SY (2014). A brief review of recent advances in stem cell biology. *Neural Regen Res*. Apr 1; **9**(7): 684-7.

Chen WJ, Lin Y, Xiong ZQ, Wei W, Ni W, Tan GH, Guo SL, He J, Chen YF, Zhang QJ, Li HF, Lin Y, Murong SX, Xu J, Wang N, Wu ZY (2011). Exome sequencing identifies truncating mutations in PRRT2 that cause paroxysmal kinesigenic dyskinesia. *Nat Genet;* **43:** 1252-5.

Chiappalone M, Casagrande S, Tedesco M, Valtorta F, Baldelli P, Martinoia S, Benfenati F (2009). Opposite changes in glutamatergic and GABAergic transmission underlie the diffuse hyperexcitability of synapsin I-deficient cortical networks. *Cereb Cortex*. Jun; **19**(6): 1422-39.

Chiappalone M., Vato A., Berdondini L., Koudelka-Hep M. and Martinoia S (2007). Network dynamics and synchronous activity in cultured cortical neurons. *Int J Neural Syst*; **17**: 87-103.

Chiappalone M, Bove M, Vato A, Tedesco M, Martinoia S (2006). Dissociated cortical networks show spontaneously correlated activity patterns during in vitro development. *Brain Res*; **1093**, 41-53.

Chin MH, Pellegrini M, Plath K, Lowry WE (2010). Molecular analyses of human induced pluripotent stem cells and embryonic stem cells. *Cell Stem Cell*. Aug 6; **7**(2): 263-9.

Chin MH, Mason MJ, Xie W, Volinia S, Singer M, Peterson C, Ambartsumyan G, Aimiuwu O, Richter L, Zhang J, Khvorostov I, Ott V, Grunstein M, Lavon N, Benvenisty N, Croce CM, Clark AT, Baxter T, Pyle AD, Teitell MA, Pelegrini M, Plath K, Lowry WE (2009). Induced pluripotent stem cells and embryonic stem cells are distinguished by gene expression signatures. *Cell Stem Cell*. Jul2; **5**(1): 111-23.

Cloarec R, Bruneau N, Rudolf G, Massacrier A, Salmi M, Bataillard M, Boulay C, Caraballo R, Fejerman N, Genton P, Hirsch E, Hunter A, Lesca G, Motte J, Roubertie A, Sanlaville D, Wong SW, Fu YH, Rochette J, Ptácek LJ, Szepetowski P (2012). PRRT2 links infantile convulsions and paroxysmal dyskinesia with migraine. *Neurology*. Nov 20; **79**(21): 2097-103.

Cohen D, Segal M (2011). Network bursts in hippocampal microcultures are terminated by exhaustion of vesicle pools. *J Neurophysiol*. Nov; **106**(5): 2314-21.

Colman A, Dreesen O (2009). Pluripotent stem cells and disease modeling. *Cell Stem Cell.* Sep 4; **5**(3): 244-7.

Costantin L, Bozzi Y, Richichi C, Viegi A, Antonucci F, Funicello M, Gobbi M, Mennini T, Rossetto O, Montecucco C, Maffei L, Vezzani A, Caleo M (2005). Antiepileptic effects of botulinum neurotoxin E. *J Neurosci*. Feb 23; **25**(8): 1943-51.

Corradi A, Fadda M, Piton A, Patry L, Marte A, Rossi P, Cadieux-Dion M, Gauthier J, Lapointe L, Mottron L, Valtorta F, Rouleau GA, Fassio A, Benfenati F, Cossette P. SYN2 is an autism predisposing gene: loss-of-function mutations alter synaptic vesicle cycling and axon outgrowth. Hum Mol Genet. 2014 Jan 1; **23**(1): 90-103.

Cowan CA, Atienza J, Melton DA, Eggan K (2005). Nuclear reprogramming of somatic cells after fusion with human embryonic stem cells. *Science*. Aug 26; **309**(5739): 1369-73.

Cowell JK (2014). LGI1: from zebrafish to human epilepsy. *Prog. Brain Res.* **213:** 159-79.

Cox JJ, Reimann F, Nicholas AK, Thornton G, Roberts E, Springell K, Karbani G, Jafri H, Mannan J, Raashid Y, Al-Gazali L, Hamamy H, Valente EM, Gorman S, Williams R, McHale DP, Wood JN, Gribble FM, Woods CG (2006). An SCN9A channelopathy causes congenital inability to experience pain. Nature; **444**: 894-8.

Crill WE (1996). Persistent sodium current in mammalian central neurons. *Annu Rev Physiol*; **58**: 349-62.

D'Adamo MC (2015). Episodic Ataxia Type 1 *GeneReviews*®.

D'Adamo MC, Imbrici P, Sponcichetti F, Pessia M (1999). Mutations in the *KCNA1* gene associated with episodic ataxia type-1 syndrome impair heteromeric voltage-gated K^+ channel function. *FASEB J*. Aug; **13**(11): 1335-45.

Dale RC, Gardiner A, Antony J, Houlden H (2012). Familial PRRT2 mutation with heterogeneous paroxysmal disorders including paroxysmal torticollis and hemiplegic migraine. *Dev Med Child Neurol*. Oct; **54**(10): 958-60.

Davis RL, Weintraub H, Lassar AB (1987). Expression of a single transfected cDNA converts fibroblasts to myoblasts. *Cell*. Dec 24; **51**(6): 987-1000.

Debanne D, Campanac E, Bialowas A, Carlier E, Alcaraz G (2011). Axon physiology. *Physiol Rev*. Apr; **91**(2): 555-602.

Delcourt M, Riant F, Mancini J, Milh M, Navarro V, Roze E, Humbertclaude V, Korff C, Des Portes V, Szepetowski P, Doummar D, Echenne B, Quintin S, Leboucq N,Singh Amrathlal R, Rochette J, Roubertie A (2015). Severe phenotypic spectrum of biallelic mutations in PRRT2 gene. *J Neurol Neurosurg Psychiatry*. Jul; **86**(7): 782-5.

Demirkiran M, Jankovic J (1995). Paroxysmal dyskinesias: clinical features and classification. *Ann Neurol*. Oct; **38**(4): 571-9.
de Vries B, Callenbach PM, Kamphorst JT, Weller CM, Koelewijn SC, Houten RT, de Coo IF, Brouwer OF, van den Maagdenberg AM (2012). PRRT2 mutation causes benign familial infantile convulsions. *Neurology*; **79:** 2154-5.

Dichgans M, Freilinger T, Eckstein G, Babini E, Lorenz-Depiereux B, Biskup S, Ferrari MD, Herzog J, van den Maagdenberg AM, Pusch M, Strom TM (2005). Mutation in the neuronal voltage-gated sodium channel SCN1A in familial hemiplegic migraine. *Lancet*. Jul 30-Aug 5; **366**(9483): 371-7.

Diecke S, Jung SM, Lee J, and Ju JH (2014). Recent technological updates and clinical applications of induced pluripotent stem cells. *Korean J Intern Med*. Sep; 29(5): 547–557.

Dityatev A, Schachner M, Sonderegger P (2010). The dual role of the extracellular matrix in synaptic plasticity and homeostasis. *Nat Rev Neurosci.* **11:** 735-46.

Djemie T, Weckhuysen S, Holmgren P, Hardies K, Van Dyck T, Hendrickx R, Schoonjans AS, Van Paesschen W, Jansen AC, De Meirleir L, Selim LA, Girgis MY, Buyse G, Lagae L, Smets K, Smouts I, Claeys KG, Van den Bergh V, Grisar T, Blatt I, Shorer Z, Roelens F, Afawi Z, Helbig I, Ceulemans B, De Jonghe P, Suls A (2014). PRRT2 mutations: exploring the phenotypical boundaries. *J Neurol Neurosurg Psychiatry*. Apr; **85**(4): 462-5.

Doi A, Park IH, Wen B, Murakami P, Aryee MJ, Irizarry R, Herb B, Ladd-Acosta C, Rho J, Loewer S, Miller J, Schlaeger T, Daley GQ, Feinberg AP (2009). Differential methylation of tissue- and cancer-specific CpG island shores distinguishes human induced pluripotent stem cells, embryonic stem cells and fibroblasts. *Nat Genet. Dec*; **41**(12): 1350-3.

Du W, Bautista JF, Yang H, Diez-Sampedro A, You SA, Wang L, Kotagal P, Lüders HO, Shi J, Cui J, Richerson GB, Wang QK (2005). Calcium-sensitive potassium channelopathy in human epilepsy and paroxysmal movement disorder. *Nat Genet*. Jul; **37**(7): 733-8.

Ebrahimi-Fakhari D, Saffari A, Westenberger A, Klein C (2015). The evolving spectrum of PRRT2-associated paroxysmal diseases. *Brain*. Dec; **138**(Pt 12): 3476-95.

Erro R, Bhatia KP, Espay AJ, Striano P (2017). The epileptic and nonepileptic spectrum of paroxysmal dyskinesias: Channelopathies, synaptopathies, and transportopathies*. Mov Disord*. Mar; **32**(3):310-318.

Erro R, Sheerin UM, Bhatia KP (2014). Paroxysmal dyskinesias revisited: a review of 500 genetically proven cases and a new classification. *Mov Disord*. Aug; **29**(9): 1108-16.

Fatt P, Katz B (1952). Spontaneous subthreshold activity at motor nerve endings. *J. Physiol*. **117**, 109–128.

Fink J, Rainier S, Wilkowski J, Jones S, Kume A, Hedera P, Albin R, Mathay J, Girbach L, Varvil T, Otterud T, and Leppert M (1996). Paroxysmal Dystonic Choreoathetosis: Tight Linkage to Chromosome 2q. *Am. J. Hum. Genet*. **59**:140-145, 1996.

Fioravante D, Regehr WD (2011). Short-term forms of presynaptic plasticity; *Curr Opin Neurobiol*. Apr; **21**(2): 269-274.

Fouad G, Servidei S, Durcan S, Bertini E, Ptacek L (1996). A Gene for Familial Paroxysmal Dyskinesia (FPD1) Maps to Chromosome 2q. *Am. J. Hum. Genet*. **59**:135-139.

Fox MA and Sanes JR (2007). Synaptotagmin I and II are present in distinct subsets of central synapses. *J. Comp. Neurol*. **503**, 280-296.

Freberg CT, Dahl JA, Timoskainen S, Collas P (2007). Epigenetic reprogramming of OCT4 and NANOG regulatory regions by embryonal carcinoma cell extract*. Mol Biol Cell*. May; **18**(5): 1543-53.

Gao X, Wehr M (2015). A coding transformation for temporally structured sounds within auditory cortical neurons. *Neuron*. Apr 8; **86**(1): 292-303.

Garbelli R, Inverardi F, Medici V, Amadeo A, Verderio C, Matteoli M Frassoni C (2008). Heterogeneous expression of SNAP-25 in rat and human brain. *J. Comp. Neurol*. **506**, 373-386.

Garcia-Manteiga JM, Bonfiglio S, Folladori L, Malosio ML, Lazarevic D, Stupka E, Cittaro D, Meldolesi J (2015). REST-Governed Gene Expression Profiling in a Neuronal Cell Model Reveals Novel Direct and Indirect Processes of Repression and Up-Regulation. *Front Cell Neurosci*. Nov 10; **9:** 438.

Gardella E, Becker F, Møller RS, Schubert J, Lemke JR, Larsen LH, Eiberg H, Nothnagel M, Thiele H, Altmüller J, Syrbe S, Merkenschlager A, Bast T, Steinhoff B, Nürnberg P, Mang Y, Bakke Møller L, Gellert P, Heron SE, Dibbens LM, Weckhuysen S, Dahl HA, Biskup S, Tommerup N, Hjalgrim H, Lerche H, Beniczky S, Weber YG (2016). Benign infantile seizures and paroxysmal dyskinesia caused by an SCN8A mutation. *Ann Neurol.* Mar; **79**(3): 428-36.

Gardiner AR, Jaffer F, Dale RC, Labrum R, Erro R, Meyer E, Xiromerisiou G, Stamelou M, Walker M, Kullmann D, Warner T, Jarman P, Hanna M, Kurian MA, Bhatia KP, Houlden H (2015). The clinical and genetic heterogeneity of paroxysmal dyskinesias. *Brain*; Dec; **138**(Pt 12): 3567-80.

Gardiner AR, Bhatia KP, Stamelou M, Dale RC, Kurian MA, Schneider SA, Wali GM, Counihan T, Schapira AH, Spacey SD, Valente EM, Silveira-Moriyama L, Teive HA, Raskin S, Sander JW, Lees A, Warner T, Kullmann DM, Wood NW, Hanna M, Houlden H (2012). PRRT2 gene mutations: from paroxysmal dyskinesia to episodic ataxia and hemiplegic migraine. *Neurology*. Nov 20; **79**(21): 2115-21.

Geisert EE Jr, Johnson HG, Binder LI (1990). Expression of microtubule-associated protein 2 by reactive astrocytes. *Proc Natl Acad Sci USA*. May; **87**(10): 3967-71.

George N, Thodeson DM, Park JY, Sirsi D (2017). Paroxysmal Choreoathetosis in a Child with SCN2A Mutation and Neonatal Seizures. Open Access *J Neurol Neurosurg*.; **4**(4): 555641.

Ghosh Z, Wilson KD, Wu Y, Hu S, Quertermous T, Wu JC (2010). Persistent donor cell gene expression among human induced pluripotent stem cells contributes to differences with human embryonic stem cells. *PLoS One*. Feb 1; **5**(2): e8975.

Gokhale PJ, Andrews PW (2006). A prospective on stem cell research. *Semin Reprod Med.*Nov; **24**(5): 289-97.
Gonzalez F, Boue S, Izpisua Belmonte JC (2011). Methods for making induced pluripotent stem cells: reprogramming a la carte. *Nature Reviews. Genetics*. **12**: 231-242.

Gordon D, Merrick D, Auld V, Dunn R, Goldin AL, Davidson N, Catterall WA (1987). Tissue-specific expression of the RI and RII sodium channel subtypes. *Proc Natl Acad Sci U S A.* Dec; **84**(23): 8682-6.

Gramowski A, Jugelt K, Weiss DG, Gross GW (2004). Substance identification by quantitative characterization of oscillatory activity in murine spinal cord networks on microelectrode arrays. *Eur J Neurosci*; **19**: 2815-2825.

Graves TD, Cha YH, Hahn AF, Barohn R, Salajegheh MK, Griggs RC, Bundy BN, Jen JC, Baloh RW, Hanna MG; CINCH Investigators (2014). Episodic ataxia type 1: clinical characterization, quality of life and genotype-phenotype correlation. *Brain*.Apr; **137**(Pt 4): 1009-18.

Guenther MG, Frampton GM, Soldner F, Hockemeyer D, Mitalipova M, Jaenisch R, Young RA (2010). Chromatin structure and gene expression programs of human embryonic and induced pluripotent stem cells. *Cell Stem Cell*. Aug 6; **7**(2): 249-57.

Gutman GA, Chandy KG, Grissmer S, Lazdunski M, McKinnon D, Pardo LA, Robertson GA, Rudy B, Sanguinetti MC, Stühmer W, Wang X (2005). International Union of Pharmacology. LIII. Nomenclature and molecular relationships of voltage-gated potassium channels. *Pharmacol Rev*. Dec; **57**(4): 473-508.

Haglid KG, Wang S, Qiner Y, Hamberger A (1994). Excitotoxicity. Experimental correlates to human epilepsy. Mol. *Neurobiol*; **4**, 9, 259-263.

Halder G, Callaerts P, Gehring WJ (1995). Induction of ectopic eyes by targeted expression of the eyeless gene in Drosophila. *Science.* Mar 24; **267**(5205): 1788-92.

Hauser WA (1994). The prevalence and incidence of convulsive disorders in children. *Epilepsia*; **35** Suppl 2: S1-6.

Hawkins RD, Hon GC, Lee LK, Ngo Q, Lister R, Pelizzola M, Edsall LE, Kuan S, Luu Y, Klugman S, Antosiewicz-Bourget J, Ye Z, Espinoza C, Agarwahl S, Shen L, Ruotti V, Wang W, Stewart R, Thomson JA, Ecker JR, Ren B (2010). Distinct epigenomic landscapes of pluripotent and lineage-committed human cells. Cell Stem Cell. 2010 May 7; **6**(5): 479-91.

He ZW, Qu J, Zhang Y, Mao CX, Wang ZB, Mao XY, Deng ZY, Zhou BT, Yin JY, Long HY, Xiao B, Zhang Y, Zhou HH, Liu ZQ (2014). PRRT2 mutations are related to febrile seizures in epileptic patients. *Int J Mol Sci*. Dec 16; **15**(12): 23408-17.

Heron SE, Dibbens LM (2013). Role of PRRT2 in common paroxysmal neurological disorders: a gene with remarkable pleiotropy. *J Med Genet*. Mar; **50**(3): 133-9.

Heron SE, Grinton BE, Kivity S, Afawi Z, Zuberi SM, Hughes JN, Pridmore C, Hodgson BL, Iona X, Sadleir LG, Pelekanos J, Herlenius E, Goldberg-Stern H, Bassan H, Haan E, Korczyn AD, Gardner AE, Corbett MA, Gécz J, Thomas PQ, Mulley JC, Berkovic SF, Scheffer IE, Dibbens LM (2012). PRRT2 mutations cause benign familial infantile epilepsy and infantile convulsions with choreoathetosis syndrome. *Am J Hum Genet*. Jan 13; **90**(1): 152-60.

Heron SE, Crossland KM, Andermann E, Phillips HA, Hall AJ, Bleasel A, Shevell M, Mercho S, Seni MH, Guiot MC, Mulley JC, Berkovic SF, Scheffer IE (2002). Sodium-channel defects in benign familial neonatal-infantile seizures*. Lancet*. Sep 14; **360**(9336): 851-2.

Hille B (2001). Ion channels and excitable membranes; *ISBN*: 9780878933211.

Hitoshi N, Burdon T, Chambers I, Smith A (1998). Self-renewal of pluripotent embryonic stem cells is mediated via activation of STAT3. *Genes Dev*. Jul 1; **12**(13): 2048–2060.

Hochedlinger K, Jaenisch R (2006). Nuclear reprogramming and pluripotency. *Nature*. Jun 29; **441**(7097): 1061-7.

Hodkin AL, Huxley AF (1952). A quantitative description of membrane current and its application to conduction and excitation in nerve. *J Physiol*. Aug; **117**(4): 500-44.

Howell KB, McMahon JM, Carvill GL, Tambunan D, Mackay MT, Rodriguez-Casero V, Webster R, Clark D, Freeman JL, Calvert S, Olson HE, Mandelstam S, Poduri A, Mefford HC, Harvey AS, Scheffer IE (2015). SCN2A encephalopathy: A major cause of epilepsy of infancy with migrating focal seizures*. Neurology*. Sep 15; **85**(11): 958-66.

Hu BY, Weick JP, Yu J, Ma LX, Zhang XQ, Thomson JA, Zhang SC (2010). Neural differentiation of human induced pluripotent stem cells follows developmental principles but with variable potency. *Proc Natl Acad Sci US A.* Mar 2; **107**(9): 4335-40.

Hu W, Tian C, Li T, Yang M, Hou H, Shu Y (2009). Distinct contributions of Nav1.6 and Nav1.2 in action potential initiation and backpropagation. *Nat Neurosci*. Aug; **12**(8): 996-1002.

Isobe K, Cheng Z, Nishio N, Suganya T, Tanaka Y, Ito S (2014). IPSCs, aging and age-related diseases. *N Biotechnol*. Sep 25; **31**(5): 411-21.

Jahn R, and Fasshauer D (2012). Molecular machines governing exocytosis of synaptic vesicles. *Nature*. **490:** 201-7.

Jarecki BW, Piekarz AD, Jackson JO 2nd, Cummins TR (2010). Human voltage-gated sodium channel mutations that cause inherited neuronal and muscle channelopathies increase resurgent sodium currents. *J Clin Invest*. Jan; **120**(1): 369-78.

Jones SL, Svitkina TM (2016). Axon Initial Segment Cytoskeleton: Architecture, Development, and Role in Neuron Polarity. *Neural Plast*; **2016**:6808293.

Joo E, Hong SB, Tae WS, Kim JH, Han SJ, Seo DW, Lee KH, Kim MH, Kim S, Lee MH, Kim BT (2005). Perfusion abnormality of the caudate nucleus in patients with paroxysmal kinesigenic choreoathetosis. *Eur J Nucl Med Mol Imaging*. **32**: 1205-1209.

Kato N, Sadamatsu M, Kikuchi T, Niikawa N, Fukuyama Y (2006). Paroxysmal kinesigenic choreoathetosis: from first discovery in 1892 to genetic linkage with benign familial infantile convulsions. *Epilepsy Res*. Aug; 70 Suppl; **1**: S174-84.
Kearney JA, Plummer NW, Smith MR, Kapur J, Cummins TR, Waxman SG, Goldin AL, Meisler MH (2001). A *gain-of-function* mutation in the sodium channel gene Scn2a results in seizures and behavioural abnormalities. *Neuroscience*; **102**(2): 307-17.

Keefer EW, Gramowski, Gross GW (2001). NMDA receptor-dependent periodic oscillations in cultured spinal cord networks. *J Neurophysiol;* **86**: 3030-3042.

Kertesz A (1967). Paroxysmal kinesigenic choreoathetosis. An entity within the paroxysmal choreoathetosis syndrome. Description of 10 cases, including 1 autopsied. Neurology. Jul; **17**(7): 680-90.

Kikuchi T, Nomura M, Tomita H, Harada N, Kanai K, Konishi T, Yasuda A, Matsuura M, Kato N, Yoshiura K, Niikawa N (2007). Paroxysmal kinesigenic choreoathetosis (PKC): confirmation of linkage to *16p11-q21*, but unsuccessful detection of mutations among 157 genes at the PKC-critical region in seven PKC families. Journal of human genetics; **52**: 334-341.

Kim C (2014). Disease modelling and cell based therapy with iPSC: future therapeutic option with fast and safe application. *Blood Research*; **49**(1): 7-14.

Kim JM, Kim JS, Ki CS, Jeon BS (2006). Episodic Ataxia Type 2 due to a Deletion Mutation in the CACNA1A Gene in a Korean Family. *Journal of Clinical Neurology (Seoul, Korea)*. **2**(4): 268-271.

Kim K, Zhao R, Doi A, Ng K, Unternaehrer J, Cahan P, Huo H, Loh YH, Aryee MJ, Lensch MW, Li H, Collins JJ, Feinberg AP, Daley GQ (2011). Donor cell type can influence the epigenome and differentiation potential of human induced pluripotent stem cells. *Nat Biotechnol*. Nov 27; **29**(12): 1117-9.

Kim K, Adelstein RS, Kawamoto S (2009). Identification of neuronal nuclei (NeuN) as Fox-3, a new member of the Fox-1 gene family of splicing factors. *J Biol Chem*. Nov 6; **284**(45): 31052-61.

Klein JP, Khera DS, Nersesyan H, Kimchi EY, Waxman SG, Blumenfeld H (2004). Dysregulation of sodium channel expression in cortical neurons in a rodent model of absence epilepsy. *Brain Res*. Mar 12; **1000**(1-2): 102-9.

Kochubey O, Lou X, Schneggenburger R (2011). Regulation of transmitter release by Ca^{2+} and synaptotagmin: insights from a large CNS synapse. *Trends Neurosci*. May; **34**(5): 237-46.

Kole MH, Ilschner SU, Kampa BM, Williams SR, Ruben PC, Stuart GJ (2008). Action potential generation requires a high sodium channel density in the axon initial segment. *Nat Neurosci*; Feb; **11**(2): 178-86.

Krützfeldt J, Poy MN, Stoffel M (2006). Strategies to determine the biological function of microRNAs. *Nat Genet*. Jun; **38** Suppl: S14-9.

Kumar KR, Lohmann K, Klein C (2012). Genetics of Parkinson disease and other movement disorders. *Curr Opin Neurol*. Aug; **25**(4): 466-74.

Kure S (1892). An atypical case of Thomsen's disease. Tokyo Igakukai Zasshi. *Journal of the Tokyo Medical Association*; **6**: 505-14.

Kyle DJ, Ilyin VI (2007). Sodium channel blockers. *J Med Chem*. May31; **50**(11): 2583-8.

Labate A, Tarantino P, Viri M, Mumoli L, Gagliardi M, Romeo A, Zara F, Annesi G, Gambardella A (2012). Homozygous *c.649dupC* mutation in PRRT2 worsens the BFIE/PKD phenotype with mental retardation, episodic ataxia, and absences. *Epilepsia*. Dec; **53**(12): 196-9.

Lance J.W. (1977) Familial paroxysmal dystonic choreoathetosis and its differentiation from related syndromes. *Ann Neurol*; **2**: 285-293.

Larsen J, Carvill GL, Gardella E, Kluger G, Schmiedel G, Barisic N, Depienne C, Brilstra E, Mang Y, Nielsen JE, Kirkpatrick M, Goudie D, Goldman R, Jähn JA, Jepsen B, Gill D, Döcker M, Biskup S, McMahon JM, Koeleman B, Harris M, Braun K, de Kovel CG, Marini C, Specchio N, Djémié T, Weckhuysen S, Tommerup N, Troncoso M, Troncoso L, Bevot A, Wolff M, Hjalgrim H, Guerrini R, Scheffer IE, Mefford HC,Møller RS; EuroEPINOMICS RES Consortium CRP (2015). The phenotypic spectrum of SCN8A encephalopathy. *Neurology*. Feb 3; **84**(5): 480-9.

Lee BI, Lesser RP, Pippenger CE, Morris HH, Lüders H, Dinner DS, Corrie WS, Murphy WF (1985). Familial paroxysmal hypnogenic dystonia. *Neurology*. Sep; **35**(9): 1357-60.

Lee HY, Huang Y, Bruneau N, Roll P, Roberson ED, Hermann M, Quinn E, Maas J, Edwards R, Ashizawa T, Baykan B, Bhatia K, Bressman S, Bruno MK, Brunt ER, Caraballo R, Echenne B, Fejerman N, Frucht S, Gurnett CA, Hirsch E, Houlden H, Jankovic J, Lee WL, Lynch DR, Mohamed S, Müller U, Nespeca MP, Renner D, Rochette J, Rudolf G, Saiki S, Soong BW, Swoboda KJ, Tucker S, Wood N, Hanna M, Bowcock A, Szepetowski P, Fu YH, Ptáček LJ (2012). Mutations in the novel protein PRRT2 cause paroxysmal kinesigenic dyskinesia with infantile convulsions. *Cell Rep*; **1:** 2-12.

Lee HY, Xu Y, Huang Y, Ahn AH, Auburger GW, Pandolfo M, Kwiecinski H, Grimes DA, Lang AE, Nielsen JE, Averyanov Y, Servidei S, Friedman A, Van Bogaert P, Abramowicz MJ, Bruno MK, Sorensen BF, Tang L, Fu YH, Ptácek LJ (2004). The gene for paroxysmal non-kinesigenic dyskinesia encodes an enzyme in a stress response pathway. *Hum Mol Genet.* Dec 15; **13**(24): 3161-70.

Lewitzky M, Yamanaka S (2007). Reprogramming somatic cells towards pluripotency by defined factors. *Curr Opin Biotechnol*. Oct; **18**(5): 467-73.

Lignani G, Raimondi A, Ferrea E, Rocchi A, Paonessa F, Cesca F, Orlando M, Tkatch T, Valtorta F, Cossette P, Baldelli P, Benfenati F (2013). Epileptogenic Q555X SYN1 mutant triggers imbalances in release dynamics and short-term plasticity. *Hum Mol Genet*. Jun 1; **22**(11): 2186-99.

Li HF, Ni W, Xiong ZQ, Xu J, Wu ZY (2013). PRRT2 *c.649dupC* mutation derived from *de novo* in paroxysmal kinesigenic dyskinesia. *CNS Neurosci Ther*; **19**: 61-5.

Li J, Zhu X, Wang X, Sun W. Feng B, Du T, Sun B, Niu f, Wei H, Wu X, Dong L, Li L, Cai X, Wang Y and Liu Y (2012). Targeted genomic sequencing identifies PRRT2 mutations as a cause of paroxysmal kinesigenic choreoathetosis. *J Med Genet*. Feb; **49**(2): 76–78.

Li M, Niu F, Zhu X, Wu X, Shen N, Peng X, Liu Y (2015). PRRT2 Mutant leads to dysfunction of glutamate signaling. *Int J Mol Sci*. Apr 23; **16**(5): 9134-51.

Lister R, Pelizzola M, Kida YS, Hawkins RD, Nery JR, Hon G, Antosiewicz-Bourget J, O'Malley R, Castanon R, Klugman S, Downes M, Yu R, Stewart R, Ren B, Thomson JA, Evans RM, Ecker JR (2011). Hotspots of aberrant epigenomic reprogramming in human induced pluripotent stem cells. *Nature*. Mar 3; **471**(7336): 68-73.

Liu H, Zhu F, Yong J, Zhang P, Hou P, Li H, Jiang W, Cai J, Liu M, Cui K, Qu X, Xiang T, Lu D, Chi X, Gao G, Ji W, Ding M, Deng H (2008). Generation of induced pluripotent stem cells from adult rhesus monkey fibroblasts. *Cell Stem Cell*. Dec 4; **3**(6): 587-90.

Liu PW, Bean BP (2014). Kv2 Channel Regulation of Action Potential Repolarization and Firing Patterns in Superior Cervical Ganglion Neurons and Hippocampal CA1 Pyramidal Neurons. *The Journal of Neuroscience*. 2014; **34**(14):4991-5002.

Liu Q, Qi Z, Wan XH, Li JY, Shi L, Lu Q, Zhou XQ, Qiao L, Wu LW, Liu XQ, Yang W, Liu Y, Cui LY, Zhang X (2012). Mutations in PRRT2 result in paroxysmal dyskinesias with marked variability in clinical expression. *J Med Genet*. Feb; **49**(2): 79-82.

Liu XR, Huang D, Wang J, Wang YF, Sun H, Tang B, Li W, Lai JX, He N, Wu M, Su T, Meng H, Shi YW, Li BM, Tang BS, Liao WP (2016). Paroxysmal hypnogenic dyskinesia is associated with mutations in the PRRT2 gene. *Neurol Genet*. Mar 22; **2**(2): e66.

Liu XR, Wu M, He N, Meng H, Wen L, Wang JL, Zhang MP, Li WB, Mao X, Qin JM, Li BM, Tang B, Deng YH, Shi YW, Su T, Yi YH, Tang BS, Liao WP (2013). Novel PRRT2 mutations in paroxysmal dyskinesia patients with variant inheritance and phenotypes. *Genes Brain Behav*. Mar; **12**(2): 234-40.

Liu YT, Nian FS, Chou WJ, Tai CY, Kwan SY, Chen C, Kuo PW, Lin PH, Chen CY, Huang CW, Lee YC, Soong BW, Tsai JW (2016). PRRT2 mutations lead to neuronal dysfunction and neurodevelopmental defects. *Oncotarget*. Jun 28; **7**(26): 39184-39196.

Lombardo AJ, Kuzniecky R, Powers RE, Brown GB (1996). Altered brain sodium channel transcript levels in human epilepsy. *Brain Res Mol Brain Res*; Jan; **35**(1-2): 84-90.

Lowry WE, Richter L, Yachechko R, Pyle AD, Tchieu J, Sridharan R, Clark AT, Plath K (2008). Generation of human induced pluripotent stem cells from dermal fibroblasts*. Proc Natl Acad Sci U S A*. Feb 26; **105**(8): 2883-8.

Lugaresi E, Cirignotta F (1981). Hypnogenic paroxysmal dystonia: epileptic seizure or a new syndrome? *Sleep*. **4**(2): 129-38.

Luo C, Chen Y, Song W, Chen Q, Gong Q, Shang HF (2013). Altered intrinsic brain activity in patients with paroxysmal kinesigenic dyskinesia by PRRT2 mutation: altered brain activity by PRRT2 mutation. *Neurol Sci.* Nov; **34**(11): 1925-31.

Ma T, Xie M, Laurent T, Ding S (2013). Progress in the reprogramming of somatic cells. *Circ Res.* Feb 1; **112**(3): 562–574.

Maeda E, Robinson HP and Kawana A (1995). The mechanisms of generation and propagation of synchronized bursting in developing networks of cortical neurons. *J Neurosci*; **15**: 6834-6845.

Maherali N, Sridharan R, Xie W, Utikal J, Eminli S, Arnold K, Stadtfeld M, Yachechko R, Tchieu J, Jaenisch R, Plath K, Hochedlinger K (2007). Directly reprogrammed fibroblasts show global epigenetic remodelling and widespread tissue contribution. *Cell Stem Cell*. Jun 7; **1**(1):.55-70.

Maljevic S, Lerche H (2014). Potassium channel genes and benign familial neonatal epilepsy. *Prog Brain Res*; **213**: 17-53.

Mandolesi G, Vanni V, Cesa R, Grasselli G, Puglisi F, Cesare P, Strata P (2009). Distribution of the SNAP25 and SNAP23 synaptosomal-associated protein isoforms in rat cerebellar cortex. *Neuroscience*; **164**:1 084-1096.

Mantegazza M, Catterall WA (2012). Voltage-Gated Na+ Channels: Structure, Function, and Pathophysiology. Jasper's Basic Mechanisms of the Epilepsies. 4th edition. Bethesda (MD): National Center for Biotechnology Information (US); Available from: https://www.ncbi.nlm.nih.gov/books/NBK98195/.

Mantegazza M, Curia G, Biagini G, Ragsdale DS, Avoli M (2012). Voltage-gated sodium channels as therapeutic targets in epilepsy and other neurological disorders. *Lancet Neurol*. Apr; **9**(4): 413-24.

Mantegazza M (2006). Effects in neocortical neurons of mutations of the Nav1.2 Na^+ channel causing benign familial neonatal-infantile seizures. *J Neurosci.* Oct 4; **26**(40): 10100-9.

Marchetto MC, Yeo GW, Kainohana O, Marsala M, Gage FH, Muotri AR (2009). Transcriptional signature and memory retention of human-induced pluripotent stem cells. *PLoS One.* Sep 18; **4**(9): e7076.

Margari L, Presicci A, Ventura P, Margari F, Perniola T (2005). Channelopathy: hypothesis of a common pathophysiologic mechanism in different forms of paroxysmal dyskinesia. *Pediatr Neurol*. Apr; **32**(4): 229-35.

Marini C, Conti V, Mei D, Battaglia D, Lettori D, Losito E, Bruccini G, Tortorella G, Guerrini R (2012). PRRT2 mutations in familial infantile seizures, paroxysmal dyskinesia, and hemiplegic migraine. *Neurology*. Nov 20; **79**(21): 2109-14.

Maximov A, Südhof TC (2005). Autonomous function of synaptotagmin 1 in triggering synchronous release independent of asynchronous release. *Neuron*. Nov 23; **48**(4): 547-54.

McGrath TM, Dure LS (2003). Paroxysmal Dyskinesias in Children. *Curr Treat Options Neurol*. Jul; **5**(4): 275-278.

Meisler MH, Helman G, Hammer MF, Fureman BE, Gaillard WD, Goldin AL, Hirose S, Ishii A, Kroner BL, Lossin C, Mefford HC, Parent JM, Patel M, Schreiber J, Stewart R, Whittemore V, Wilcox K, Wagnon JL, Pearl PL, Vanderver A, Scheffer IE (2016). SCN8A encephalopathy: Research progress and prospects. *Epilepsia*. Jul; **57**(7): 1027-35.

Meisler MH, O'Brien JE, Sharkey LM (2010). Sodium channel gene family: epilepsy mutations, gene interactions and modifier effects. *J Physiol.* Jun 1; **588**(Pt 11): 1841-8.

Méneret A, Gaudebout C, Riant F, Vidailhet M, Depienne C, Roze E (2013). PRRT2 mutations and paroxysmal disorders. *Eur J Neurol*. Jun; **20**(6): 872-8.

Michetti C, Castroflorio E, Marchionni I, Forte N, Sterlini B, Binda F, Fruscione F, Baldelli P, Valtorta F, Zara F, Corradi A, Benfenati F (2017). The PRRT2 knockout mouse recapitulates the neurological diseases associated with PRRT2 mutations. *Neurobiol Dis*. Mar; **99**: 66-83.

Milescu, L.S., Bean, B.P., Smith, J.C (2010). Isolation of somatic Na^+ currents by selective inactivation of axonal channels with a voltage prepulse. *J Neurosci* 30, 7740-7748.

Millar AG, Bradacs H, Charlton MP, Atwood HL (2002) Inverse relationship between release probability and readily releasable vesicles in depressing and facilitating synapses. *J Neurosci;* **22**: 9661-9667.

Montagna P (1992). Nocturnal paroxysmal dystonia and nocturnal wandering. *Neurology*. Jul; **42**(7 Suppl 6): 61-7.

Nachbauer W, Nocker M, Karner E, Stankovic I, Unterberger I, Eigentler A, Najmabadi H, Hu H, Garshasbi M, Zemojtel T, Abedini SS, Chen W, Hosseini M,Behjati F, Haas S, Jamali P, Zecha A, Mohseni M, Püttmann L, Vahid LN, Jensen C, Moheb LA, Bienek M, Larti F, Mueller I, Weissmann R, Darvish H, Wrogemann K, Hadavi V, Lipkowitz B, Esmaeeli-Nieh S, Wieczorek D, Kariminejad R, Firouzabadi SG, Cohen M, Fattahi Z, Rost I, Mojahedi F, Hertzberg C, Dehghan A, Rajab A, Banavandi MJ, Hoffer J, Falah M, Musante L, Kalscheuer V, Ullmann R, Kuss AW,Tzschach A, Kahrizi K, Ropers HH (2011). Deep sequencing reveals 50 novel genes for recessive cognitive disorders. *Nature*. Sep 21; **478**(7367): 57-63.

Nakagawa M, Koyanagi M, Tanabe K, Takahashi K, Ichisaka T, Aoi T, Okita K, Mochiduki Y, Takizawa N, Yamanaka S (2008). Generation of induced pluripotent stem cells without MYC from mouse and human fibroblasts. *Nat Biotechnol*. Jan; **26**(1): 101-6.

Namadurai S, Yereddi NR, Cusdin FS, Huang CL, Chirgadze DY, Jackson AP (2015). A new look at sodium channel β subunits. *Open Biol*. Jan; **5**(1): 140192.

Nichols J, Smith A (2009). Naive and primed pluripotent states. *Cell Stem Cell*. Jun 5; **4**(6): 487-92.

Noh GJ, Jane Tavyev Asher Y, Graham JM Jr (2012). Clinical review of genetic epileptic encephalopathies. *Eur J Med Genet*. May; **55**(5): 281-98.

Ogiwara I, Miyamoto H, Morita N, Atapour N, Mazaki E, Inoue I, Takeuchi T, Itohara S, Yanagawa Y, Obata K, Furuichi T, Hensch TK, Yamakawa K. (2007) Nav1.1 localizes to axons of parvalbumin-positive inhibitory interneurons: a circuit basis for epileptic seizures in mice carrying an *SCNA1* gene mutation. *J Neurosci*. May 30; **27**(22): 5903-14.

Ohi Y, Qin H, Hong C, Blouin L, Polo JM, Guo T, Qi Z, Downey SL, Manos PD, Rossi DJ, Yu J, Hebrok M, Hochedlinger K, Costello JF, Song JS, Ramalho-Santos M (2011). Incomplete DNA methylation underlies a transcriptional memory of somatic cells in human iPS cells. *Nat Cell Biol*. May; **13**(5): 541-9.

Okumura A, Shimojima K, Kubota T, Abe S, Yamashita S, Imai K, Okanishi T, Enoki H, Fukasawa T, Tanabe T, Dibbens LM, Shimizu T, Yamamoto T (2013). PRRT2 mutation in Japanese children with benign infantile epilepsy. *Brain Dev*. Aug; **35**(7): 641-6.

Ono S, Yoshiura K, Kinoshita A, Kikuchi T, Nakane Y, Kato N, Sadamatsu M, Konishi T, Nagamitsu S, Matsuura M, Yasuda A, Komine M, Kanai K, Inoue T, Osamura T, Saito K, Hirose S, Koide H, Tomita H, Ozawa H, Niikawa N, Kurotaki N (2012). Mutations in PRRT2 responsible for paroxysmal kinesigenic dyskinesias also cause benign familial infantile convulsions. *J Hum Genet*.May; **57**(5): 338-41.

Osafune K, Caron L, Borowiak M, Martinez RJ, Fitz-Gerald CS, Sato Y, Cowan CA, Chien KR, Melton DA (2008). Marked differences in differentiation propensity among human embryonic stem cell lines. *Nat Biotechnol*. Mar; **26**(3): 313-5.

Paiva ARC, Park I, Principe JC (2010). A comparison of binless spike train measures. *Neural Comput Applic*; **19**: 405-419.

Pang ZP, Südhof TC (2010). Cell biology of Ca^{2+}-triggered exocytosis. *Curr Opin Cell Biol.* Aug; **22**(4): 496-505.

Pang ZP, Melicoff E, Padgett D, Liu Y, Teich AF, Dickey BF, Lin W, Adachi R, Südhof TC (2006a). Synaptotagmin-2 is essential for survival and contributes to Ca^{2+} triggering of neurotransmitter release in central and neuromuscular synapses. *J Neurosci*. Dec 27; **26**(52): 13493-504.

Pang ZP, Sun J, Rizo J, Maximov A, Südhof TC (2006b). Genetic analysis of synaptotagmin 2 in spontaneous and Ca^{2+}-triggered neurotransmitter release. *EMBO J*. May 17; **25**(10):2039-50.

Pfaffl, M.W (2001). A new mathematical model for relative quantification in real-time RT-PCR. *Nucleic Acids Res* 29, e45.

Pietrobon D (2010). Insights into migraine mechanisms and $Ca_V2.1$ calcium channel function from mouse models of familial hemiplegic migraine. *J Physiol*. Jun 1; **588**(Pt 11): 1871-8.

Polo JM, Liu S, Figueroa ME, Kulalert W, Eminli S, Tan KY, Apostolou E, Stadtfeld M, Li Y, Shioda T, Natesan S, Wagers AJ, Melnick A, Evans T, Hochedlinger K (2010). Cell type of origin influences the molecular and functional properties of mouse induced pluripotent stem cells. *Nat Biotechnol Aug*; **28**(8): 848-55.

Pozzi D, Lignani G, Ferrea E, Contestabile A, Paonessa F, D'Alessandro R, Lippiello P, Boido D, Fassio A, Meldolesi J, Valtorta F, Benfenati F, Baldelli P (2013) REST/NRSF-mediated intrinsic homeostasis protects neuronal networks from hyperexcitability. *EMBO J;* **32**: 2994-3007.

Prajumwongs P, Weeranantanapan O, Jaroonwitchawan T, Noisa P (2016). Human Embryonic Stem Cells: A Model for the Study of Neural Development and Neurological Diseases. *Stem Cells International*; **2016**: 2958210.

Ragsdale DS, McPhee JC, Scheuer T, Catterall WA (1996). Common molecular determinants of local anesthetic, antiarrhythmic, and anticonvulsant block of voltage-gated Na^+ channels. *Proc Natl Acad Sci USA.* Aug 20; **93**(17): 9270-5.

Ragsdale DS, McPhee JC, Scheuer T, Catterall WA (1994). Molecular determinants of state-dependent block of Na+ channels by local anesthetics. *Science*.Sep 16; **265**(5179): 1724-8.

Rajakulendran S, Graves TD, Labrum RW, Kotzadimitriou D, Eunson L, Davis MB, Davies R, Wood NW, Kullmann DM, Hanna MG, Schorge S (2010). Genetic and functional characterisation of the P/Q calcium channel in episodic ataxia with epilepsy. *J Physiol*.Jun 1; **588**(Pt 11): 1905-13.

Rasband MN (2010). The axon initial segment and the maintenance of neuronal polarity. *Nat Rev Neurosci*. Aug; **11**(8): 552-62.

Raskind WH, Bolin T, Wolff J, Fink J, Matsushita M, Litt M, Lipe H, Bird TD (1998). Further localization of a gene for paroxysmal dystonic horeoathetosis to a 5-cM region on chromosome 2q34*. Hum Genet*. Jan; **102**(1): 93-7.

Reubinoff BE, Itsykson P, Turetsky T, Pera MF, Reinhartz E, Itzik A, Ben-Hur T (2001). Neural progenitors from human embryonic stem cells. *Nat Biotechnol*. Dec; **19**(12): 1134-40.

Riant F, Roze E, Barbance C, Méneret A, Guyant-Maréchal L, Lucas C, Sabouraud P, Trébuchon A, Depienne C, and Tournier-Lasserve E (2012). PRRT2 mutations cause hemiplegic migraine. *Neurology*; **79:** 2122-2124.

Ricciardi S, Ungaro F, Hambrock M, Rademacher N, Stefanelli G, Brambilla D, Sessa A, Magagnotti C, Bachi A, Giarda E, Verpelli C, Kilstrup-Nielsen C, Sala C, Kalscheuer VM, Broccoli V (2012). CDKL5 ensures excitatory synapse stability by reinforcing NGL-1-PSD95 interaction in the postsynaptic compartment and is impaired in patient iPSC-derived neurons. *Nat Cell Biol.*Sep; **14**(9): 911-23.

Rieke, F., Warland, D., de Ruyter van Steveninck, R., Bialek, W (1997). Spikes, exploring the neural code (*MIT Press*).

Rogawski MA (2000). KCNQ2/KCNQ3 K^+ channels and the molecular pathogenesis of epilepsy: implications for therapy. *Trends Neurosci*. Sep; **23**(9): 393-8.

Rossi P, Sterlini B, Castroflorio E, Marte A, Onofri F, Valtorta F, Maragliano L, Corradi A, Benfenati F (2016). A Novel Topology of Proline-rich Transmembrane Protein 2 (PRRT2): hints for an intracellular function at the synapse. *J Biol Chem*. Mar 18; **291**(12): 6111-23.

Russell MB, Ducros A (2011). Sporadic and familial hemiplegic migraine: pathophysiological mechanisms, clinical characteristics, diagnosis, and management. *Lancet Neurol*. May; **10**(5): 457-70.

Ryan DP, Ptácek LJ (2010). Episodic neurological channelopathies. *Neuron*; Oct 21; **68**(2): 282-92.

Saheki Y, De Camilli P (2012). Synaptic vesicle endocytosis. *Cold Spring Harb Perspect Bio*l. Sep 1; **4**(9): a005645.

Sällman Almén M, Bringeland N, Fredriksson R, Schiöth HB (2012). The dispanins: a novel gene family of ancient origin that contains 14 human members. *PLoS One*; **7**(2): e31961.

Scalmani P, Rusconi R, Armatura E, Zara F, Avanzini G, Franceschetti S, Mantegazza M (2006). Effects in neocortical neurons of mutations of the $Na_V1.2$ Na^+ channel causing benign familial neonatal-infantile seizures. *J Neurosci*. Oct 4; **26**(40): 10100-9.

Scharfman HE, Brooks-Kayal AR (2014) Is plasticity of GABA-ergic mechanisms relevant to epileptogenesis? *Adv Exp Med Biol* 813: 133-150.

Scheffer IE, Grinton BE, Heron SE, Kivity S, Afawi Z, Iona X, Goldberg-Stern H, Kinali M, Andrews I, Guerrini R, Marini C, Sadleir LG, Berkovic SF, and Dibbens LM (2012). PRRT2 phenotypic spectrum includes sporadic and fever-related infantile seizures. *Neurology*. **79:** 2104-2108.

Schneggenburger R, Sakaba T, Neher E (2002) Vesicle pools and short-term synaptic depression: lessons from a large synapse. *Trends Neurosci;* **25**: 206-212.

Schneggenburger R, Meyer AC, Neher E (1999) Released fraction and total size of a pool of immediately available transmitter quanta at a calyx synapse. *Neuron;* **23**: 399-409.

Schneider R, Poewe W, Delazer M, Boesch S (2014). Episodic ataxia type 2: phenotype characteristics of a novel CACNA1A mutation and review of the literature. *J Neurol*.May; **261**(5): 983-91.

Scholl UI, Choi M, Liu T, Ramaekers VT, Häusler MG, Grimmer J, Tobe SW, Farhi A, Nelson-Williams C, Lifton RP (2009). Seizures, sensorineural deafness, ataxia, mental retardation, and electrolyte imbalance (SeSAME syndrome) caused by mutations in KCNJ10. *Proc Natl Acad Sci U S A*. Apr 7; **106**(14): 5842-7.

Schubert J, Paravidino R, Becker F, Berger A, Bebek N, Bianchi A, Brockmann K, Capovilla G, Dalla Bernardina B, Fukuyama Y, Hoffmann GF, Jurkat-Rott K, Anttonen AK, Kurlemann G, Lehesjoki AE, Lehmann-Horn F, Mastrangelo M, Mause U, Müller S, Neubauer B, Püst B, Rating D, Robbiano A, Ruf S, Schroeder C, Seidel A, Specchio N, Stephani U, Striano P, Teichler J, Turkdogan D, Vigevano F, Viri M, Bauer P, Zara F, Lerche H, Weber YG (2012). PRRT2 mutations are the major cause of benign familial infantile seizures. *Hum Mutat*. Oct; **33**(10): 1439-43.

Schwenk J, Baehrens D, Haupt A, Bildl W, Boudkkazi S, Roeper J, Fakler B, Schulte U (2014). Regional diversity and developmental dynamics of the AMPA-receptor proteome in the mammalian brain. *Neuron*. Oct 1; **84**(1): 41-54.

Schwenk J, Harmel N, Brechet A, Zolles G, Berkefeld H, Müller CS, Bildl W, Baehrens D, Hüber B, Kulik A, Klöcker N, Schulte U, Fakler B (2012). High-resolution proteomics unravel architecture and molecular diversity of native AMPA receptor complexes. *Neuron*. May 24; **74**(4): 621-33.

Shahaf G, Marom S (2001). Learning in networks of cortical neurons. *J Neurosci;* **21**: 8782-8788.

Shanks NF, Savas JN, Maruo T, Cais O, Hirao A, Oe S, Ghosh A, Noda Y, Greger IH, Yates JR 3rd, Nakagawa T. (2012) Differences in AMPA and kainate receptor interactomes facilitate identification of AMPA receptor auxiliary subunit GSG1L. *Cell Rep*. Jun 28; **1**(6): 590-8.

Shimmura C, Suda S, Tsuchiya KJ, Hashimoto K, Ohno K, Matsuzaki H, Iwata K, Matsumoto K, Wakuda T, Kameno Y, Suzuki K, Tsujii M, Nakamura K, Takei N, Mori N (2011). Alteration of plasma glutamate and glutamine levels in children with high-functioning autism. *PLoS One*; **6**(10): e25340.

Shinawi M, Liu P, Kang SH, Shen J, Belmont JW, Scott DA, Probst FJ, Craigen WJ, Graham BH, Pursley A, Clark G, Lee J, Proud M, Stocco A, Rodriguez DL, Kozel BA, Sparagana S, Roeder ER, McGrew SG, Kurczynski TW, Allison LJ, Amato S, Savage S, Patel A, Stankiewicz P, Beaudet AL, Cheung SW, Lupski JR (2010). Recurrent reciprocal *16p11.2* rearrangements associated with global developmental delay, behavioural problems, dysmorphism, epilepsy, and abnormal head size. *J Med Genet*. May; **47**(5): 332-41.

Silveira-Moriyama L, Gardiner AR, Meyer E, King MD, Smith M, Rakshi K, Parker A, Mallick AA, Brown R, Vassallo G, Jardine PE, Guerreiro MM, Lees AJ, Houlden H, Kurian MA (2013). Clinical features of childhood-onset paroxysmal kinesigenic dyskinesia with PRRT2 gene mutations. *Dev Med Child Neurol*. Apr; **55**(4): 327-34.

Smallwood SA, Kelsey G (2012). De novo DNA methylation: a germ cell perspective. *Trends Genet*. Jan; **28**(1): 33-42.

Soldner F, Hockemeyer D, Beard C, Gao Q, Bell GW, Cook EG, Hargus G, Blak A, Cooper O, Mitalipova M, Isacson O, Jaenisch R. (2009) Parkinson's disease patient-derived induced pluripotent stem cells free of viral reprogramming factors. *Cell Mar* 6; **136**(5): 964-77.

Soza-Ried J, Fisher AG (2012). Reprogramming somatic cells towards pluripotency by cellular fusion. *Curr Opin Genet Dev*. Oct; **22**(5): 459-65.

Spacey and Adams (2013) GeneReviews®; 1998-2018.

Stadtfeld M, Hochedlinger K (2010). Induced pluripotency: history, mechanisms, and applications. *Genes & Development*, **24**(20), 2239-2263.

Stadtfeld M, Maherali N, Borkent M, Hochedlinger K (2010). A reprogrammable mouse strain from gene-targeted embryonic stem cells. *Nat Methods*.Jan; **7**(1): 53-5.

Stelzl U, Worm U, Lalowski M, Haenig C, Brembeck FH, Goehler H, Stroedicke M, Zenkner M, Schoenherr A, Koeppen S, Timm J, Mintzlaff S, Abraham C, Bock N, Kietzmann S, Goedde A, Toksöz E, Droege A, Krobitsch S, Korn B, Birchmeier W, Lehrach H, Wanker EE (2005). A human protein-protein interaction network: a resource for annotating the proteome. *Cell*; **122:** 957-68.

Strzelczyk A, Bürk K, Oertel WH (2011). Treatment of paroxysmal dyskinesias. Expert Opin Pharmacother; **12**(1): 63-72.

Südhof TC (2013). Neurotransmitter release: the last millisecond in the life of a synaptic vesicle. *Neuron*. Oct 30; **80**(3): 675-90.

Südhof TC and Rizo J (2011). Synaptic vesicle exocytosis. *Cold Spring Harb. Perspect. Biol*. Dec; **3**(12): a005637.

Südhof TC (2008). Neuroligins and neurexins link synaptic function to cognitive disease*. Nature*; **455**: 903-911.

Suls A, Dedeken P, Goffin K, Van Esch H, Dupont P, Cassiman D, Kempfle J, Wuttke TV, Weber Y, Lerche H, Afawi Z, Vandenberghe W, Korczyn AD, Berkovic SF, Ekstein D, Kivity S, Ryvlin P, Claes LR, Deprez L, Maljevic S, Vargas A, Van Dyck T, Goossens D, Del-Favero J, Van Laere K, De Jonghe P, Van Paesschen W (2008). Paroxysmal exercise-induced dyskinesia and epilepsy is due to mutations in SLC2A1, encoding the glucose transporter GLUT1. *Brain*.Jul; **131**(Pt 7): 1831-44.

Sun J, Pang ZP, Qin D, Fahim AT, Adachi R, Südhof TC (2007). A dual-Ca^{2+}-sensor model for neurotransmitter release in a central synapse. *Nature*. Nov 29; **450**(7170): 676-82.

Suresh J, Radojicic M, Pesce LL, Bhansali A, Wang J, Tryba AK. Marks JD, van Drongelen W (2016). Network burst activity in hippocampal neuronal cultures: the role of synaptic and intrinsic currents. *J Neurophysiol*; **115**: 3073-3089.

Suter MR, Bhuiyan ZA, Laedermann CJ, Kuntzer T, Schaller M, Stauffacher MW, Roulet E, Abriel H, Decosterd I, Wider C (2015). *p.L1612P*, a novel voltage-gated sodium channel Nav1.7 mutation inducing a cold sensitive paroxysmal extreme pain disorder*. Anesthesiology*. Feb; **122**(2): 414-23.

Swoboda KJ, Soong B, McKenna C, Brunt ER, Litt M, Bale JF Jr, Ashizawa T, Bennett LB, Bowcock AM, Roach ES, Gerson D, Matsuura T, Heydemann PT, Nespeca MP, Jankovic J, Leppert M, Ptácek LJ (2000). Paroxysmal kinesigenic dyskinesia and infantile convulsions: clinical and linkage studies. *Neurology*; **55:** 224-30.

Szepetowski P, Rochette J, Berquin P, Piussan C, Lathrop GM, Monaco AP (1997). Familial infantile convulsions and paroxysmal choreoathetosis: a new

neurological syndrome linked to the pericentromeric region of human chromosome 16. *Am J Hum Genet*; **61:** 889-98.

Tada M, Takahama Y, Abe K, Nakatsuji N, Tada T (2001). Nuclear reprogramming of somatic cells by in vitro hybridization with ES cells. *Curr Biol*. Oct 2; **11**(19):1553-8.

Takahashi K, Yamanaka S (2015). A developmental framework for induced pluripotency. *Development*. Oct 1; **142**(19): 3274-85.

Takahashi K, Tanabe K, Ohnuki M, Narita M, Ichisaka T, Tomoda K, Yamanaka S (2007). Induction of pluripotent stem cells from adult human fibroblasts by defined factors. *Cell*. Nov 30; **131**(5): 861-72.

Takahashi K, Yamanaka S (2006). Induction of pluripotent stem cells from mouse embryonic and adult fibroblast cultures by defined factors. *Cell*. Aug 25; **126**(4): 663-76.

Tan GH, Liu YY, Wang L, Li K, Zhang ZQ, Li HF, Yang ZF, Li Y, Li D, Wu MY, Yu CL, Long JJ, Chen RC, Li LX, Yin LP, Liu JW, Cheng XW, Shen Q, Shu YS, Sakimura K, Liao LJ, Wu ZY, Xiong ZQ (2017). PRRT2 deficiency induces paroxysmal kinesigenic dyskinesia by regulating synaptic transmission in cerebellum. *Cell Res*. Jan; **28**(1): 90-110.

Tanabe Y, Hashimoto K, Shimizu C, Hirakawa A, Harano K, Yunokawa M, Yonemori K, Katsumata N, Tamura K, Ando M, Kinoshita T, Fujiwara Y (2013). Paclitaxel-induced peripheral neuropathy in patients receiving adjuvant chemotherapy for breast cancer. *Int J Clin Oncol*. Feb; **18**(1): 132-8.

Tang G (2005). siRNA and miRNA: an insight into RISCs. *Trends Biochem Sci; F*eb; **30**(2):106-14.

Taverna E, Huttner WB (2010). Neural progenitor nuclei IN motion. *Neuron*. Sep 23; **67**(6): 906-14.

Thomson JA, Itskovitz-Eldor J, Shapiro SS, Waknitz MA, Swiergiel JJ, Marshall VS, Jones JM (1998). Embryonic stem cell lines derived from human blastocysts. *Science*. Nov 6; **282**(5391): 1145-7.

Toader O, Forte N, Orlando M, Ferrea E, Raimondi A, Baldelli P, Benfenati F, Medrihan L (2013). Dentate gyrus network dysfunctions precede the symptomatic phase in a genetic mouse model of seizures. *Front Cell Neurosci*. Aug 30; **7**: 138.

Todorov B, Kros L, Shyti R, Plak P, Haasdijk ED, Raike RS, Frants RR, Hess EJ, Hoebeek FE, De Zeeuw CI, van den Maagdenberg AM (2012). Purkinje cell-specific ablation of Cav2.1 channels is sufficient to cause cerebellar ataxia in mice. *Cerebellum*. Mar; **11**(1): 246-58.

Tokuzawa Y, Kaiho E, Maruyama M, Takahashi K, Mitsui K, Maeda M, Niwa H, Yamanaka S (2003). Fbx15 is a novel target of Oct3/4 but is dispensable for

embryonic stem cell self-renewal and mouse development. Mol Cell Biol. Apr; **23**(8): 2699-708.

Tomita Ha, Nagamitsu S, Wakui K, Fukushima Y, Yamada K, Sadamatsu M, Masui A, Konishi T, Matsuishi T, Aihara M, Shimizu K, Hashimoto K, Mineta M, Matsushima M, Tsujita T, Saito M, Tanaka H, Tsuji S, Takagi T, Nakamura Y, Nanko S, Kato N,Nakane Y, Niikawa N (1999). Paroxysmal kinesigenic choreoathetosis locus maps to chromosome *16p11.2-q12.1*. *Am J Hum Genet*. Dec; **65**(6): 1688-97.

Tottene A, Conti R, Fabbro A, Vecchia D, Shapovalova M, Santello M, van den Maagdenberg AMJM, Ferrari MD, Pietrobon D. (2009) Enhanced excitatory transmission at cortical synapses as the basis for facilitated spreading depression in $Ca_V2.1$ knockin migraine mice. *Neuron*; **61**: 762-773.

Turrigiano G (2011). Too many cooks? Intrinsic and synaptic homeostatic mechanisms in cortical circuit refinement. *Annu Rev Neurosci*.; **34**: 89-103.

Unno T, Wakamori M, Koike M, Uchiyama Y, Ishikawa K, Kubota H, Yoshida T, Sasakawa H, Peters C, Mizusawa H, Watase K (2012). Development of Purkinje cell degeneration in a knocking mouse model reveals lysosomal involvement in the pathogenesis of SCA6*. Proc Natl Acad Sci USA*.Oct 23; **109**(43): 17693-8.

Unterberger I and Trinka E. (2008) Diagnosis and Treatment of Paroxysmal Dyskinesias Revisited. *Ther Adv Neurol Disord*. Sep; **1**(2): 4-11.

Vacher H, Mohapatra DP, Trimmer JS (2008). Localization and targeting of voltage-dependent ion channels in mammalian central neurons. *Physiol Rev.Oct*; **88**(4): 1407-47.

Vajda I, van Pelt J, Wolters PS, Chiappalone M, Martinoia S, van Someren E, van Ooyen A (2008). Low frequency stimulation induces stable transitions in stereotypical activity of cortical networks. *Biophys J*; **94**: 5028–5039.

Valente P, Castroflorio E, Rossi P, Fadda M, Sterlini B, Cervigni RI, Prestigio C, Giovedì S, Onofri F, Mura E, Guarnieri FC, Marte A, Orlando M, Zara F, Fassio A, Valtorta F, Baldelli P, Corradi A, Benfenati F (2016a). PRRT2 Is a Key Component of the Ca^{2+}- Dependent Neurotransmitter Release Machinery. *Cell Rep*. Apr 5; **15**(1): 117-31.

Valente P, Orlando M, Raimondi A, Benfenati F, Baldelli P (2016b). Fine Tuning of Synaptic Plasticity and Filtering by GABA Released from Hippocampal Autaptic Granule Cells. *Cereb Cortex*. Mar; **26**(3): 1149-67.

Valente P, Casagrande S, Nieus T, Verstegen AM, Valtorta F, Benfenati F, Baldelli P (2012) Site-specific synapsin I phosphorylation participates in the expression of post-tetanic potentiation and its enhancement by BDNF. *J Neurosci* **32**: 5868-5879.

Valtorta F, Benfenati F, Zara F, Meldolesi J (2016). PRRT2: from Paroxysmal Disorders to Regulation of Synaptic Function. *Trends Neurosci*. Oct; **39**(10): 668-679.

Van Pelt J, Wolters PS, Corner MA, Rutten WLC, Ramakers GJA (2004). Long-Term Characterization of Firing Dynamics of Spontaneous Bursts in Cultured Neural Networks. IEEE Trans. *Biomed. Engineer*. **51**: 2051-2062.

van Vliet R, Breedveld G, de Rijk-van Andel J, Brilstra E, Verbeek N, Verschuuren-Bemelmans C, Boon M, Samijn J, Diderich K, van de Laar I, Oostra B, Bonifati V, Maat-Kievit A (2012). PRRT2 phenotypes and penetrance of paroxysmal kinesigenic dyskinesia and infantile convulsions. Neurology. Aug 21; **79**(8): 777-84.

Verderio C, Pozzi D, Pravettoni E, Inverardi F, Schenk U, Coco S, Proux-Gillardeaux V, Galli T, Rossetto O, Frassoni C, Matteoli M (2004). SNAP-25 modulation of calcium dynamics underlies differences in GABA-ergic and glutamatergic responsiveness to depolarization. *Neuron*, **41:** 599–610.

Vermeer S, Koolen DA, Visser G, Brackel HJ, van der Burgt I, de Leeuw N, Willemsen MA, Sistermans EA, Pfundt R, de Vries BB (2007). A novel microdeletion in 1(p34.2p34.3), involving the SLC2A1 (GLUT1) gene, and severe delayed development. *Dev Med Child Neurol*. May; **49**(5): 380-4.

Vigevano F, Fusco L, DiCapua M, Ricci S, Sebastianelli R, Lucchini P (1992). Benign infantile familial convulsions. *Eur J Pediatr*; **151:** 608-12.

Wakayama T, Tabar V, Rodriguez I, Perry ACF, Studer L and Mombaerts P (2001). Differentiation of embryonic stem cell lines generated from adult somatic cells by nuclear transfer. *Science*; **292**, 740-743.

Walch-Solimena C, Blasi J, Edelmann L, Chapman ER, von Mollard GF, Jahn R (1995). The t-SNAREs syntaxin 1 and SNAP-25 are present on organelles that participate in synaptic vesicle recycling. *J Cell Biol*. Feb; **128**(4): 637-45.

Wan W, Cao L, Kalionis B, Xia S, Tai X (2015). Applications of Induced Pluripotent Stem Cells in Studying the Neurodegenerative Diseases. *Stem Cells Int*; **2015**:382530.

Wang D, Kranz-Eble P, De Vivo DC (2000). Mutational analysis of GLUT1 (SLC2A1) in Glut-1 deficiency syndrome. Hum Mutat. 2000 Sep; **16**(3): 224-31.

Wang HX, Li HF, Liu GL, Wen XD, Wu ZY (2016). Mutation Analysis of MR-1, SLC2A1, and CLCN1 in 28 PRRT2-negative Paroxysmal Kinesigenic Dyskinesia Patients. *Chin Med J*. May 5; **129**(9): 1017-21.

Wang J, Zhao W, Liu H, He H, Shao R (2017a). Myofibrillogenesis regulator 1 (MR-1): a potential therapeutic target for cancer and PNKD. *J Drug Target*. Nov; **15**: 1-6.

Wang J, Gao H, Bao X, Zhang Q, Li J, Wei L, Wu X, Chen Y and Yu S (2017b). *SCN8A* mutations in Chinese patients with early onset epileptic encephalopathy and benign infantile seizures. *BMC Medical Genetics;* **18**: 104.

Wang JL, Cao L, Li XH, Hu ZM, Li JD, Zhang JG, Liang Y, San-A, Li N, Chen SQ, Guo JF, Jiang H, Shen L, Zheng L, Mao X, Yan WQ, Zhou Y, Shi YT, Ai SX, Dai MZ, Zhang P, Xia K, Chen SD, Tang BS (2011). Identification of PRRT2 as the causative gene of paroxysmal kinesigenic dyskinesias. *Brain.* Dec; **134**(Pt 12): 3493-3501.

Waszkielewicz AM, Gunia A, Szkaradek N, Słoczyńska K, Krupińska S, Marona H (2013). Ion channels as drug targets in central nervous system disorders. *Curr Med Chem*. **20**(10): 1241-85.

Watanabe K, Yamamoto N, Negoro T, Takaesu E, Aso K, Furune S, Takahashi I (1987). Benign complex partial epilepsies in infancy. *Pediatr Neurol*; **3:** 208-11.

Waxman SG (2012). Sodium channels, the electrogenisome and the electrogenistat: lessons and questions from the clinic. *J. Physiol*. **590**, 2601-2612.

Weiss LA, Shen Y, Korn JM, Arking DE, Miller DT, Fossdal R, Saemundsen E, Stefansson H, Ferreira MA, Green T, Platt OS, Ruderfer DM, Walsh CA, Altshuler D, Chakravarti A, Tanzi RE, Stefansson K, Santangelo SL, Gusella JF, Sklar P, Wu BL, Daly MJ (2008). Autism Consortium. Association between microdeletion and microduplication at *16p11.2* and autism. *N Engl J Med.* Feb 14; **358**(7): 667-75.

Wernig M, Meissner A, Foreman R, Brambrink T, Ku M, Hochedlinger K, Bernstein BE, Jaenisch R (2007). In vitro reprogramming of fibroblasts into a pluripotent ES-cell-like state. *Nature;* Jul 19; **448**(7151): 318-24.

Whitaker WR, Faull RL, Dragunow M, Mee EW, Emson PC, Clare JJ (2001). Changes in the mRNAs encoding voltage-gated sodium channel types II and III in human epileptic hippocampus. *Neuroscience*; **106**(2): 275-85.

Wilson KD, Venkatasubrahmanyam S, Jia F, Sun N, Butte AJ, Wu JC (2009). MicroRNA profiling of human-induced pluripotent stem cells. Stem Cells Dev; Jun; **18**(5): 749-58.

Wu L, Tang HD, Huang XJ, Zheng L, Liu XL, Wang T, Wang JY, Cao L, and Chen SD (2014). PRRT2 truncated mutations lead to nonsense-mediated mRNA decay in Paroxysmal Kinesigenic Dyskinesia. *Parkinsonism Relat. Disord*. **20:** 1399-404.

Xu J, Mashimo T, Südhof TC (2007). Synaptotagmin-1, -2, and -9: Ca^{2+} sensors for fast release that specify distinct presynaptic properties in subsets of neurons. *Neuron*. May 24; **54**(4): 567-81.

Xu YN, Guan N, Wang ZD, Shan ZY, Shen JL, Zhang QH, Jin LH, Lei L (2009). ES cell extract-induced expression of pluripotent factors in somatic cells. *Anat Rec (Hoboken)*. Aug; **292**(8): 1229-34.

Yamanaka S (2010). Patient-specific pluripotent stem cells become even more accessible. *Cell Stem Cel;* Jul 2; **7**(1): 1-2.

Yamanaka S (2009). A fresh look at iPS cells. *Cell*. Apr 3; **137**(1): 13-7.

Yang Y, Wang Y, Li S, Xu Z, Li H, Ma L, Fan J, Bu D, Liu B, Fan Z, Wu G, Jin J, Ding B, Zhu X, Shen Y (2004). Mutations in SCN9A, encoding a sodium channel α subunit, in patients with primary erythermalgia. *J Med Genet*. Mar; **41**(3): 171-4.

Yang Y, Xia Z, Liu Y (2000). SNAP-25 functional domains in SNARE core complex assembly and glutamate release of cerebellar granule cells. *J. Biol. Chem*. **275**, 29482-29487.

Yang W, Zhang Y, Xu X, Wang S, Yang Z, Wu Y, Liu X, and Xiru Wu (2013). Phenotypes and *PRRT2* mutations in Chinese families with benign familial infantile epilepsy and infantile convulsions with paroxysmal choreoathetosis. *BMC Neurol*. **13**: 209.

Yu FH, Mantegazza M, Westenbroek RE, Robbins CA, Kalume F, Burton KA, Spain WJ, McKnight GS, Scheuer T, Catterall WA (2006). Reduced sodium current in GABA-ergic interneurons in a mouse model of severe myoclonic epilepsy in infancy. *Nat Neurosci*. Sep; **9**(9): 1142-9.

Yu J, Hu K, Smuga-Otto K, Tian S, Stewart R, Slukvin II, Thomson JA (2009). Human induced pluripotent stem cells free of vector and transgene sequences. *Science*. May 8; **324**(5928): 797-801.

Yu J, Vodyanik MA, Smuga-Otto K, Antosiewicz-Bourget J, Frane JL, Tian S, Nie J, Jonsdottir GA, Ruotti V, Stewart R, Slukvin II, Thomson JA (2007). Induced pluripotent stem cell lines derived from human somatic cells. *Science*. Dec 21; **318**(5858):1917-20.

Zhang C, Kasner SE (2015). Paroxysmal Atrial Fibrillation in Cryptogenic Stroke: an Overlooked Explanation? *Curr Atheroscler Rep*. Dec; **17**(12): 66.

Zhang YH, Burgess R, Malone JP, Glubb GC, Helbig KL, Vadlamudi L, Kivity S, Afawi Z, Bleasel A, Grattan-Smith P, Grinton BE, Bellows ST, Vears DF, Damiano JA, Goldberg-Stern H, Korczyn AD, Dibbens LM, Ruzzo EK, Hildebrand MS, Berkovic SF, Scheffer IE (2017). Genetic epilepsy with febrile seizures plus: Refining the spectrum. *Neurology*. Sep 19; **89**(12): 1210-1219.

Zhang SC, Wernig M, Duncan ID, Brüstle O, Thomson JA (2001). In vitro differentiation of transplantable neural precursors from human embryonic stem cells. *Nat Biotechnol*. Dec; **19**(12): 1129-33.

Zhao J, Jiang WJ, Sun C, Hou CZ, Yang XM, Gao JG (2013). Induced pluripotent stem cells: origins, applications, and future perspectives. *Journal of Zhejiang University: Science B*. **14**(12): 1059-1069.

Zhao P, Luo Z, Tian W, Yang J, Ibáñez DP, Huang Z, Tortorella MD, Esteban MA, Fan W (2014). Solving the puzzle of Parkinson's disease using induced pluripotent stem cells. *Exp Biol Med (Maywood).* Nov; **239**(11): 1421-32.

Zhou B, Chen Q, Zhang Q, Chen L, Gong Q, Shang H, Tang H, Zhou D (2010). Hyperactive putamen in patients with paroxysmal kinesigenic choreoathetosis: a resting-state functional magnetic resonance imaging study. *Mov Disord*. Jul 15; **25**(9): 1226-31.

Zucker RS, Regehr WG (2002). Short-term synaptic plasticity. Annu Rev Physiol; **64**: 355-405.

8. APPENDIX

8.1. List of abbreviations and acronyms

β-gal: β-galactosidase

AA: Amino-acid

AIS: Axon initial segment

AMPA: α-amino-3-hydroxy-5-methyl-4-isoxazolepropionic acid

AP: Action potential

BAP: Bacterial alkaline phosphatase

BIC: Bicuculline

BDNF: Brain derived neurotrophic factor

BFIE: Benign familial infantile epilepsy

CACNA1A: Calcium voltage-gated channel subunit α1 A

CGP 35348: 3-Aminopropyl-diethoxymethyl phosphinic acid hidrate

C-MYC: Proto-oncogene C-MYC

CNQX: 6-cyano-7-nitroquinoxaline-2, 3-dione

Ca_V: Voltage-gated calcium channels

D-APV: D-2-amino-5-phosphonovaleric acid

DIV: Days in vitro

DSP: Dispanin

E: Embryonic day

EA: Episodic ataxia

EAA: Excitatory amino acid

EB: embryoid body

ECAT: ES cell-associated transcript

EEG: Electroencephalography

eEPSC: Excitatory evoked post-synaptic current

eIPSC: Inhibitory evoked post-synaptic current

ESC: Embryonic stem cell

Fbxo15: F-box only protein 15

FGF-2: Fibroblast growth factor-2

GABA: γ-Aminobutyric acid

GDNF: Glial cell-derived neurotrophic factor

GFP: Green fluorescent protein

G/Gmax-V: Normalized conductance-voltage curve

GLUA1: Glutamate AMPA receptor subunit 1

ICCA: Infantile convulsion and choreoathetosis

ID: Intellectual disability

IPSC: Induced-pluripotent stem cell

ISI: Interstimulus interval

JK^+: K^+ current density

JNa^+: Na^+ current density

KCNMA1: Potassium calcium-activated channel subfamily α1 M

KCNA1: Potassium voltage-gated channel subfamily A member 1

KCNQ2/3: Potassium voltage-gated channel subfamily Q member 2/3

KLF4: Kruppel-like factor 4

KO: Knock-out

K_V: Voltage-gated potassium channel

LIF: Leukaemia inhibitory factor

MAP2: Microtubule-Associated Protein 2

MEF: Mouse embryonic fibroblast

MiRNA: Micro RNA

mEPSC: Miniature postsynaptic current

mIPSC: Miniature postsynaptic current

MR-1: Myofibrillogenesis regulator 1

MRI: Magnetic resonance imaging

Na_V: Voltage-gated sodium channel

NeuN: Neuronal nuclei

NPC: Neural progenitor cell

OCT3/4: Octamer-binding transcription factor ¾

P: Post-natal day

PBS: Phosphate-buffered saline

PD: Paroxysmal dyskinesia

PED: Paroxysmal exercise-induced dyskinesia

PHD: Paroxysmal hypnogenic dyskinesia

PKD: Paroxysmal kinesigenic dyskinesia

PNKD: Paroxysmal non-kinesigenic dyskinesia

PPR: Paired-pulse ratio

PR: Probability of release

PRRT2: Proline-rich transmembrane protein 2

PSC: Post-synaptic current

PSD95: Post-synaptic density 95 kDa

RRP: Readily releasable pool

RRP_{syn}: Readily releasable pool of synchronous release

SCN1A: Sodium voltage-gated channel α subunit 1

SLC2A1: Solute carrier family 2 facilitated glucose transporter member 1

SNAP25: Synaptosomal-associated protein 25 kDa

SNARE: Soluble N-ethylmaleimide-sensitive factor (NSF) attachment protein (SNAP) receptor

SOX2: Sex determining region Y-box 2

Syp1: Synaptophysin-1

Syt 1/2: Synaptotagmin1/2

SV: Synaptic vesicle

STP: Short-term plasticity

TTX: Tetrodotoxin

$V_{0.5}$: Half-maximal potential

VAMP-2: Vesicle-associated membrane protein 2

VGLUT1: Vesicular glutamate transporter 1

V_h: Holding potential

WT: Wild-type

8.2. Articles

Valente P., Romei A., Fadda M., Sterlini B., Lonardoni D., Fruscione F., Castroflorio E., Michetti C., Giansante G., Valtorta F., Tsai JW., Zara F., Nieus T., Corradi A., Fassio A., Baldelli P., Benfenati F. Constitutive inactivation of the PRRT2 gene alters short-term synaptic plasticity and promotes network hyperexcitability in hippocampal neurons. *Cerebral Cortex*, **2018**.

Fruscione F., Valente P., Sterlini B., Romei A., Baldassari S., Fadda M., Prestigio C., Giansante G., Sartorelli J., Rossi P., Rubio A., Gambardella A., Nieus T., Broccoli V., Fassio A., Baldelli P., Corradi A., Zara F., Benfenati F. PRRT2 controls neuronal excitability by negatively modulating Na^+ channel 1.2/1.6 activity. *Brain*, **2017**.

Piccini A., Castroflorio E., Valente P., Guarnieri F., Aprile D., Michetti C., Bramini M., Giansante G., Pinto B., Savardi A., Cesca F., Bachi A., Cattaneo A., Wren J.D., Fassio A., Valtorta F., Benfenati F., Giovedì S. APache: a novel AP-2 interacting protein involved in synaptic vesicle trafficking and *in vitro* neuronal development. *Cell Report*, **2017**.